

INFORMATION TO USERS

The most advanced technology has been used to photograph and reproduce this manuscript from the microfilm master. UMI films the text directly from the original or copy submitted. Thus, some thesis and dissertation copies are in typewriter face, while others may be from any type of computer printer.

The quality of this reproduction is dependent upon the quality of the copy submitted. Broken or indistinct print, colored or poor quality illustrations and photographs, print bleedthrough, substandard margins, and improper alignment can adversely affect reproduction.

In the unlikely event that the author did not send UMI a complete manuscript and there are missing pages, these will be noted. Also, if unauthorized copyright material had to be removed, a note will indicate the deletion.

Oversize materials (e.g., maps, drawings, charts) are reproduced by sectioning the original, beginning at the upper left-hand corner and continuing from left to right in equal sections with small overlaps. Each original is also photographed in one exposure and is included in reduced form at the back of the book.

Photographs included in the original manuscript have been reproduced xerographically in this copy. Higher quality 6" x 9" black and white photographic prints are available for any photographs or illustrations appearing in this copy for an additional charge. Contact UMI directly to order.

U·M·I

University Microfilms International
300 North Zeeb Road
Ann Arbor, Michigan 48106
U·M·I

Order Number 1343024

**Inhibition of hydrogen-oxygen-nitrogen diffusion flames by
potassium and potassium superoxide**

Mitson, Scott Charles, M.S.

University of Nevada, Reno, 1990

Copyright ©1990 by Mitson, Scott Charles. All rights reserved.

U·M·I
300 N. Zeeb Rd.
Ann Arbor, MI 48106

University of Nevada

Reno

Inhibition of Hydrogen-Oxygen-Nitrogen Diffusion
Flames by Potassium and Potassium Superoxide


A thesis submitted in partial fulfillment of the requirements
for the degree of Master of Science in Metallurgical Engineering

by

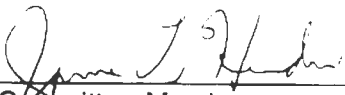
Scott Charles Mitson

September 1990

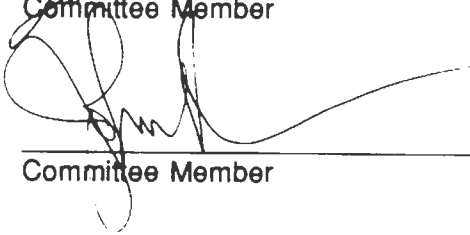
The thesis of Scott Charles Mitson is approved:



Major Professor / Committee Member



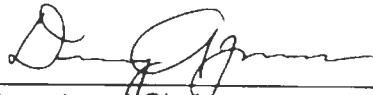
Committee Member



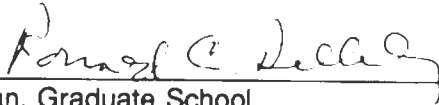
Committee Member



Thesis Director / Major Advisor



Department Chair



Dean, Graduate School

University of Nevada

Reno

September 1990

c Copyright by Scott Charles Mitson 1990
All Rights Reserved

ACKNOWLEDGEMENTS

This research was supported by grants from the U.S. Air Force Office of Scientific Research and the Morton Thiokol Corporation. I wish to express my thanks to Dr. Eugene Miller. Without his guidance and assistance, this effort would not have been completed.

ABSTRACT

The afterburning of hydrogen and carbon monoxide in rocket plume gases is inhibited by the addition of potassium salts to the rocket propellant formulation. The mechanism of the inhibition is not completely understood, but it is believed to involve chain breaking of H and OH reactions by K° , KOH, and KO_2 . The present study is directed toward clarifying the reactions involved. Inhibition effects are reported of K° and KO_2 vapor on the combustion of preheated nitrogen-diluted hydrogen-oxygen opposed-jet diffusion flames for various lean to rich mixtures with overall stoichiometric ratios (ϕ) ranging from 0.72 to 1.21. These effects are interpreted from the spectral emission measured from incremental scans of a flat flame in the 3800 - 3000 cm^{-1} range for water and OH bands. It is concluded that K° vapors inhibit the combustion of hydrogen over the range studied of 0.1 to 1692 molar ppm for lean to rich flames with ϕ 's of 0.98 to 1.21. KO_2 inhibits at concentrations equivalent to its equilibrium vapor pressure at 160° to 320°C for ϕ 's of 0.72 to 1.21.

TABLE OF CONTENTS

	Page number
Table of Contents	
Title page	
Signature page	i
Acknowledgements	ii
Abstract	iii
Table of contents	iv
List of Figures	v
List of Tables	vi
Introduction	1
Theoretical Background	2
Previous Research	4
Radiation Processes	19
Experimental Apparatus	24
Experimental Procedure	29
Experimental Results	32
Discussion	40
Conclusions	44
References	45
Appendix 1 Previous Research; Experimental Detail	48
Appendix 2 Apparatus Standard Operating Procedure	65
Appendix 3 S. O. P. Comments	70
Appendix 4 Heat Transfer; Thermocouple Errors	75
Appendix 5 Settings, Data, Spectra	89
Appendix 6 Methane Combustion Inhibition by Bromine Compounds	137

LIST OF FIGURES

Figure		Page number
Figure 1	Schematic of Opposed-jet Burner and Optical System	27
Figure 2	Heated Burner for K ^o -Additive Vaporization	28
Figure 3	Burner with Thermocouple Location Scale	30
Figure 4	Spectral Intensity vs Inlet Fuel Gas Temperature and Stoichiometric Ratio, No Additive	34
Figure 5	Spectral Intensity vs Inlet Fuel Gas Temperature and Stoichiometric Ratio, K ^o Addition	35
Figure 6	Spectral Intensity vs Inlet Oxidizer Gas Temperature and Stoichiometric Ratio, No Additive	37
Figure 7	Spectral Intensity vs Inlet Oxidizer Gas Temperature and Stoichiometric Ratio, KO ₂ Addition	38

LIST OF TABLES

Table	Page number
Table 1 N_2 - H_2 - K° / O_2 - N_2 Test Conditions	36
Table 2 N_2 - H_2 / O_2 - N_2 - KO_2 Test Conditions	39
Table 3 Flame Chemical Reactions and Rate Coefficients	43

INTRODUCTION

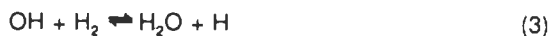
Visible primary and secondary smoke has been largely eliminated from solid rocket plumes by the removal of ammonium perchlorate oxidizer and most of the other solid energy and ballistic modifier additives from the propellant formulation. The combustion gases from these propellants, however, contain significant concentrations of hydrogen and carbon monoxide. When mixed with ambient air in the plume, they react to form water and carbon dioxide with visible flash and increased infrared and ultraviolet radiation. Also, some of the secondary smoke advantage of these so-called minimum-smoke propellants over reduced-smoke propellants (formulations containing ammonium perchlorate oxidizer and low content of solid energy and ballistic modifiers) is lost since the additional water formed by afterburning is available for condensation to smoke. The research reported here was directed toward preventing or at least inhibiting the signatures related to afterburning.

It is known that potassium salts inhibit the reaction of hydrogen and carbon monoxide to water and carbon dioxide. Potassium salts, such as KNO_3 and K_2SO_4 , have been added to propellant charges at a level of 1 - 3 wt pct to suppress gun muzzle flash and rocket plume flash and infrared signatures. The mechanism by which the potassium salts inhibit afterburning is not completely understood, but it probably involves K° , KOH and KO_2 reacting with H and OH radicals to break the chain reactions controlling the combustion of hydrogen and carbon monoxide. Experimental evidence suggests that the reactions take place in the vapor phase.

In the present research, the effects of K° and KO_2 vapor on the afterburning reactions of hydrogen were evaluated in the flat diffusion flame of $\text{N}_2\text{-H}_2/\text{O}_2\text{-N}_2$. An opposed-jet burner, modified from one described by Hahn, Wendt and Tyson¹, was used to produce the flame. An infrared spectrophotometer, to which was added an external optical system and a staged slit, recorded incrementally the emission spectra of narrow segments of flame zone in the $3800 - 3000 \text{ cm}^{-1}$ water and OH band range. The spectra were used to interpret the effects of the K° and KO_2 .

THEORETICAL BACKGROUND

The most important reactions involved in afterburning are,



There has been disagreement about the correct mechanism for the suppression of afterburning by potassium. Jensen, Jones and Mace² concluded from their experiment with premixed fuel-rich H₂-O₂-N₂ flames that atomic potassium reacts as follows:



On the other hand, Friedman and Levy³ found atomic potassium to be ineffective for a methane-air diffusion flame and stated that reaction (6) was unlikely to occur early enough in the reaction sequence to be important. They suggested that potassium salts first form molten K₂O which reacts with water to form gaseous KOH. They argued that the formation rate for the KOH by the reverse reaction of equation (7)⁴ is orders of magnitude greater than the rate of equation (6) for K^o and OH.

Kaskan⁵ proposed an alternative mechanism,



[†] M is any third body; ^o indicates activated, having higher energy

and



based on observations of hydroxyl radicals in a lean flame. Jensen in a later paper, however, was able to explain Kaskan's results without resorting to the postulation of the reactions of KO_2 .

Plume calculations were made by Jensen & Jones⁷ from which they concluded that the reverse reaction (9) was a significant source of OH, enhancing afterburning. They noted, however, that there is a lack of reliable thermochemical data for KO_2 making speculations about its effects uncertain.

One other reaction of KO_2 is relevant to the present study, and it too can be a significant source of OH. This reaction is



PREVIOUS RESEARCH

Friedman and Levy³ investigated the effect of sodium and potassium metal vapors on opposed-jet methane/air diffusion flames (1963). They found that neither of these two were effective inhibitors, as judged by the criterion of "flame strength", described below. They also investigated the effects of organic halides on similar flames and found these to be effective. Friedman and Levy utilized an opposed-jet technique that had been developed by A. E. Potter et al.¹¹ for studying diffusion flames in which the parameter measuring the stability of the flame, the flame strength, was defined. Since the opposed-jet technique had not previously been applied to a study of the flame inhibition by potassium, Friedman and Levy found it prudent to perform preliminary experiments with known gaseous inhibitors, i.e. organic halides, before investigating the alkali metal vapors. Previous research had demonstrated inhibition of premixed methane flames by the same organic halides¹³. (See Appendix 6 for a discussion of the inhibition of methane/air flames by bromine compounds.)

Their experimental technique involved the observation of a hole formation in the central region of a flat, circular diffusion flame between the opposing gas jets. Potter et al. described how, if the flame is maintained centered between the two jets while the flows are progressively increased, a hole appears on the flame axis at a reproducible flow rate, enlarges if the flows are increased, and disappears again if the flows are reduced. Friedman and Levy used the criterion of first detectable appearance of a hole as the measure of "flame strength". They made comparisons of hole-point fuel flow rate with and without inhibitor at constant burner geometry. It appears from their paper that the air flow rate was varied in a manner to some extent independently of the flow rate of fuel, thus varying the fuel-to-air ratio.

With methyl bromide as the fuel additive, Friedman and Levy found the flow rate of fuel for hole-point at room temperature to be approximately 78% of that for no additive and at 733

Kelvin found it to be approximately 85%. In both cases the methyl bromide concentration was 10 mole percent of the fuel flow. No change in fuel flow rate for hole formation was noted for sodium concentrations up to 0.26 mole percent. Likewise, no change in fuel flow rate for hole formation was noted for potassium concentrations up to as high as 3.5 mole percent.

Friedman and Levy concluded, based on this evidence, that there was lack of any inhibitory effect by elementary potassium [or sodium] introduced into the fuel side of a methane-air diffusion flame at concentrations comparable to those at which bromine inhibitors exert easily measurable effects in the same apparatus. This behavior must be contrasted with that reported for potassium salts in premixed flames, which are at least as potent in reducing burning velocity as bromine inhibitors. They go on further to say that "We therefore conclude that the known inhibitory effects of alkali metal salts must arise from species other than the alkali metal atoms and we propose that the effective species is the gaseous alkali metal hydroxide." Based upon kinetic data available at the time, their calculations indicated that three-body reactions of potassium metal with H, OH, and O at atmospheric pressure would be several orders of magnitude slower than any competing two-body reactions of very low activation energy. Therefore



could not occur early enough in the flame to affect the propagation. Instead they suggested that potassium salts are decomposed to molten K_2O which reacts with water to form $2KOH$. KOH then reacts to scavenge radicals by such means as



In their discussion Friedman and Levy state that "Even though the inhibitor potassium hydroxide does not regenerate itself by the proposed sequence, the concentration of inhibitor necessary to be effective is comparable with the concentrations of H and OH in the equilibrium products, and a single functioning of each inhibitor molecule may be quite adequate for the

observed effects." Thus the thermal decomposition of potassium carbonate, for instance, to potassium oxide, followed by reaction with water to potassium hydroxide, and then reaction with the H or OH radical to form K^o or KO, respectively, was predicted to proceed at a rate "several orders of magnitude" more quickly than the three-body reaction of elemental potassium and OH to form KOH.

Walter E. Kaskan⁵ (1965) investigated the reaction of alkali atoms in lean premixed H₂/O₂/N₂ flames. It had been proposed by other researchers that the major equilibrium reaction of alkali metals in these H₂/air premixed flames was:



Kaskan's results did not indicate this to be correct and he suggested that the appropriate reaction was



He also suggested that there was an analogy between this reaction and that for forming HO₂. Most of the previous work was done on fuel rich or near-stoichiometric H₂/air flames.

Hydrogen atom concentrations were determined by a method which correlates [H] to the intensity of the Lithium resonance line. OH, Na^o, and K^o concentrations were determined by photometric methods. The sources were a discharge in water vapor for OH measurement, and a tungsten-strip filament lamp for alkali-atom measurements. Alkali atoms were determined by resonance-line absorption, employing the Na^o 5889, 5896 Å doublet, and the K^o 7665, 7699 Å doublet. Flame gas temperatures were generally measured with silica-coated thermocouples, and occasionally were checked by a Na^o-reversal measurement.

The procedure followed consisted of burning various lean H₂/air flames and following the absorption of both OH and alkali atoms as a function of distance from the burner. In all of the flames studied both the concentrations of OH and Na^o or K^o decreased with increasing distance

[†] A^o represents an alkali metal atom.

from the burner. The rate of decrease of both OH and the alkali atoms was faster the leaner the flame, but more so for alkali atoms. Most runs were made in duplicate. The first flame was a lean H_2 /air flame which provided an observable, but relatively slow, decay of alkali, and the second would differ only in that a small amount of O_2 was added to speed up the decay.

The rates of decay were shown to be directly proportional to alkali atom concentration, indicating the observed effects were first order in alkali atoms. If, as proposed by the previous researchers, the main reaction was



it was shown that the relation of $[A]$ to $[OH]$ should be cubic in $[OH]$. However the plot of $\log [A]/([A]_{tot} - [A])$ against $\log [OH]$ was linear, but had a slope of 2, not 3. The remainder of the analysis suggested that the data are better interpreted by assuming the reaction responsible for alkali atom concentration decay is :



In 1978 D. E. Jensen and G. A. Jones published "Reaction Rate Coefficients for Flame Calculations"⁴ which contained an updated list of recommended rate coefficients for chemical reactions occurring in flames. The rate coefficients were expressed as functions of temperature for the range $1000 < T < 3000$ Kelvin, and were either taken from experiments described in the scientific literature or estimated by comparison with rate coefficients for analogous reactions. An estimate of the uncertainties of the values listed was also included, as were reaction equilibrium constants as functions of temperature. An emphasis was placed on reactions of metal derivatives.

They note two particularly difficult points in the description of the chemical kinetics in the case of reactions involving "third bodies" or "collision partners" - typically denoted "M". The first is that different third bodies have different efficiencies in these reactions. The list gives rate coefficients averaged for the more effective third bodies such as CO_2 , H_2O , and N_2 , present in

typical flames. The concentration $[M]$ is taken as the sum of concentrations of all gas phase species present. A second difficulty is that the third body reactions (and their reverse reactions) actually take place via stepwise processes involving excited molecular or atomic states, vibrational and electronic. They additionally state that the "collision frequencies" to which kineticists often refer rate coefficients are generally those calculated on the assumption that all chemical species are in ground electronic, vibrational, and rotational states, and that this common usage is "sometimes rather misleading".

In the following year (1979) D. E. Jensen, G. A. Jones, and A. C. H. Mace² published the results of an investigation of fuel-rich, premixed H_2/O_2-N_2 flames with a potassium compound additive. They hoped to test the validity of the proposed reaction scheme for recombination of H and OH radicals in the flames



and



In addition they hoped to derive more accurate rate coefficients for the forward and reverse reactions of these two. Upon publication of their previous list of rate coefficients it was clear that the values presently accepted were only "order-of-magnitude estimates based on flame experiments not specifically designed for kinetic measurements". The previously reported values for these two forward reactions were $4 \cdot 10^{-12} \exp(-1000/T) \text{ cm}^3 \text{ molecule}^{-1} \text{ sec}^{-1}$ and $6 \cdot 10^{-28} T^{-1} \text{ cm}^6 \text{ molecule}^{-2} \text{ sec}^{-1}$ respectively. The more accurate values which they provide in this work are $1.8 \cdot 10^{-11} \exp(-1000/T)$ and $1.5 \cdot 10^{-27} T^{-1}$, respectively.

The flames used were atmospheric-pressure, laminar, shielded, cylindrical, premixed, fuel-rich $H_2 + O_2 + N_2$ flames in which the distance above (downstream of) the primary reaction zones was a linear measure of reaction time available for recombination of the free radicals produced in

above-equilibrium amounts in these zones. The authors state that under the conditions of this work, the only flame radicals present in significant quantities were H and OH, with the concentrations of other species such as O and HO₂ being extremely low. Calculations based on JANAF Thermochemical Tables (1971) and supplemented for such species as K[°] and KO₂ by kinetic data from their list of rate coefficients of the previous year suggested that no potassium-containing species other than K[°] and KOH would be formed in the flames used at concentrations high enough to contribute significantly either to reaction rates or to the total potassium concentration. Therefore they assumed that $[K]_{TOTAL} = [K] + [KOH]$.

Potassium was added to the flame as potassium dipivaloylmethane in the form of vapor from a supply reservoir. Deposition of additive in the supply system and burner was minimized by the heating of both. Photometric determinations of [H] and [K] were performed on the flame. [OH] and [KOH] were calculated assuming that [H] and [OH] were related by



and that [K] and [KOH] were in equilibrium through



For the purposes of these determinations, potassium was first supplied to the flames at known concentrations from a calibrated atomizer and the curve of growth of the integrated emission intensity of the 766.5 nm wavelength potassium resonance line, against [K] was constructed using the above relations. Hydrogen atom concentrations were measured by the Li[°]/Na[°] comparison method, lithium and sodium being supplied in known proportions from the atomizer.

In tests of similar flames with and without potassium additive it was seen that potassium accelerated the rate of hydrogen atom removal and that the fraction of the recombination due to the presence of the potassium is proportional to the total concentration of potassium, which they claim is consistent with a homogenous acceleration process. The researchers tabulated the rate

coefficients derived from this work for both the forward and reverse directions and state that the values obtained are consistent with earlier thermochemical studies of K and KOH in flames.⁴ They further conclude that the mechanism for flame radical removal consisting of the reactions mentioned above is cyclic; the observed decreases in [H] and [OH] caused by addition of potassium exceed $[K]_{total}$, which implies that K^o and KOH must be successively regenerated during the acceleration process. In that sense, the acceleration of radical removal could be loosely termed a catalysis, although not strictly so.

Jensen and Jones published again in 1981, "Theoretical Aspects of Secondary Combustion In Rocket Exhausts"⁷. This was a computational technique based on a two-equation turbulence model, coupled with detailed nonequilibrium chemistry, used for predictions of whether or not secondary combustion of excess fuels would occur in the exhaust from an additive-modified double-base (nitrocellulose-nitroglycerin) propellant rocket motor. The purpose of the paper was to describe in outline a method of predicting whether or not secondary combustion occurs in the exhaust of any low altitude rocket, to summarize results of applying this method to a particular rocket motor with small proportions of potassium additive incorporated in its solid propellant, and to discuss both method and results in a manner that brings out the need for improved prediction techniques.

They found that the concentrations of the major species H₂, CO, CO₂, H₂O, and N₂ do not vary significantly with the proportion of potassium-containing additive in the propellant. Those of the minor species were found to vary with additive level, and the higher the level, the greater the rate of recombination in the nozzle of the free radicals present. Slight variations of exit temperature and pressure with additive level were also apparent. With potassium excluded from the calculations in a particular exhaust stream, a significant rise in gas temperature with increasing axial distance occurs near the nozzle exit. This indicated that secondary combustion of hydrogen and carbon monoxide was taking place. For the same conditions except with 0.8 percent by weight

potassium in the propellant, a decrease of 400 to 500 Kelvin was noted in the maximum temperature found in the secondary combustion zone; 1.0 percent totally eliminated the region of temperature increase and hence, suppressed the secondary combustion. In calculations of a variety of other exhausts, it was found that the minimum concentration of potassium necessary to completely suppress the secondary combustion under most conditions would be more nearly 2.5 percent by weight.

The authors list six reactions containing potassium which were considered in their analysis:



One interesting aspect of the work was that the inclusion of reactions involving KO_2 led to promotion of secondary combustion. As oxygen from the air is mixed with the propellant products, the reaction



is predicted to be a significant source of active free radicals. They qualify this analysis with the comment that much of the uncertainty in the influence of KO_2 stems from the lack of reliable thermochemical data for this species. Overall they view their approach to the analysis of the chemistry of the rocket exhausts as adequate as used within this method.

W. A. Hahn, J. O. L. Wendt, and T. J. Tyson published a paper in 1981 entitled "Analysis

of the Flat Laminar Opposed Jet Diffusion Flame with Finite Rate Detailed Chemical Kinetics¹¹. The fuel in their flame was moist CO, which was burned with O₂ and N₂. The main intent of the work reported was to study pollutant formation. Their stated objectives were to mathematically model the flame and to develop procedures to solve the model, to gather experimental data for comparison with the predicted results, and if the previous two objectives were accomplished and in agreement, to introduce small quantities of an additive (fuel impurity) into the flame and compare predictions to measured values.

The model was solved for combustion of a moist carbon monoxide opposed-jet diffusion flame. The reaction set included seven elementary reactions and eight chemical species.



The forward and reverse rate coefficients were taken from Engleman¹². The concentrations of carbon monoxide and water in the fuel stream were 36.2 percent and 3.0 percent, respectively, the diluent being nitrogen, while the oxidizing stream contained 19.1 percent oxygen in nitrogen. The initial guess employed for the solution of the differential equations used in the model was the solution of the equivalent Burke-Schuman flame (infinitely fast reactions assumed). This approach provided the basic profiles of CO, O₂, CO₂, and temperature. The temperature profile calculated

matched the measured profile (after correcting measured values for radiation heat losses) in maximum temperature (approximately 1540 Kelvin) quite well, but the rest of the temperatures tended to be 200 - 300 Kelvin too high in the model (except where the flame zone transition to inlet gases occurred, of course). The predicted versus measured profiles for CO, CO₂, O₂, H₂, and H₂O were in very good agreement at selected points in the flame, but in other locations deviated significantly. The interpretation of this fact is that the free radical concentrations were far above those predicted by the equilibrium calculations in the model which tended to alter the reactant profiles. The measured reaction zone thickness, which the authors state is a key parameter in the prediction of the formation of trace species in this type of flame, was in close agreement with that predicted. It was noted that water decomposes in the fuel-rich region, and the so-formed free radicals and H₂ molecules diffuse into the fuel-lean side of the flame where, in a very narrow region, water is formed again. The predicted peak values of the free radicals varied from 1000 to 3000 parts per million, existing mainly on the fuel-lean portion of the flame zone. No measurement of the actual free radical concentrations were carried out, although as stated above, it was inferred that they generally were higher than predicted, as evidenced by the measured values of the major species. In general, the authors felt that there was sufficient agreement between predicted and measured characteristics of the flame to claim the model a success.

"Kinetic Investigation of the Third-order Rate Processes between K^o + O₂ + M by Time-resolved Atomic Resonance Absorption Spectroscopy"⁸, published in 1982 by David Husain and John M.C. Plane, compared rate constants for this reaction obtained from the pulsed photochemical method following the flash photolysis of KI vapor to those reported by Kaskan and Carabetta from their atomic resonance absorption studies on premixed, fuel-lean H₂/O₂/N₂ flames. This investigation found the rate constants determined by Kaskan for potassium were three orders of magnitude too low. A prior report by these authors similarly found that the rate constants reported by Kaskan for sodium were also three orders of magnitude too low. The tests were undertaken in a very rigorous method, and three different third bodies were investigated : He, N₂, and CO₂.

A table of the results for the third-order rate constants ($k/\text{cm}^6 \text{ molecule}^{-2} \text{ sec}^{-1}$) for

$(\text{K}^\circ, \text{Na}^\circ) + \text{O}_2 + \text{M}$ follows:

<u>M</u>	<u>K[°] (753-873 K)</u>	<u>Na[°] (724-844 K)</u>
He	1.3×10^{-30} (784 K)	$(6 \pm 1) \times 10^{-31}$
N ₂	2.2×10^{-30} (784 K)	$(1 \pm 0.2) \times 10^{-30}$
CO ₂	5.0×10^{-30} (784 K)	2×10^{-30}
(H ₂ + N ₂ + H ₂ O)**	1.02×10^{-30}	8.2×10^{-34}

** Kaskan's flame

David E. Jensen in 1982, published the paper "Alkali-metal Compounds in Oxygen-rich Flames : A Reinterpretation of Experimental Results"⁶. Jensen reviewed principally the work of three teams of investigators who had previously published research on premixed oxygen-rich H₂/O₂/N₂ flames. These investigators were Kaskan and Carabetta, McEwan and Phillips, and Husain and Plane. Kaskan had at his disposal rate coefficients for the formation of the superoxides of both sodium and potassium that were in error by three orders of magnitude. Both Kaskan and Carabetta and McEwan and Phillips introduced some errors into the conclusions drawn from their work by utilizing alkali metal concentrations that were too low and by not recognizing some inherent bias in techniques used to calculate the concentrations of some of the chemical species in the flames. Husain and Plane provided evidence supporting Jensen's interpretation of the earlier work.

The researchers studying these flames have variously considered compounds formed in significant proportions to be the hydroxides, AOH, the monoxides, AO, and the superoxides, AO₂. One difficulty associated with this work, however, is that the nature of the compounds formed had generally been inferred from dependencies of depletions of free alkali atom concentrations upon flame composition and temperature rather than established by direct observation. The evidence for formation of hydroxides appears strong because of the self-consistency of interpretations invoking their presence and because flame determinations of hydroxide bond energies agree with

the results of independent experiments. Evidence for formation of AO_2 is less convincing, partly because the measurements performed on alkali-seeded oxygen-rich flames for certain parameters present greater experimental difficulties than do the corresponding determinations performed on fuel-rich flames. The earlier experiments were also interpreted based upon reaction rate data which was later seen to be in error.

Jensen took Kaskan's data from the potassium experiments and assumed that the only alkali species present in significant quantities were K° and KOH . He then took the OH concentrations and increased them by 50% to bring them "into line with a preferred value for the oscillator strength of the appropriate OH band". After calculations based upon recent (and more accurate kinetic data), Jensen compared the predicted results to the experimental results and found good agreement. Thus the experimental data reported by Kaskan for potassium could be quantitatively interpreted on the basis of the up-to-date kinetic work on the reactions



and



without the need for inclusion of any compound other than the hydroxide.

The reinterpretation of the sodium experiments of Kaskan met with greater difficulty. When the same techniques mentioned above were applied to the sodium flame data, the predicted sodium concentrations $[\text{Na}]$ were found to be too low near the main reaction zone and too high further downstream. Inclusion of NaO_2 in the model reportedly gave even worse agreement. Kaskan reported measured OH concentrations to be higher in cooler flames, which is contrary to expectations. Jensen took this discrepancy as justification to increase the measured values for $[\text{OH}]$ at all points by a factor of two. He also reduced the forward and reverse rate coefficients for



by a factor of 2.5 (within the uncertainty bounds). The predictions were recalculated, and this time

good agreement was achieved. Almost in passing, Jensen notes that this model could not be applied to McEwan and Phillip's data due to a lack of data correlating [OH] at atmospheric pressure to [OH] at other pressures. He does state that McEwan had assumed that the concentration of NaOH would be equal to the concentration of H based solely upon the reaction



McEwan had found low concentrations of H, which led them to the conclusion that NaOH was not the main compound formed and that significant proportions of NaO₂ must be present. The concentration of H was determined by the Li/Na comparison method. According to Jensen, this method yields erroneously low H concentration values in this type of flame.

Summarizing, Jensen felt that his interpretation of the results of these experiments on sodium and potassium in oxygen-rich H₂/O₂/N₂ flames removes the conflict between the rate coefficients for the superoxide formations obtained by Husain and Plane and the original apparent values derived by the previously mentioned investigators. Husain and Plane's work yielded revised values for Na-O₂ and K-O₂ bond energies and reaction rate coefficients. He suggests that further experiments of widely varying temperature and composition be undertaken to more rigorously test his hypotheses. Additionally, in such work it would be necessary to determine flame radical concentrations with great precision and highly desirable to observe compounds directly (either by spectrophotometric means or by mass spectrometric sampling) rather than to infer their presence by indirect methods.

J. A. Silver, M. S. Zahniser, A. C. Stanton, and C. E. Kolb published the results of similar work "Temperature Dependent Termolecular Reaction Rate Constants for Potassium and Sodium Superoxide Formation" in 1984. They measured the rate constants as a function of temperature in the range of 300 to 700 Kelvin in the low pressure third order limit from 1 to 8 torr total pressure with N₂, He, and Ar as third bodies. Laser induced fluorescence was used to monitor the disappearance of Na^o or K^o as a function of O₂ and M. Their findings were in agreement with the results of Husain and Plane.

"Afterburning Suppression Kinetics"¹⁴ by T. S. Singh, D. P. Weaver, and J. D. Eversole and "Kinetic Mechanisms for Ionization and Afterburning Suppression"¹⁶ by Weaver and Singh both address the inhibition effects of KOH on premixed H₂/O₂/N₂ flames. The effect of KOH addition on laminar burning velocity, peak mole fractions for H and OH, the rate of fuel and oxidizer decay, the rate of production of product species, and the rate of temperature rise were studied theoretically. Computations were performed for both fuel rich and fuel lean flames. The researchers also performed their analyses with HBr as the suppressant additive. The predictions resultant from the computational model developed for the base-line H₂/O₂/N₂ flames and for the flames inhibited by either HBr or KOH were compared to predictions of other computational models and experimental data reported previously by other researchers.

Weaver modified computational models previously developed by Coffee et al.¹⁶ and Kee et al.¹⁷ for the base-line flames and found the predicted characteristics to be in good agreement with the experimental results of Dixon-Lewis¹⁸ and Eversole and Singh¹⁹. Supplementing the model with reactions involving HBr and related species yielded predictions in good agreement with experimental results reported by Dixon-Lewis et al.^{20,21} and Charles Westbrook^{22,23}.

Weaver found that a 5-step reaction scheme involving potassium-containing species (with associated chemical, physical, and thermodynamic parameters) combined with the base-line flame model accurately predicted the experimental data reported by Jensen et al.² and Mitani et al.²⁴, but not so for Hynes et al.²⁶. The 5-step reaction scheme included the forward and reverse reactions



It is of interest that both Weaver and Jensen concluded that the first two reactions were of primary importance in flame inhibition by potassium compounds, while Hynbs concluded (as had Friedman and Levy²) that reaction two was of negligible significance .

RADIATION PROCESSES¹⁰

The radiation from any system in equilibrium will be continuous and the same as for a black body at the same temperature as the system. Fully aerated flames usually show an emission spectrum of discrete bands. In small flames the emission of radiation by molecules and particles is not balanced by the absorption of radiation, so that there is a steady deactivation of excited molecules and radiation cooling of particles (if present) which has to be made up by collision processes within the flame gases. If these collision processes are not sufficiently efficient then the distribution of energy among excited molecules or the temperature of solid particles may differ from that for equilibrium at the temperature of the flame gases.

The distribution of radiation with wavelength (in cm) is given by Planck's radiation law. In a constant temperature enclosure at temperature T (Kelvin), the radiation density between wavelengths λ and $\lambda+d\lambda$ is equal to

$$8\pi hc\lambda^{-5}d\lambda/(\exp(c_2/\lambda T)-1) ,$$

where c is the velocity of light, h is Planck's constant, and c_2 is the second radiation constant ($c_2 = 1.438 \text{ cm deg}$).

For practical use, Wien's law will give the intensity of radiation, in ergs/sec per unit solid angle normal to the surface of a black body

$$I_\lambda = 2E_\lambda A c_1 \lambda^{-5} \exp(-c_2/\lambda T) d\lambda ,$$

where c_1 is the first radiation constant, $0.588 \times 10^{-5} \text{ erg cm}^2 \text{ sec}^{-1}$, and A is in cm^2 .

This holds with sufficient accuracy as long as λT is less than 0.2 cm deg. It begins to fail for long wavelengths or very high temperatures. For a black body the emissivity E_λ is equal to 1 for all wavelengths. In practice, flames do not usually approximate a black body. For fully aerated flames E_λ is close to zero for most values of λ but may reach fairly high values, near 1, for a limited number of emission bands, the strongest of which are in the infra-red. For a black body the wavelength λ_{max} for maximum intensity varies with temperature, and is given by Wien's

displacement law,

$$\lambda_{\text{max}}T = 2.89 \times 10^7 \text{ , cm K .}$$

The total radiation (over a hemisphere) from unit area of a black body at temperature T is given by the Stefan-Boltzmann law,

$$W = \sigma T^4 = 5.67 \times 10^{-12} T^4 \text{ , watts cm}^2 \text{ .}$$

The four previous fundamental laws are most useful for dealing with bodies emitting a continuous spectrum, but their application to small flames, which emit discrete banded spectra, is limited. However, it should be remembered that if the flame gases are in thermodynamic equilibrium, in which the energy is equally partitioned among its various possible forms, then the emissivity at any wavelength E_λ cannot be greater than 1, and the Planck radiation law and Wien's law may be used to predict the maximum possible brightness at any wavelength.

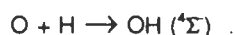
For molecules in the gaseous state, the energy of each molecule is restricted to a limited number of possible values, i.e. is quantized, and the wavelengths of radiation which the molecule can emit or absorb are limited to a relatively small number of lines in the spectrum. Spectra in the visible and ultra-violet regions are generally due to changes of electronic energy, i.e. to a transition of an electron from one energy level within the molecule to another. This change determines the position of the band system as a whole. Accompanying changes in the vibrational energy of the atoms of the molecule determine the position of individual bands within the band system. Accompanying changes of rotational energy of the molecule as a whole determine the fine structure of individual bands. Band spectra in the near infra-red are due to changes of vibrational and rotational energy of the molecules, while spectra in the far infra-red are due to changes of rotational energy.

None of the ordinary molecules which are stable products of combustion of hydrocarbon flames, such as H_2O , CO_2 , CO , O_2 , or N_2 radiate strongly in the visible or ultra-violet regions. The only product of combustion which has an appreciable equilibrium concentration which does give a strong visible/ultra-violet spectrum is the hydroxyl radical, OH , which gives a band system in the

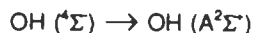
ultra-violet, with a band maximum at 3064 Å. In some very hot flames there may be weak emission of the Schumann-Runge bands of O₂ giving band structure from the blue into the ultra-violet. Generally speaking, we may say that burnt flame gases do not give appreciable emission or absorption in the visible region and the only strong feature in the ultra-violet is the OH band system.

Several chemical species do radiate significantly in the infrared region, including H₂O, CO₂, CO, and OH. H₂O has strong vibration bands at 1.8, 2.7, and 6.3 μm and a rotational band that covers the region from 10 to about 100 μm. The OH vibrational bands cover the near infra-red area to about 4 μm, with a strong peak at 2.8 μm. It follows from Wien's displacement law that at typical flame temperatures the maximum emission for H₂ flames will tend to be in the near infra-red between about 3 μm and 1 μm, depending upon the temperature of the flame. For small premixed, laboratory flames the radiation is mainly in the near infra-red. For fuel-lean flames about 10% of the heat of combustion is lost by radiation, rising to about 18% for stoichiometric flames, and then falls off for increasingly fuel-rich flames. For clear flames the radiation in the visible and ultra-violet usually accounts for less than 0.4% of the heat of combustion.

When a chemical reaction leads directly to the formation of an atom or a molecule in an electronically excited state, from which radiation may occur, then we may have a light emission (in the visible or ultra-violet regions) out of all proportion to that to be expected from thermal emission at equilibrium. This phenomenon is referred to as chemiluminescence. Chemiluminescence phenomena result from mechanisms involved when the flame is in a state of either non-thermal equilibrium or non-chemical equilibrium. For OH there are at least two recognized processes for chemiluminescence. In low pressure (0.01 atm) hydrogen-oxygen flames the pre-association of O plus H is thought to occur²⁸ and produces a high-energy, low-stability OH state :



The OH (⁴Σ) concentration depends upon the product of the concentrations of free atoms (approximately 11% for H and 4% for O). By a radiationless transition,



leading to selective excitation to vibrational levels $v' = 2$ and 3 , from which radiation may occur.

At the base of premixed, low-temperature hydrogen flames the recombination



occurs; this has an intensity proportional to the cube of the concentration of free atoms or radicals but gives a fairly normal distribution of rotational and vibrational energy.

Departures from equilibrium in flame gases have an effect upon flame radiation, but there are also other effects. The most obvious type of failure to reach equilibrium will be through incomplete combustion. The main chemical processes are normally completed in a very short time during passage through the reaction zone of the flame, but in some cases the chemical reactions are not complete. This is especially the case with low-temperature flames, wherein reactions requiring large activation energies may not take place with sufficient speed. Thus reactions are most likely to be incomplete for flames with inactive diluents such as nitrogen, or those with excess fuel or oxidizer. Apart from these major chemical effects, there is evidence for other chemical abnormalities. Many of these may be due to the slowness with which free atoms recombine. The main reactions are probably of the chain type, proceeding by bimolecular collisions; this applies to both chain propagation and chain branching. Chain termination involving removal of free atoms or active radicals usually, however, requires a surface or a three-body reaction and tends to be less rapid. Thus free atoms or radicals may persist past the main reaction zone. The abnormally high intensity of the (2,1) and (3,2) bands of OH in H_2 /air flames at atmospheric pressure is due to an excess population of free atoms; in this case, H and O atoms recombine directly through inverse predissociation to form OH in the vibrational levels with $v' = 2$ and 3 .

The measurements made in this research were in the near IR, in the vibrational-rotational regime. Although various non-equilibrium phenomenon have been cited (Gaydon, above), most studies have indicated that the spectra of OH, H_2O , CH, CO, and CO_2 , in the wavelengths studied,

are in thermal and chemical equilibrium. These experiments were performed on hydrogen-oxygen-nitrogen flames, and the spectra of H_2O , and OH was recorded as a measurement of the effects of K, KO_2 , and preheat temperature.

EXPERIMENTAL APPARATUS

A schematic sketch of the opposed-jet burner and optical system arrangement used is shown in Figure 1. One half of the burner pair was utilized to vaporize the K° and KO_2 . The heated burner is shown in Figure 2. It was 2-inch diameter by 16-inch long, and made of schedule 40 cold-drawn pipe (pickled and annealed) of Inconel Alloy 600 for corrosion resistance at high temperatures. It was concentric at the heating end with an 8-inch long Coors mullite alumina tube (2.66-inch ID by 3.14-inch OD) bonded to it with Sauereisen Electric Heater Cement No. 6 Powder. Nichrome wire was wound around the periphery of the mullite tube and heated electrically. Power was supplied to heat the burner by a VWR Powerstat variable transformer with a 0 to 140 volt, 10 Amp output. The other end of the burner was cooled by water in a copper-tube coil heavily silver-soldered (solder thickness approximately one-half copper tube diameter) to the Inconel tube. Gases entering the cool end of the burner passed through a plenum chamber into the heated section packed with 990 grams of 1/16-inch Coors Type M mullite alumina balls held in place at both ends with stainless steel screening. The balls served two purposes - to provide a flat velocity profile needed to obtain the flat flame, and to hold the potassium additives in place in an evaporation boat while being vaporized and mixed with the other gases. The additive boat was 2.5 inches long by 0.5 inch wide, oriented with the long axis parallel to the tube axis, and located near the tube midplane between 3.5 and 6 inches on the thermocouple location scale. The boat temperature was assumed equal to that of the surrounding gas/packed bed. The exterior of the burner was insulated with a Nomex blanket. Thermocouples were used to measure the temperature of the gases in the vaporization section and at the exit of the burner. The thermocouples were Omega Chromel/Alumel type K in a 1/8-inch diameter, 12-inch long, shielded cable (cain-18E-12; shielded probe). Omega series 7000 analog pyrometers (7045-K-2000), provided the temperature indication for a range of 0 to 1100 degrees Celsius. The pyrometers were factory calibrated for ten ohms external thermocouple resistance and were provided with a

ten ohm calibrating resistor bobbin. Resistor bobbin calibration was performed in the laboratory on the assembled system.

The other half of the burner pair was similar in design but did not include the heating coils nor the cooling jacket. The packing in this burner was 3 mm Kimax glass beads. A 2.5-inch by 4-inch long schedule 80, AISI 316 stainless steel pipe nipple fitted on the gas inlet end with a 2.5-inch, AISI 316 stainless steel pipe was utilized. The outlet end was configured to provide a jet of gas of similar diameter to the jet of the opposing burner.

An external optical system was used to convert a Beckman 4240 IR spectrophotometer with a thermopile detector from absorption to emission measurements. A single-path mode was utilized. The optical system comprised front surface 2-in plane mirrors (one stationary, one adjustable) and a 6-in spherical mirror of $f/1.8$ (stationary) all from Oriel Optics. The mirrors were held in adjustable mounts on an optical bench and positioned by means of rod carriers. These permitted positioning of the burner and optics easily and reproducibly. The slit used was variable in width between 0.05 and 4 mm, and was 12 mm high. It was mounted on a translating base in the sample compartment of the spectrometer. Magnification of the image on the slit was 0.8. The flame image was focused on the spectrometer slit, and the flame scanned by translating the slit. The slit width in all the tests was 0.25 mm. Scans were made over seven increments of 0.637 mm starting at the flame edge. The spectrometer was capable of detecting spectra from the near-to the far-infrared. However, the most important effects were noted in the water-OH bands in the spectral region $3800 - 3000 \text{ cm}^{-1}$.

A conventional metering system incorporating calibrated rotameters, valves and tubing was used for introducing N_2 , O_2 , and H_2 into the burners. Brooks Instrument Model 1355-8506 Sho-Rate "150" flowmeters with R-6-15-A tubes were used to meter the fuel-side nitrogen and both oxygen and nitrogen on the air-side flows. Stainless steel floats were used to measure the fuel-side nitrogen and the air-side oxygen; a Carboloy float, for the air-side nitrogen. The maximum flow, expressed in liters per minute of air at STP, for the stainless steel floats was 16.4; for the carboloy

float, 23.0. A Matheson model 7631T flowmeter with a 603 tube and stainless steel float was used to meter the hydrogen gas flow to the fuel-side. The maximum flow for this unit was 19.5 liters per minute of hydrogen at STP. Flow meters were calibrated with a Curtin Matheson Scientific Precision Scientific wet test gas meter accurate to $\pm 0.5\%$. The flow system and burner arrangement provided the stable flat flame required to make measurements of the effects of the additives.

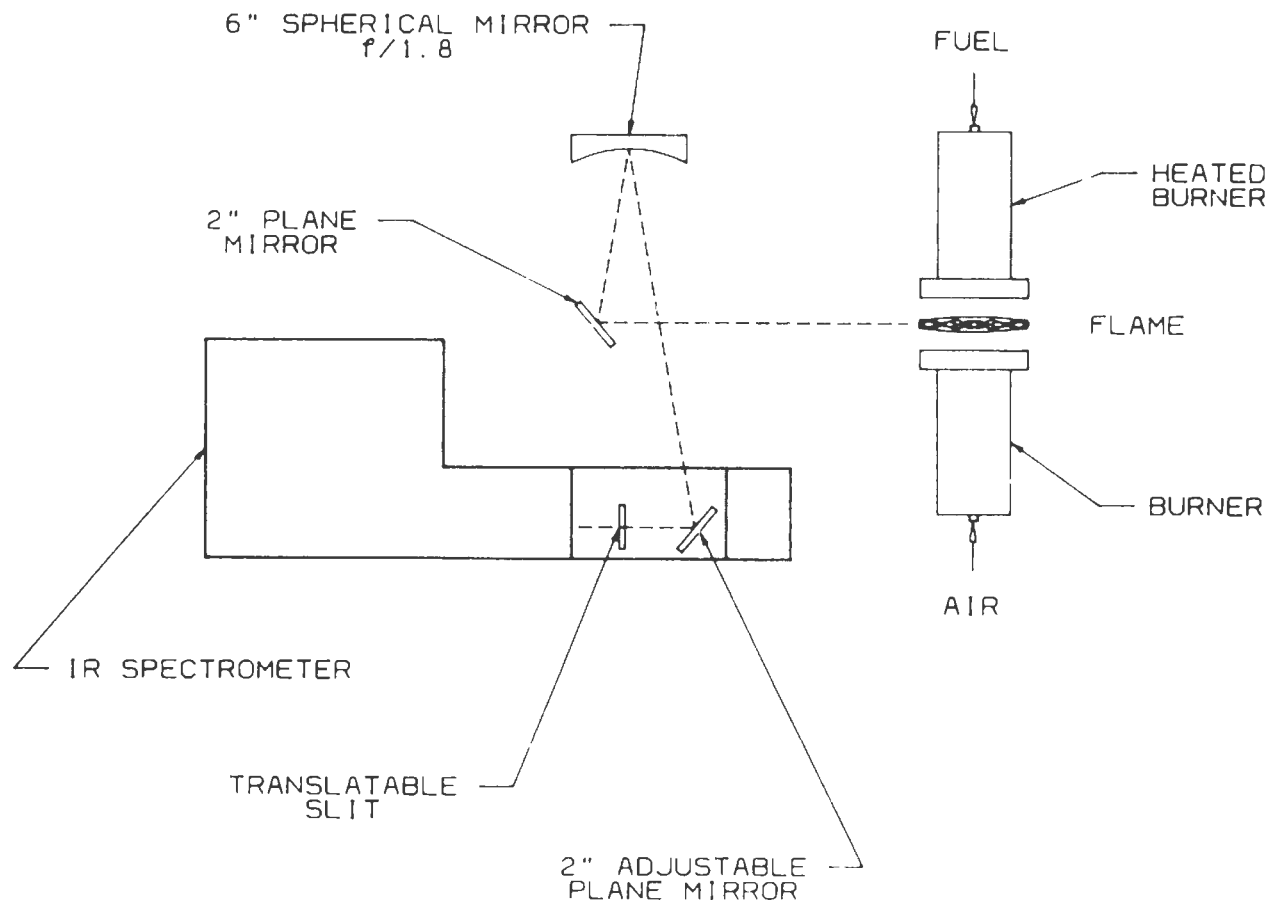


FIGURE 1. SCHEMATIC OF OPPOSED-JET BURNER & OPTICAL SYSTEM (TOP VIEW)

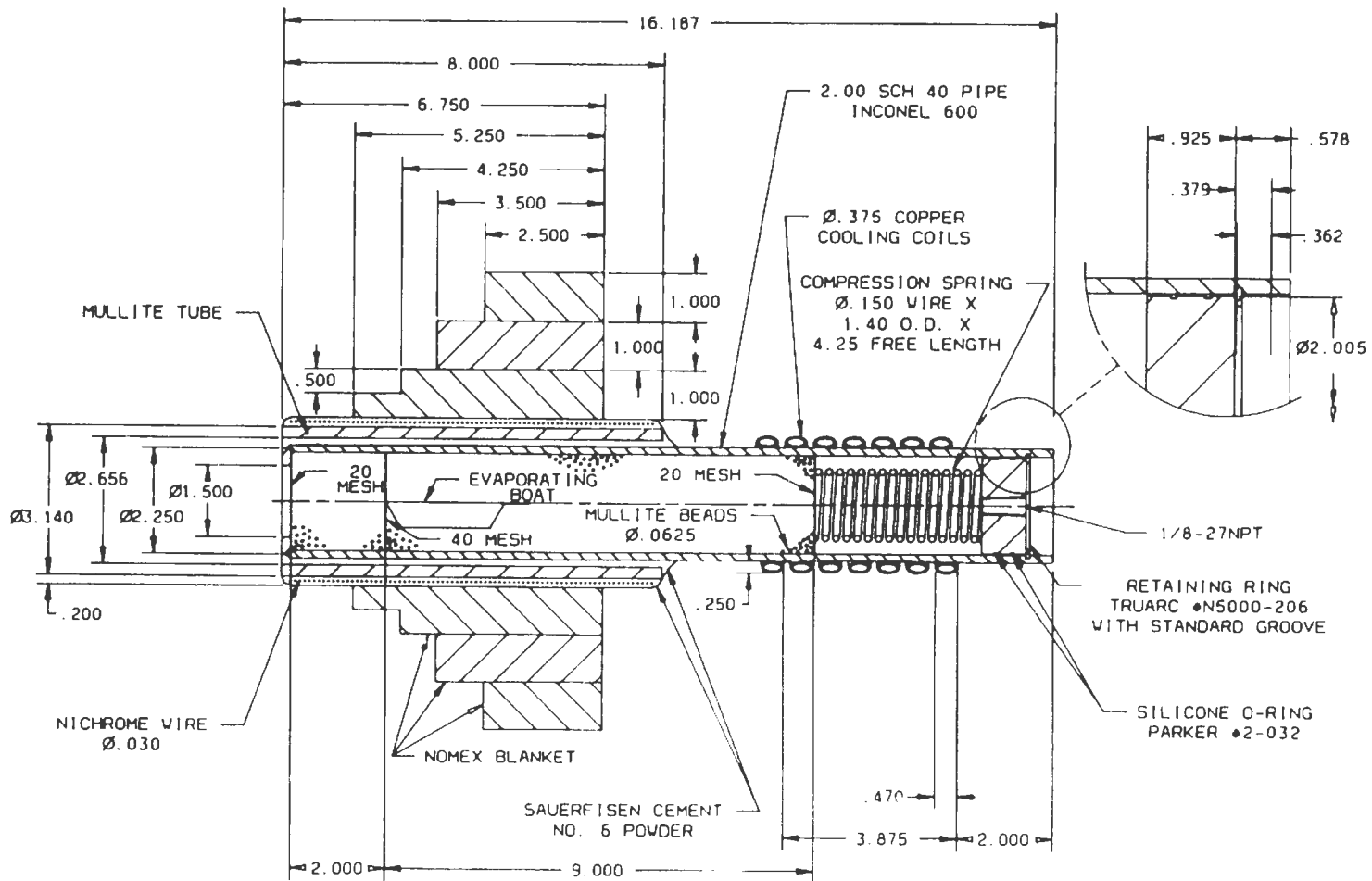
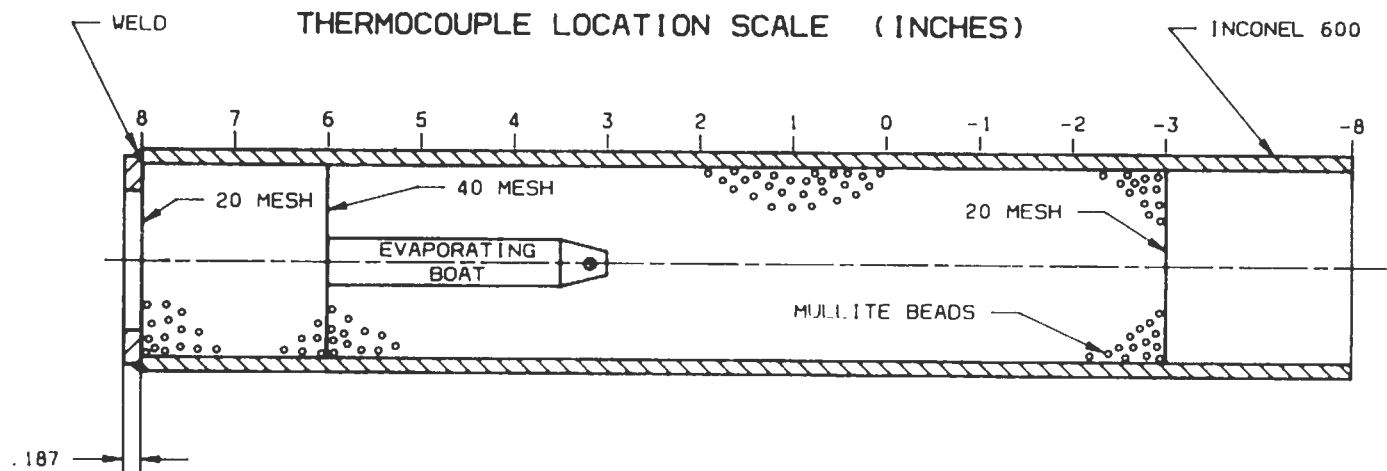


FIGURE 2. HEATED BURNER: FUEL SIDE FOR POTASSIUM ADDITIVE VAPORIZATION; AIR SIDE FOR POTASSIUM SUPEROXIDE ADDITIVE VAPORIZATION.

EXPERIMENTAL PROCEDURE

Once all systems were prepared (see Appendix 1 and Appendix 2 for details), the gas flows were established and the flame ignited. The temperature of the exit ends of the burners increased rapidly from ambient as heat was transferred from the flame to the burners. To maintain a uniform temperature distribution throughout the additive burner, heat was applied to the central portion of this burner. This insured that the bead-filled section had a uniform temperature over the additive area, and that the gases flowing through it were heated to temperatures close to the wall temperatures (See calculations in Appendix 4). Temperature distributions had to be known for additive and no-additive runs to separate thermal and chemical effects on the flame. The natural temperature increase of the exit end of the additive burner was asymptotic, approaching 300°C after two hours. The temperature rises approximately 3°C per minute initially, then rises more slowly as the maximum temperature is approached. The highest temperature rise rate utilized during experimental runs was generally about 2°C per minute. As the rise rate decreased to approximately 0.5°C per minute, use of a secondary heating element on the exit end of the burner was implemented. The combination of the two heating elements and flame heating were used to cover a range of "gas preheat" (or "burner exit", or "flame inlet") temperatures from 150° to 350°C.

The gas preheat temperature and additive temperature were determined by thermocouple measurements of the wall (Inconel 600 pipe) temperature at two locations on the burner. For the potassium additive experiments, the locations were 7.75" and 6"; for the potassium superoxide additive experiments, 8" and 5" (See Figure 2 for burner configuration and Figure 3 for thermocouple location scale). Sufficient heat transfer occurred within the packed bed of the burner to bring the gas temperature to within 5 degrees Celsius of the wall temperature at the locations measured. Calculations which justify this statement are included in Appendix 4.



NOTE: BURNER CONFIGURATION DEPICTED IS FOR "WITH ADDITIVE" CONDITION
 BURNER CONFIGURATION FOR "NO ADDITIVE" IS SAME WITH EXCEPTONS:

- A) NO EVAPORATING BOAT PRESENT
- B) 20 MESH SCREEN DEPICTED AT -3 ON THERMOCOUPLE
 LOCATION SCALE WOULD APPEAR AT -2.8 INCH (APPROX.)

FIGURE 3. BURNER WITH THERMOCOUPLE LOCATION SCALE (TOP VIEW - CROSS SECTION)

An initial scan was performed approximately 30 minutes after flame ignition. A scan consisted of eight individual determinations of flame emission intensity versus wavenumber (3800 to 3000 cm^{-1}), made at evenly-spaced increments from the flame edge, through the main reaction zone, to the opposite flame edge. An entire scan across the flame was accomplished in 8 minutes. Two minutes time between scans was allowed for temperature measurement and recording, and gas flow rate checks. Subsequent scans were conducted at progressively higher gas-preheat temperatures. The flame conditions (fuel to air ratio, temperature rise rate and actual temperatures) were the same for runs with or without additive. This ensured that the effect of the additive upon the flame was the only variable. Repetitive tests were made to verify reproducibility. For duplicate tests performed with this apparatus, reproducibility of $\pm 5\%$ in spectral intensity vs wave number and ± 5 degrees Celsius in temperature was demonstrated. The following table illustrates the capability of this system to reproduce a particular "temperature versus time" for duplicate tests. Experimental data from all the tests can be found in Appendix 5. As mentioned above, Appendices 1 and 2 have detailed information regarding apparatus and procedures.

	Run #1	Run #2
Time	Temperature**	Temperature**
(minutes)	(degrees C)	(degrees C)
0	120	120
11	155	155
21	175	180
31	200	205
41	220	225
51	230	240

** Temperatures recorded at 7.75 inches on thermocouple location scale; indicated temperatures were accurate to approx. $\pm 2.5^\circ\text{C}$ and were reported to the nearest multiple of five degrees Celsius.

EXPERIMENTAL RESULTS .

Since the H_2/N_2 or the N_2/O_2 gases were heated during vaporization of the K^o or KO_2 , it was necessary to establish first the intensity of radiation of the flame in the spectral range of interest as a function of temperature of the gases exiting the heated burner. Subsequently, the spectra were measured with additives in the flame.

A. N_2-H_2/O_2-N_2 flames, No additives:

Tests were conducted with the following compositions:

	<u>Flow, L per min</u>		
Fuel-	H_2 ,	5.2	
Side	N_2 ,	4.1	
Oxidizer-	N_2 ,	8.7	
side	O_2 ,	2.5	$\phi = 0.98$
		2.4	$\phi = 1.08$
		2.15	$\phi = 1.21$

The H_2/N_2 gas mixture was heated to a temperature ranging from 118°C to 350°C.

The oxidizer-side gases were at room temperature.

The results of the measurements are given in Figure 4 where the spectral area for the 3800 - 3000 cm^{-1} range in arbitrary units are plotted as a function of the burner exit gas temperature, i.e. the inlet fuel gas temperature to the flame zone. The lines correlating the data were derived by a least square fit with a standard error of estimate of 0.225 spectral area units.

For tests with KO_2 additive, the KO_2 was added to the oxygen-side of the flame to avoid decomposition of the KO_2 and reaction with H_2 in the heater. Therefore, an additional series of tests was made in which the N_2/O_2 gases were heated to a range of

temperatures from 190° to 313°C. In these tests the H₂/N₂ gases exited the burner tube at room temperature. These results are plotted in Figure 6. The standard error of estimate of the correlation is 0.049 spectral area units. The flame widths for these tests were approximately one scan interval less than when the fuel gases were heated.

B. N₂-H₂-K^o/O₂-N₂ Flames:

The vaporization temperature of the potassium was always lower than the burner exit temperature. The overall stoichiometric ratio, ϕ , burner gas exit temperature, potassium vaporization temperature, and the potassium concentration for the tests are given in Table 1. Figure 5 is a plot of the spectral area for the 3800 - 3000 cm⁻¹ range as a function of the inlet fuel gas temperature and ϕ . For clarity of presentation only the regression lines for no-addition are shown.

K^o depressed the combustion uniformly in the flame, i.e. there was no change in the width of the flame zone or the shape of the spectral area as a function of location. Spectral area was reduced at all ϕ values studied. Greater reductions were observed as ϕ was reduced.

C. N₂-H₂/N₂-O₂-KO₂ Flames:

Overall stoichiometric ratio, ϕ , burner gas exit temperature, and KO₂ vaporization temperature for this series are given in Table 2. Concentrations of KO₂ in the flame are unknown since vapor pressure data are unavailable. The results obtained for ϕ of 0.72 and 1.21 are given in Figure 7; the integrated spectral area for the 3800 - 3000 cm⁻¹ range is plotted as a function of inlet oxidizer gas temperature and ϕ . KO₂, as was the case with the K^o additive, depressed combustion uniformly throughout the flame. Greater reductions in spectral area also were observed for the lower ϕ 's.

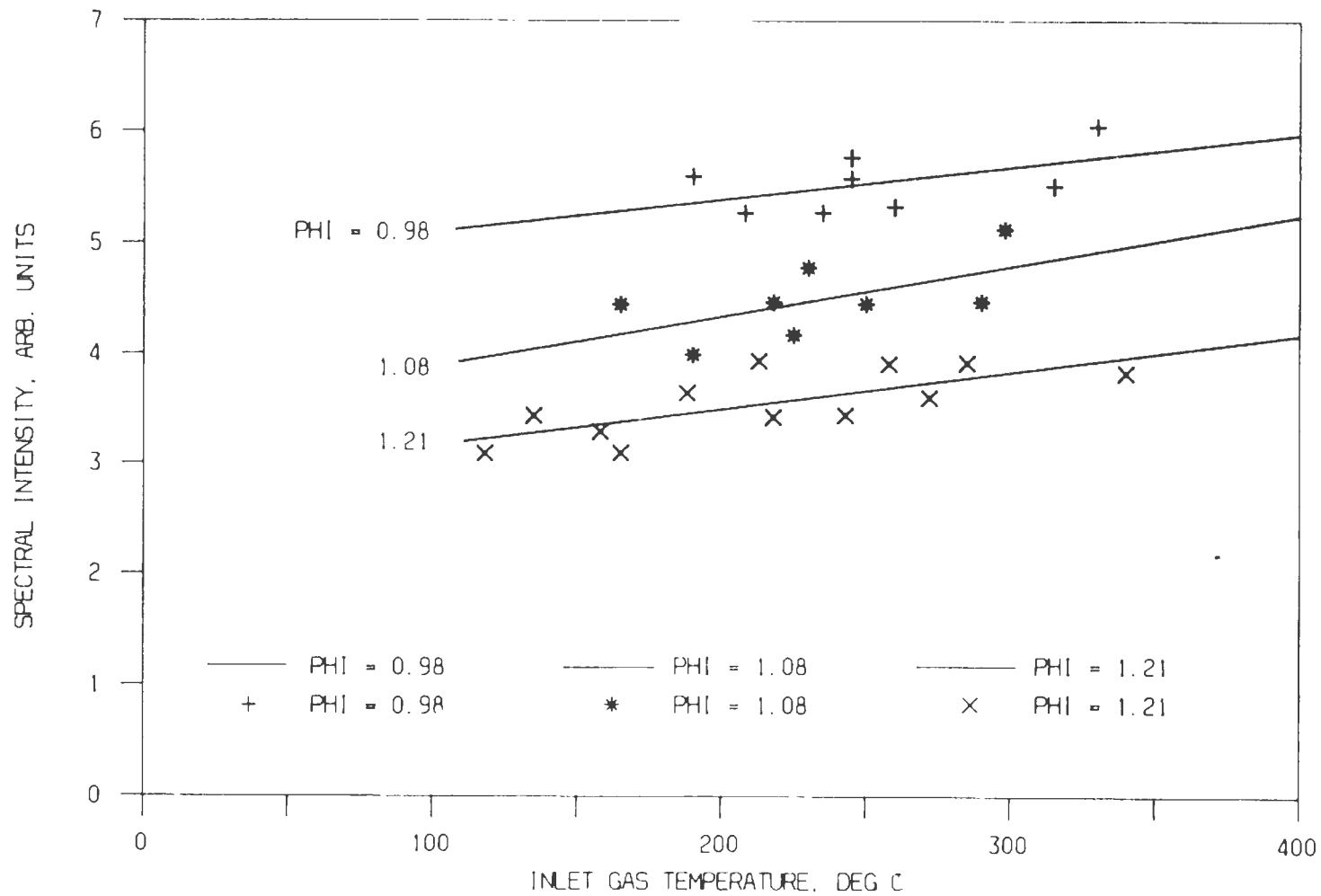


FIGURE 4. SPECTRAL INTENSITY VS. INLET FUEL GAS TEMP AND STOICH. RATIO, NO ADDITIVE 34

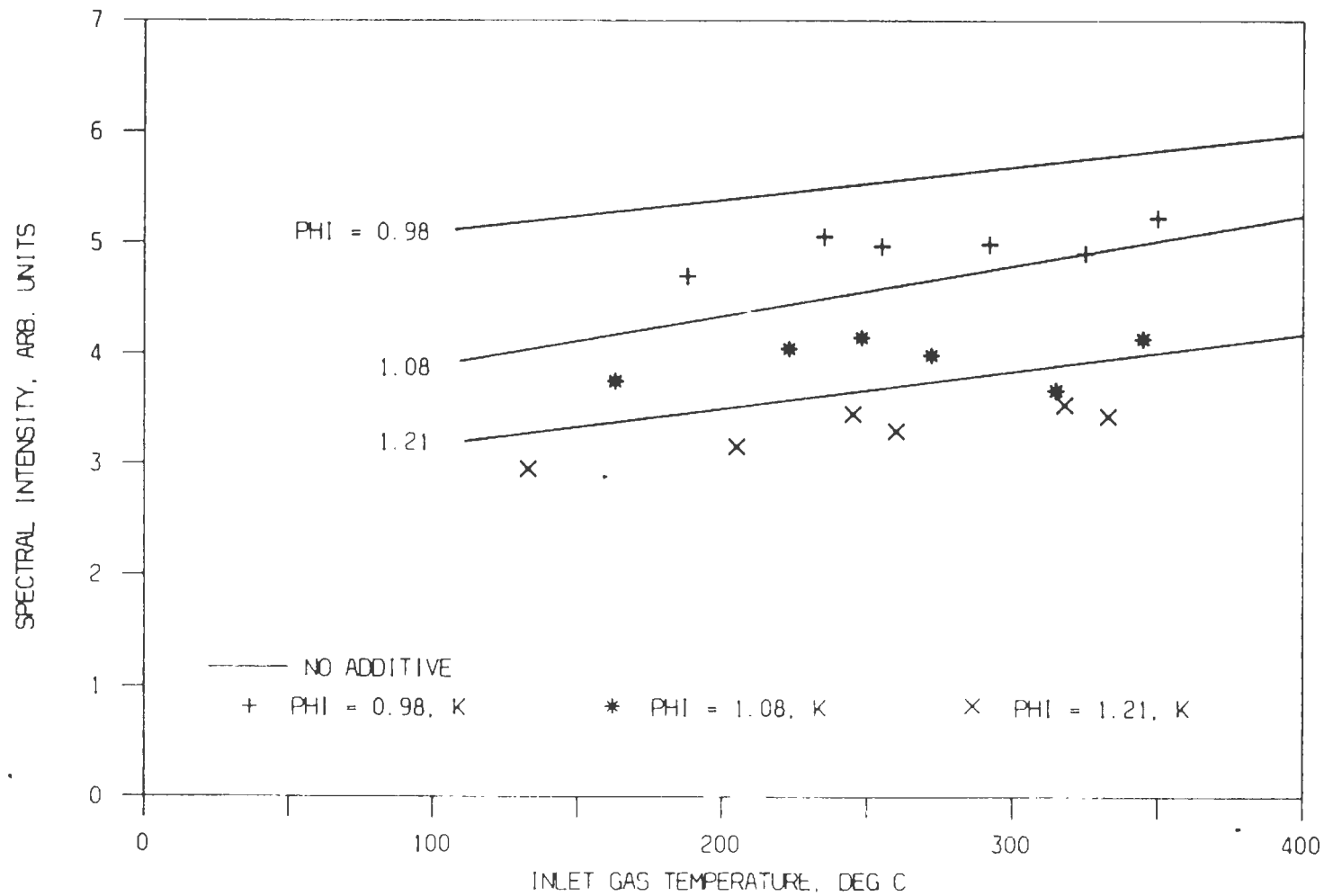


FIGURE 5. SPECTRAL INTENSITY VS. INLET FUEL GAS TEMP AND STOICH. RATIO, K ADDITION

TABLE 1

N₂-H₂-K^o/O₂-N₂ Test Conditions

ϕ	Gas Exit Temperature, Degree C	K ^o Vaporization Temperature, Degree C	K ^o Concentration, Molar ppm**
0.98	188	158	1.7
	235	218	27.7
	255	245	60.0
	292	282	292.3
	325	320	892.3
	350	343	1692.0
1.08	163	128	0.3
	223	205	16.9
	248	232	49.2
	272	270	200.9
	315	313	723.1
	345	335	1338.5
1.21	133	100	0.1
	205	185	6.8
	245	228	43.1
	260	255	115.4
	318	300	492.3
	333	328	1107.7

** Molar ppm = mole fraction x 10⁶

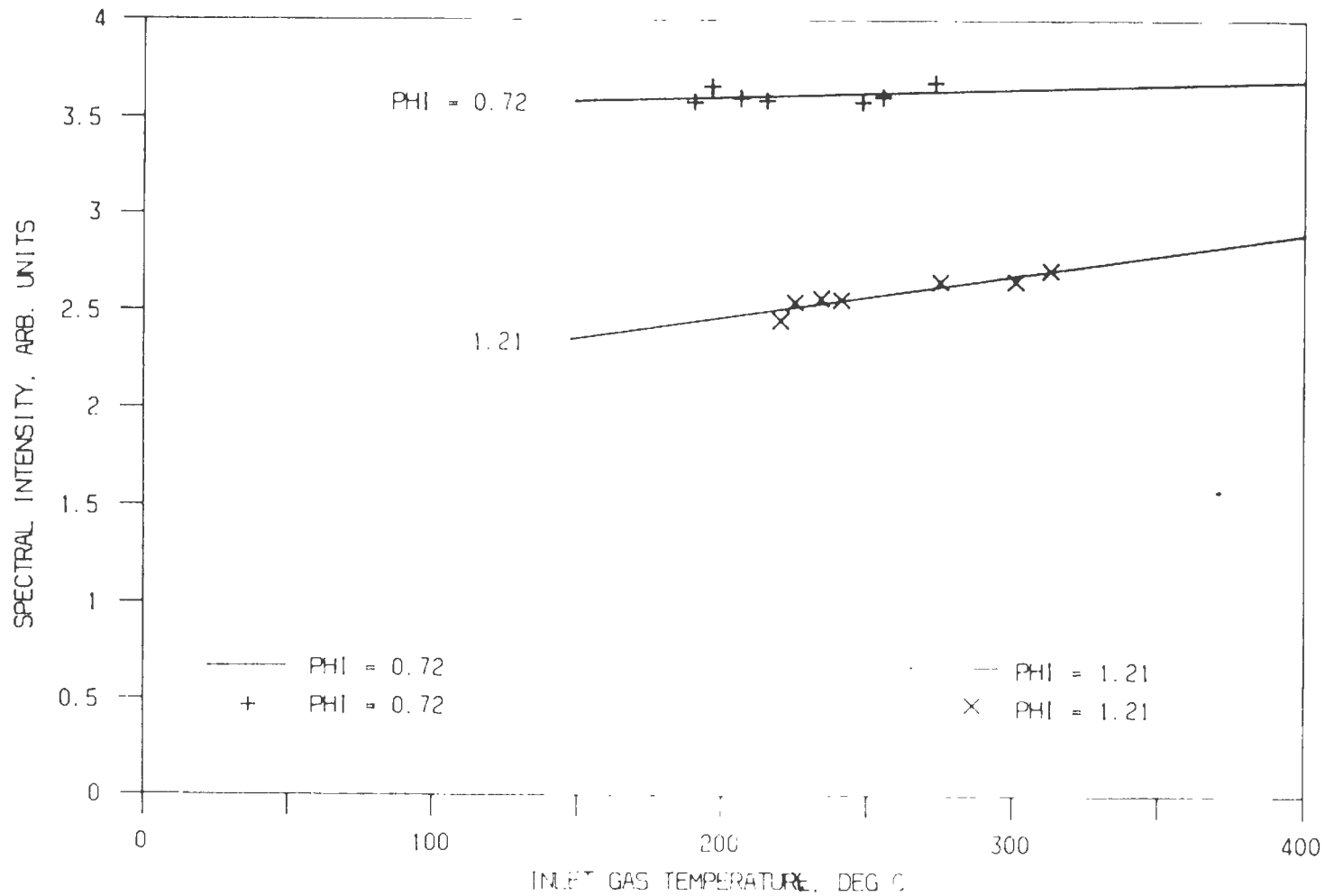


FIGURE 6. SPECTRAL INTENSITY VS. INLET OXIDIZER GAS TEMP AND STOICH. RATIO, NO ADDITIVE 37

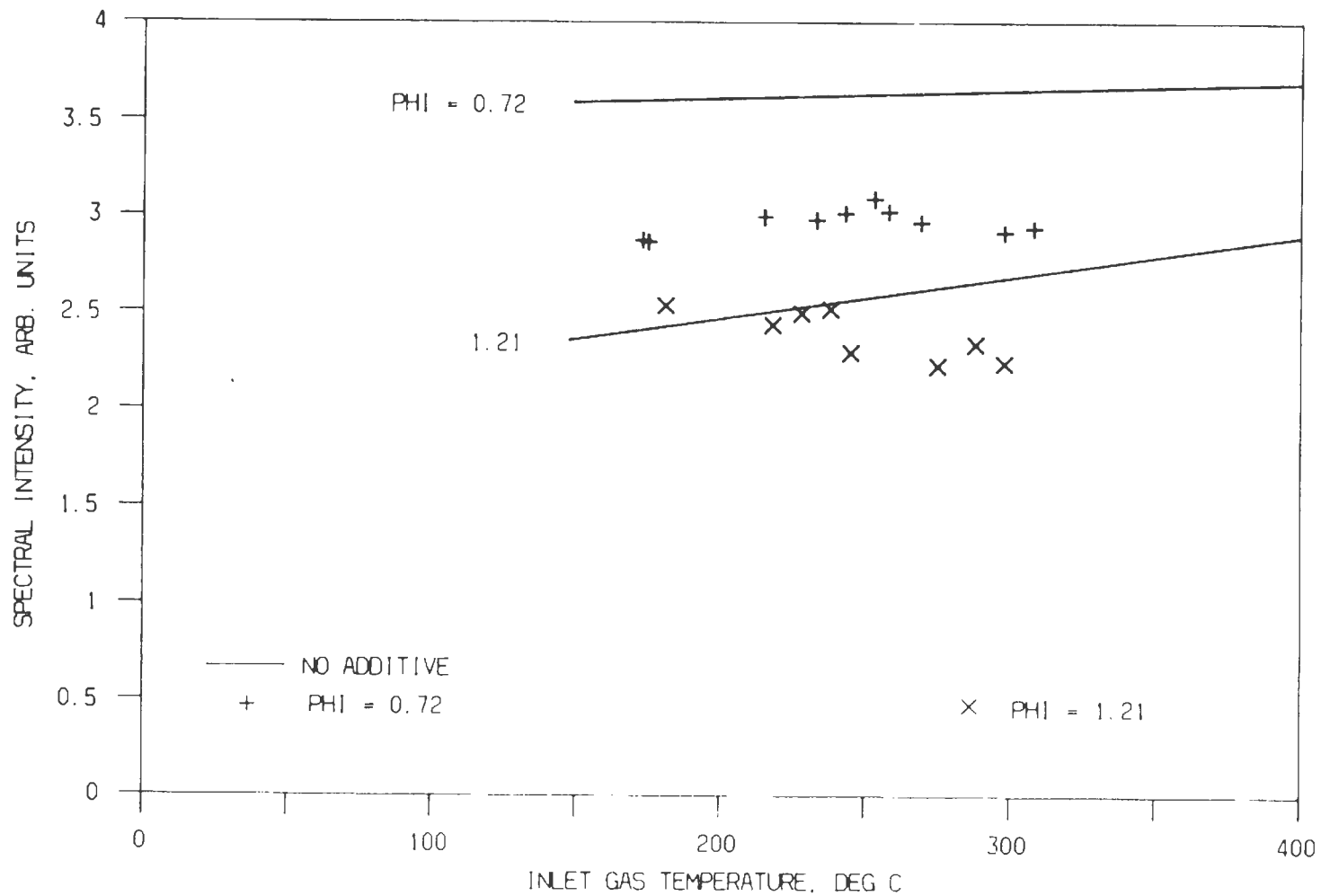


FIGURE 7. SPECTRAL INTENSITY VS. INLET OXIDIZER GAS TEMP AND STOICH. RATIO, KO_2 ADDITION

TABLE 2

N₂-H₂/O₂-N₂-KO₂ Test Conditions

ϕ	Gas Exit Temperature, Degree C	KO ₂ Vaporization Temperature, Degree C
0.72	173	83
	173	88
	215	115
	233	128
	243	138
	253	153
	258	168
	269	179
	298	198
	308	208
1.21	181	108
	218	123
	228	133
	238	143
	245	148
	275	175
	298	200
	298	213

DISCUSSION

The reaction rate coefficients of equations (1) through (10) for both the forward and reverse reactions, taken from references 4, and 7, are given in Table 3 for temperatures of 1000 and 2000 K. The kinetic coefficients for equation (10), the reaction of $K^\circ + O_2 + M$ were increased by three orders of magnitude, in conformance with the more recent results reported by references 8 and 9. The reaction rate coefficients, considered together with concentration of the reactants, give some insight into the relative importance of the flame reactions taking place. The reaction numbers referred to in what follows are taken from Table 3.

A. N_2-H_2/N_2-O_2 Flames - No Additives:

As the overall stoichiometric ratio is reduced, and the flame becomes leaner, the increased O_2 and O concentration should drive reactions (1), (4), and the reverse reaction of (5) to produce more OH radicals. This is what was observed, as shown in figures 4 and 6. At a ϕ of 1.21, less OH was developed when the O_2-N_2 gases were preheated than when the H_2-N_2 gases were preheated. This suggests that the reverse reaction of (1) is more important when the O_2-N_2 are preheated.

B. $N_2-H_2-K^\circ/N_2-O_2$ Flames:

K° inhibits the formation of OH and water in the range of ϕ between 0.98 and 1.21, even at low concentrations of K° vapor. Since OH concentrations in the flame are higher at the lower values of ϕ , the observed larger quenching effects of K° under these conditions may only be relative to these larger concentrations.

Friedman and Levy argue that reaction (6) for K° is too slow to be significant in the inhibition reactions. The inhibition by K° may indeed be through a KOH mechanism, as they propose, but possibly by a different path. The reverse reaction of K° with H_2O to produce $KOH + H$, equation (7), the subsequent reactions of $KOH + OH$ to KO_2 and H by equation (10), and $KO_2 + OH$ to KOH and O_2 by equation (9) would be rapid enough to

explain the inhibition by K° . This argument is supported by an examination of the magnitudes of the reaction rate constants in Table 3. This path is more likely than their proposal of the formation of solid K_2O , its vaporization, and reaction with water to form KOH. It is not clear why K° did not inhibit in the Friedman and Levy experiments. They also used an opposed diffusion flame but at a much larger ϕ value, about 3.5. Perhaps, their flame had a higher concentration of H which would inhibit the reverse reaction (7) - effectively preventing inhibition by the K° . Further, their use of flame strength, i.e. the flow rate of air to methane at which a hole appears on the flame axis, may not be a sensitive enough measure of the effect of K° .

C. $N_2-H_2/N_2-O_2-KO_2$ Flames:

KO_2 is relatively stable, that is its decomposition reaction rate constant becomes comparable to the reactions of KO_2 with OH and H_2 at higher temperatures well into the flame zone. At the flame edge, KO_2 is available to react with the OH and H to quench the hydrogen chain reaction. In the lean flame studied, at an ϕ of 0.72, the forward reaction rate of reaction (9) dominates in the removal of OH, augmented further into the flame zone by the decomposition of KO_2 to K° by equation (8) and the further reactions of K to deplete OH. For the richer ϕ of 1.21, there is competition between the depletion of OH by equation (9) and its formation by equation (10). At lower KO_2 concentrations, at $\phi = 1.21$, and lower burner exit gas temperatures, KO_2 is not effective in inhibition.

The experimental conclusions do not support Jensen and Jones⁷ computations that KO_2 promotes the combustion of hydrogen. In their paper, however, they acknowledged a need for more precise characterization of the KO_2 reactions. The more recent experimental results of Hussain and Plane⁸ and Silver et al⁹ indicate the forward reaction coefficient of $K^\circ + O_2 + M$ to be three orders of magnitude larger than the value used by Jensen and Jones.

Jensen⁶ also took exception to Kaskan's hypothesis⁵ that KO_2 was important in the inhibition of lean hydrogen premixed flames. The present studies support Kaskan's argument that KO_2 could be important in such flames.

TABLE 3

Fluorine Chemical Reactions and Rate Coefficients**

Eq. No.	Reaction	Forward Rate Coef. 1000 K	Forward Rate Coef. 2000 K	Reverse Rate Coef. 1000 K	Reverse Rate Coef. 2000 K
(1)	$H + O_2 \rightleftharpoons OH + O$	6.3×10^{-14}	3.9×10^{-12}	1.4×10^{-11}	1.7×10^{-11}
(2)	$H + OH + M \rightleftharpoons HOH + M^*$	1.5×10^{-31}	3.8×10^{-32}	8.0×10^{-33}	2.2×10^{-20}
(3)	$OH + H_2 \rightleftharpoons HOH + H$	2.4×10^{-12}	1.5×10^{-11}	5.7×10^{-15}	1.5×10^{-12}
(4)	$O + H_2 \rightleftharpoons OH + H$	3.4×10^{-13}	6.4×10^{-12}	4.2×10^{-19}	5.8×10^{-22}
(5)	$OH + OH \rightleftharpoons HOH + O$	5.8×10^{-12}	7.6×10^{-12}	1.1×10^{-14}	1.0×10^{-12}
(6)	$K^{\circ} + OH + M \rightleftharpoons KOH + M^*$	1.5×10^{-30}	7.5×10^{-31}	8.1×10^{-22}	7.1×10^{-13}
(7)	$KOH + H \rightleftharpoons K^{\circ} + HOH$	6.6×10^{-12}	1.1×10^{-11}	1.0×10^{-18}	2.3×10^{-14}
(8)	$K^{\circ} + O_2 + M \rightleftharpoons KO_2 + M^*$	3.0×10^{-30}	1.5×10^{-30}	9.6×10^{-17}	1.8×10^{-10}
(9)	$KO_2 + OH \rightleftharpoons KOH + O_2$	2.0×10^{-11}	2.0×10^{-11}	2.4×10^{-15}	1.7×10^{-13}
(10)	$KO_2 + H_2 \rightleftharpoons KOH + OH$	1.4×10^{-16}	2.0×10^{-14}	5.0×10^{-18}	5.7×10^{-16}

**Bimolecular rate coefficients in units of ml-molecule⁻¹-second⁻¹; termolecular rate coefficients in ml²-molecule⁻²-second⁻¹.

CONCLUSIONS

Both additives, K° and KO_2 inhibit afterburning of hydrogen, the magnitude of the observed effects depending on the overall mixture ratio in the diffusion flame. K° inhibits afterburning for rich ($\phi = 1.21$) and near-stoichiometric mixtures ($\phi = 0.98-1.08$). KO_2 is effective, even at low concentrations, at a lean mixture, $\phi = 0.72$, and at higher concentrations for $\phi = 1.21$. While K° and KO_2 appear to be more effective for leaner mixtures, the observed greater reduction in the spectral intensity may be a consequence of the larger concentrations of OH for the lean mixtures.

The present research confirms the Jensen, Jones and Mace conclusion that potassium is effective as an after burning inhibitor for hydrogen premixed flames. It is not clear why Friedman and Levy observed no effect when potassium was added to their methane-air diffusion flames. Further, the present results support Kaskan's proposed mechanism of inhibition by KO_2 . They are not in agreement with the Jensen & Jones computer prediction of enhancement of afterburning by KO_2 . The latter computations were completed, however, before the experimental data of references 8 and 9 were available, which gave improved rate constant values.

REFERENCES

- (1) Hahn, W. A., Wendt, J.O.L., and Tyson, T. J., "Analysis of the Flat Laminar Opposed Jet Diffusion Flame with Finite Rate Detailed Chemical Kinetics," Combustion Science and Technology Vol. 27, 1981, pp. 1-17
- (2) Jensen, D. E., Jones, G. A., and Mace, A. C. H., "Flame Inhibition by Potassium," J. Chem. Soc. Faraday Trans. 1, Vol. 75, 1979, pp. 2377-2385
- (3) Friedman, R., and Levy, J. B., "Inhibition of Opposed-Jet Methane-Air Diffusion Flames. The effects of Alkali Metal Vapors and Organic Halides," Combustion and Flame Vol. 7, 1963, pp. 195-291
- (4) Jensen, D. E., and Jones, G. A., "Reaction Rate Coefficients for Flame Calculations," Combustion and Flame Vol. 32, 1978, pp. 1-34
- (5) Kaskan, W. E., "The Reaction of Alkali Atoms in Lean Flames," *10th Symposium (International) on Combustion*, The Combustion Institute, 1965, pp.41-46
- (6) Jensen, D. E., "Alkali-metal Compounds in Oxygen-rich Flames: A Reinterpretation of Experimental Results," J. Chem. Soc. Faraday Trans., 1982, pp. 2835-2842
- (7) Jensen, D. E., and Jones, G. A., "Theoretical Aspects of Secondary Combustion in Rocket Exhausts," Combustion and Flame, Vol 41, 1981, pp. 71-85
- (8) Hussain, D., and Plane, J. M. C., "Kinetic Investigation of the Third-order Rate Processes between $K + O_2 + M$ by Time-resolved Atomic Resonance Absorption Spectroscopy," J. Chem. Soc. Faraday Trans 2, Vol. 78, 1982, pp. 1175-1194
- (9) Silver, J. A., Zahnesir, M. S., Starton, A.C., and Kolb, C. E., "Temperature Dependent Termolecular Reaction Rate Constants," *20th Symposium (International) on Combustion*, The Combustion Institute, 1984, pp. 605-612

- (10) Gaydon, A. G., Flames - Their Structure, Radiation, and Temperature, Chapman and Hall, 4th Ed., 1979
- (11) Potter, A. E. and Butler, J. N., J. Amer. Rocket Soc., Vol. 29, 1959, pp. 54-56; and Potter, A. E., Heimel, S. and Butler, J. N., Eighth Symposium (International) on Combustion, pp. 1027-34, Williams and Wilkins: Baltimore, 1962
- (12) Engleman, V. S. (1978). "Survey and evaluation of kinetic data on reactions in methane/air combustion," U.S. Environmental Protection Agency, Office of Research and Development, Washington, D.C. Environmental Protection Technology Series, Publ.No. EPA-600/2-76-003
- (13) Rosser, Jr, W. A., Wise, H. and Miller, J.; Seventh Symposium (International) on Combustion, pp 175-182. Butterworths: London, 1959
- (14) Singh, T. S., Weaver, D. P., and Eversole, J. D.; Afterburning Suppression Kinetics, AFRL-TR-87-001, Air Force Rocket Propulsion Laboratory, Edwards Air Force Base, Calif., 1987
- (15) Weaver, D. P. and Singh, T.; Kinetic Mechanisms for Ionization and Afterburning Suppression, AFAL-TR-87-049, Air Force Astronautics Laboratory, Edwards Air Force Base, Calif., 1987
- (16) Coffee, T. P., and Heimerl, J. M., Sensitivity Analysis for Premixed, Laminar, Steady-State Flames, ARBRL-TR-02457, U.S. Army Ballistic Research Laboratory, Aberdeen Proving Ground, MD, 1983
- (17) Kee, R. J., Grcar, J. F., Smooke, M. D., and Miller, J. A., "A Fortran Program for Modeling Steady Laminar One-Dimensional Premixed Flames," Sandia Report SAND85-8240, 1985
- (18) Dixon-Lewis, G., "Kinetic Mechanism, Structure, and Properties of Premixed Flames in Hydrogen-Oxygen-Nitrogen Mixtures," Proceedings, Royal Soc. of London, Vol. 292, 1979, pp. 45-99
- (19) Eversole, J. D., and Singh, T., "Suppression in Premixed $H_2/O_2/N_2$ Laminar Flames," Western States Section, Combustion Institute Meeting, Paper No. WSS/CI/84-52, 1982
- (20) Dixon-Lewis, G., "Mechanisms of Inhibition of Hydrogen-Air Flames by HBr and Its

- Relevance to the General Problem of Flame Inhibition," Combustion and Flame, Vol.36, 1979, pp. 1-14
- (21) Dixon-Lewis, G., and Simpson, R., "Aspects of Flame Inhibition by Halogen Compounds," *16th Symposium (International) on Combustion*, The Combustion Institute, 1976, p. 1111
- (22) Westbrook, Charles K., "Inhibition of Hydrocarbon Oxidation in Laminar Flames and Detonations by Halogenated Compounds," *19th Symposium (International) on Combustion*, The Combustion Institute, 1982, pp. 127-141
- (23) Westbrook, Charles, K., "Flame Inhibition by CF_3Br ," Preprint UCRL-88180, Lawrence Livermore National Laboratory, Livermore, CA, 1982
- (24) Mitani, Tohru, Niloka, and Takashi, "Extinction Phenomenon of Premixed Flames with Alkali Metal Compounds," Combustion and Flame, Vol. 55, 1984, pp. 13-21
- (25) Hynes, J. A., Steinberg, M., and Schofield, K., "The Chemical Kinetics and Thermodynamics of Sodium Species in Oxygen-Rich Hydrogen Flames," J. Chem. Phys., Vol. 80, 1984, pp. 2565-2597
- (26) Gaydon, A. G., The Spectroscopy of Flames, 2nd Edition, Chapman and Hall, London, 1974, pp. 103, 110, 122

APPENDIX 1 Previous research with experimental detail included.

Friedman and Levy³ investigated the effect of sodium and potassium metal vapors on opposed-jet methane/air diffusion flames (1963). They found that neither of these two were effective inhibitors, as judged by the criterion of "flame strength", described below. They also investigated the effects of organic halides on similar flames and found these to be effective. Friedman and Levy utilized an opposed-jet technique that had been developed by A. E. Potter et al.¹¹ for studying diffusion flames in which the parameter measuring the stability of the flame, the flame strength, was defined. Since the opposed-jet technique had not previously been applied to a study of the flame inhibition, Friedman and Levy found it prudent to perform preliminary experiments with known gaseous inhibitors, i.e. organic halides, before investigating the alkali metal vapors. Previous research had demonstrated inhibition of premixed methane flames by the same organic halides.

Their experimental technique involved the observation of a hole formation in the central region of a flat, circular diffusion flame between the opposing gas jets. The methane, air, and gaseous additives were metered by calibrated critical-flow orifices and accurate 0 to 200 lb/sq.in. Heise pressure gages. Sodium and potassium vapors were metered by bubbling the methane stream through the molten metal additive in a nickel saturator device. The saturator and feed lines were immersed in a fused-salt bath operated at temperatures up to nearly 773 Kelvin. The burner consisted of opposed coaxial vertical tubes of 3.86 mm bore and variable separation (typically about 1 cm). The lower fuel jet was mounted in a copper block not quite entirely submerged in the bath. Thermocouple probing indicated that the effluent gas was essentially at the bath temperature. The upper tube, carrying a downward flow of air, was jacketed with water at approximately 338 Kelvin, reportedly to provide a constant temperature while avoiding

condensation from the flame. The flame was shielded from drafts with a metal sleeve having a replaceable Pyrex window consisting of a microscope slide. Frequent replacement of the window was found necessary due to a solid deposit formed during the experiments with alkali metal addition. They found the mass ratio of air to methane for satisfactory flames to be about 2.7 both when the methane was at room temperature and when the methane was at about 733 Kelvin. Potter et al. described how, if the flame is maintained centered between the two jets while the flows are progressively increased, a hole appears on the flame axis at a reproducible flow rate, enlarges if the flows are increased, and disappears again if the flows are reduced. Friedman and Levy used the criterion of first detectable appearance of a hole as the measure of "flame strength". They made comparisons of hole-point fuel flow rate with and without inhibitor at constant burner geometry. It appears from their paper that the air flow rate was varied in a manner to some extent independently of the flow rate of fuel, thus varying the fuel-to-air ratio.

With methyl bromide as the fuel additive, Friedman and Levy found the flow rate of fuel for hole-point at room temperature to be approximately 78% of that for no additive and at 733 Kelvin found it to be approximately 85%. In both cases the methyl bromide concentration was 10 mole percent of the fuel flow. No change in fuel flow rate for hole formation was noted for sodium concentrations up to 0.26 mole percent. Likewise, no change in fuel flow rate for hole formation was noted for potassium concentrations up to as high as 3.5 mole percent.

Friedman and Levy concluded, based on this evidence, that there was lack of any inhibitory effect by elementary potassium [or sodium] introduced into the fuel side of a methane-air diffusion flame at concentrations comparable to those at which bromine inhibitors exert easily measurable effects in the same apparatus. This behavior must be contrasted with that reported for potassium salts in premixed flames, which are at least as potent in reducing burning velocity as bromine inhibitors. They state that "We therefore conclude that the known inhibitory effects of alkali metal salts must arise from species other than the alkali metal atoms and we propose that the effective

species is the gaseous alkali metal hydroxide." Based upon kinetic data available at the time, their calculations indicated that three-body reactions of potassium metal with H, OH, and O at atmospheric pressure would be several orders of magnitude slower than any competing two-body reactions of very low activation energy. Therefore



could not occur early enough in the flame to affect the propagation. Instead they suggested that potassium salts are decomposed to molten K_2O which reacts with water to form $2KOH$. KOH then reacts to scavenge radicals by such means as



In their discussion Friedman and Levy state that "Even though the inhibitor potassium hydroxide does not regenerate itself by the proposed sequence, the concentration of inhibitor necessary to be effective is comparable with the concentrations of H and OH in the equilibrium products, and a single functioning of each inhibitor molecule may be quite adequate for the observed effects." Thus the thermal decomposition of potassium carbonate, for instance, to potassium oxide, followed by reaction with water to potassium hydroxide, and then reaction with the H or OH radical to form K° or KO, respectively, was predicted to proceed at a rate "several orders of magnitude" more quickly than the three-body reaction of elemental potassium and OH to form KOH.

Walter E. Kaskan⁵ (1965) investigated the reaction of alkali atoms in lean premixed $H_2/O_2/N_2$ flames. It had been proposed by other researchers that the major equilibrium reaction of alkali metals in these H_2 /air premixed flames was:



Kaskan's results did not indicate this to be correct and he suggested that the appropriate reaction

was



He also suggested that there was an analogy between this reaction and that for forming HO_2 . Most of the previous work was done on fuel rich or near-stoichiometric H_2 /air flames.

His experimental apparatus consisted of a gas-handling system and a cooled porous metal burner providing a flat flame three inches in diameter, surrounded by an annular shield flame 0.5 inch wide. Solutions of either sodium chloride or potassium chloride were introduced into the inner flame through an atomizer. The burner was moveable in the vertical direction. The optical system, consisting of sources, mirrors, and a monochromator with photoelectric recording, providing a narrow beam of probing light. The beam passed over the burner parallel to its surface and perpendicular to the flow. The spatial resolution was reported to be approximately 1 mm. Hydrogen atom concentrations were determined by a method which correlates $[H]$ to the intensity of the Lithium resonance line. OH , Na° , and K° concentrations were determined by photometric methods. The sources were a discharge in water vapor for OH measurement, and a tungsten-strip filament lamp for alkali-atom measurements. Alkali atoms were determined by resonance-line absorption, employing the Na° 5889, 5896 doublet, and the K° 7665, 7699 doublet. Flame gas temperatures were generally measured with silica-coated thermocouples, and occasionally were checked by a Na° -reversal measurement.

The procedure followed consisted of burning various lean H_2 /air flames and following the absorption of both OH and alkali atoms as a function of distance from the burner. In all of the flames studied both the concentrations of OH and Na° or K° decreased with increasing distance from the burner. The rate of decrease of both OH and the alkali atoms was faster the leaner the flame, but more so for alkali atoms. Most runs were made in duplicate. The first flame was a lean H_2 /air flame which provided an observable, but relatively slow, decay of alkali, and the second would differ only in that a small amount of O_2 was added to speed up the decay.

The rates of decay were shown to be independent of alkali atom concentration, indicating that the observed effects were first order in alkali atoms. If, as proposed by the previous researchers, the main reaction was



it was shown that the relation of $[A]$ to $[OH]$ should be cubic in $[OH]$. However the plot of $\log [A]/([A]_{tot}-[A])$ against $\log [OH]$ was linear, but had a slope of 2, not 3. The remainder of the analysis suggested the data are better interpreted by assuming the reaction responsible for alkali atom concentration decay is :



In 1978, D. E. Jensen and G. A. Jones published "Reaction Rate Coefficients for Flame Calculations" which contained an updated list of recommended rate coefficients for chemical reactions occurring in flames. The rate coefficients were expressed as functions of temperature for the range $1000 < T < 3000$ Kelvin, and were either taken from experiments described in the scientific literature or estimated by comparison with rate coefficients for analogous reactions. An estimate of the uncertainties of the values listed was also included, as were reaction equilibrium constants as functions of temperature. An emphasis was placed on reactions of metal derivatives.

They note two particularly difficult points in the description of the chemical kinetics in the case of reactions involving "third bodies" or "collision partners" - typically denoted "M". The first is that different third bodies have different efficiencies in these reactions. The list gives rate coefficients averaged for the more effective third bodies such as CO_2 , H_2O , and N_2 , present in typical flames. The concentration $[M]$ is taken as the sum of concentrations of all gas phase species present. A second difficulty is that the third body reactions (and their reverse reactions) actually take place via stepwise processes involving excited molecular or atomic states, vibrational and electronic. They additionally state that the "collision frequencies" to which kineticists often refer

rate coefficients are generally those calculated on the assumption that all chemical species are in ground electronic, vibrational, and rotational states, and that this common usage is "sometimes rather misleading".

In the following year (1979) D. E. Jensen, G. A. Jones, and A. C. H. Mace² published the results of an investigation of fuel-rich, premixed H₂/O₂-N₂ flames with a potassium compound additive. They hoped to test the validity of the proposed reaction scheme for recombination of H and OH radicals in the flames



and



In addition they hoped to derive more accurate rate coefficients for the forward and reverse reactions of these two. Upon publication of their previous list of rate coefficients it was clear that the values presently accepted were only "order-of-magnitude estimates based on flame experiments not specifically designed for kinetic measurements". The previously reported values for these two forward reactions were $4 \cdot 10^{-12} \exp(-1000/T) \text{ cm}^3 \text{ molecule}^{-1} \text{ sec}^{-1}$ and $6 \cdot 10^{-28} T^{-1} \text{ cm}^6 \text{ molecule}^{-2} \text{ sec}^{-1}$, respectively. The more accurate values which they provide in this work are $1.8 \cdot 10^{-11} \exp(-1000/T)$ and $1.5 \cdot 10^{-27} T^{-1}$ respectively.

The flames used were atmospheric-pressure, laminar, shielded, cylindrical, premixed, fuel-rich H₂ + O₂ + N₂ flames in which the distance above (downstream of) the primary reaction zones was a linear measure of reaction time available for recombination of the free radicals produced in above-equilibrium amounts in these zones. The authors state that under the conditions of this work, the only flame radicals present in significant quantities were H and OH, with the concentrations of other species such as O and HO₂ being extremely low. Calculations based on JANAF Thermochemical Tables (1971) and supplemented for such species as K[•] and KO₂ by

kinetic data from their list of rate coefficients of the previous year suggested that no potassium-containing species other than K° and KOH would be formed in the flames used at concentrations high enough to contribute significantly either to reaction rates or to the total potassium concentration. Therefore they assumed that $[K]_{TOTAL} = [K] + [KOH]$.

Potassium was added to the flame as potassium dipivaloylmethane in the form of vapor from a supply reservoir. Deposition of additive in the supply system and burner was minimized by the heating of both. Photometric determinations of $[H]$ and $[K]$ were performed on the flame. $[OH]$ and $[KOH]$ were calculated assuming that $[H]$ and $[OH]$ were related by



and that $[K]$ and $[KOH]$ were in equilibrium through



For the purposes of these determinations, potassium was first supplied to the flames at known concentrations from a calibrated atomizer and the curve of growth of the integrated emission intensity of the 766.5 nm wavelength potassium resonance line, against $[K]$ was constructed using the above relations. Hydrogen atom concentrations were measured by the Li°/Na° comparison method, lithium and sodium being supplied in known proportions from the atomizer.

In tests of similar flames with and without potassium additive it was seen that potassium accelerated the rate of hydrogen atom removal and that the fraction of the recombination due to the presence of the potassium is proportional to the total concentration of potassium, which they claim is consistent with a homogenous acceleration process. The researchers tabulated the rate coefficients derived from this work for both the forward and reverse directions and state that the values obtained are consistent with earlier thermochemical studies of K° and KOH in flames. They further conclude that the mechanism for flame radical removal consisting of the reactions mentioned above is cyclic; the observed decreases in $[H]$ and $[OH]$ caused by addition of

potassium exceed $[K]_{total}$, which implies that K° and KOH must be successively regenerated during the acceleration process. In that sense, the acceleration of radical removal could be loosely termed a catalysis, although not strictly so.

Jensen and Jones published again in 1981, "Theoretical Aspects of Secondary Combustion in Rocket Exhausts"⁷. This was a computational technique based on a two-equation turbulence model, coupled with detailed nonequilibrium chemistry, used for predictions of whether or not secondary combustion of excess fuels would occur in the exhaust from an additive-modified double-base (nitrocellulose-nitroglycerin) propellant rocket motor. The purpose of the paper was to describe in outline a method of predicting whether or not secondary combustion occurs in the exhaust of any low altitude rocket, to summarize results of applying this method to a particular rocket motor with small proportions of potassium additive incorporated in its solid propellant, and to discuss both method and results in a manner that brings out the need for improved prediction techniques. They utilized equations for conservation of the axial component of momentum, the radial component of momentum, the stagnation enthalpy, chemical species, turbulence kinetic energy, eddy energy dissipation rate, the ideal gas equation of state, and the continuity equation applied to a local elementary fluid volume. The assumptions used in the method were that the flow is quasi-steady (the average motion is steady and the governing equations are time averaged), the flow is treated as locally incompressible, turbulent density fluctuations are neglected, the Reynolds stresses are taken to be expressible in terms of mean velocity gradients, molecular transport is not a rate-determining process, the laminar viscosity is small by comparison with the turbulence eddy viscosity, coupling of fluid dynamic and chemical effects can be accomplished legitimately by combining local time-mean values, the flow is adiabatic, and turbulence is locally isotropic.

They found that the concentrations of the major species H_2 , CO, CO_2 , H_2O , and N_2 do not vary significantly with the proportion of potassium-containing additive in the propellant. Those of the minor species were found to vary with additive level, and the higher the level, the greater the

rate of recombination in the nozzle of the free radicals present. Slight variations of exit temperature and pressure with additive level were also apparent. With potassium excluded from the calculations in a particular exhaust stream, a significant, rise in gas temperature with increasing axial distance occurs near the nozzle exit. This indicated that secondary combustion of hydrogen and carbon monoxide was taking place. For the same conditions except with 0.8 percent by weight potassium in the propellant, a decrease of 400 to 500 Kelvin was noted in the maximum temperature found in the secondary combustion zone; 1.0 percent totally eliminated the region of temperature increase and hence, suppressed the secondary combustion. In calculations of a variety of other exhausts, it was found that the minimum concentration of potassium necessary to completely suppress the secondary combustion under most conditions would be more nearly 2.5 percent by weight.

The authors list six reactions containing potassium which were considered in their analysis:



One interesting aspect of the work was that the inclusion of reactions involving KO_2 led to promotion of secondary combustion. As oxygen from the air is mixed with the propellant products, the reaction



is predicted to be a significant source of active free radicals. They qualify this analysis with the comment that much of the uncertainty in the influence of KO_2 stems from the lack of reliable thermochemical data for this species. Overall they view their approach to the analysis of the chemistry of the rocket exhausts as adequate as used within this method.

W. A. Hahn, J. O. L. Wendt, and T. J. Tyson published a paper in 1981 entitled "Analysis of the Flat Laminar Opposed Jet Diffusion Flame with Finite Rate Detailed Chemical Kinetics"¹. The fuel in their flame was moist CO, which was burned with O_2 and N_2 . The main intent of the work was to study pollutant formation. The objectives were to mathematically model the flame and to develop procedures to solve the model, to gather experimental data for comparison with the predicted results, and if the previous two objectives were accomplished and in agreement, to introduce small quantities of an additive (fuel impurity) into the flame and compare predictions to measured values. Most of the prior work they cited was thought to have not included proper sets of kinetic data. This did not allow the older models to be useful in studying the formation of trace species. Early models also suffered from the assumption of inviscid, incompressible jets. To meet their stated objectives they had to combine the following features into one coherent model of the flat, laminar, opposed-jet diffusion flame: 1) coupling of momentum and energy conservation equations; 2) inclusion of detailed finite-rate combustion chemistry, with no restrictions on high or low activation energies or on fast or slow reaction rates; 3) inclusion of variable transport and thermodynamic properties; and 4) determination of the correct ratio of velocities of the opposing jets in order to provide a laboratory flat flame with a specified stretching rate. The specific flame to be examined utilized moist carbon monoxide as the fuel, and the fuel impurity and pollutant considered were ammonia and nitric oxide, respectively.

Metered amounts of fuel (CO; Matheson, C.P. grade), oxygen, and nitrogen are mixed and fed to the two opposing burners through Teflon tubing. The flow rate of these gases is measured with critical flow orifices of size ranging from .1 to 0.625 mm; the flow range that could be covered

with these orifices was 0.3 liter/min to 25 liter/min of N_2 . Water was introduced into the fuel gas by bubbling it through a flask. Chemically bound nitrogen contained in the fuel was simulated by the addition of anhydrous ammonia to the fuel stream. The flow rate of this additive was measured with a restriction and an inclined differential manometer. The fluid used in the manometer was a light oil, which did not absorb ammonia to a measurable extent.

The combustion chamber was a 30x30x30 cm, sealed aluminum box which contained the two vertically mounted opposed burners, an uncooled quartz probe (I.D. = 0.06 cm), a platinum ignition wire, and a Pt, Pt/10% Rh thermocouple, mounted on the probe. The thermocouple bead was 0.15 mm in diameter and uncoated. The two burners were made of 6.25 cm diameter stainless steel tubes filled with glass beads and sealed at the ends with a stainless steel porous disk. The burners were mounted on independent screws to allow variation of their separation and positioning with respect to the sample probe. Two gliding bars on each burner kept them aligned to within 0.25 cm. The quartz probe, with attached thermocouple, was mounted on a two-dimensional traversing mechanism, to allow both vertical and radial concentration and temperature profiles.

A sample was drawn with a vacuum pump at approximately 0.13 liter/min. This represented a residence time of 7 msec in the tip of the probe before the sample was quenched. The sample lines were kept warm with heating tape, and water contained in the sample was condensed in a flask immersed in an ice bath only after passing through a gas chromatograph sampling loop. The sample loop was filled at the same time that the sample flowed through a Thermo Electron Model 10-A, self-contained, Chemiluminescent NO/NO_x analyzer with stainless steel and molybdenum converters. When the NO reading reached a steady value, the sample loop was assumed full and was pressurized to 15 psig, and then injected into a Perkin-Elmer, Sigma II Gas Chromatograph, where it was analyzed for CO, CO₂, O₂, H₂, H₂O, and HCN using a 3-m mole sieve and a 1.8-m Porapak T column. The oven temperature was set at 110 degrees C and

the carrier gas was 0.999999 helium at a flow rate of 10 ml/min. The sensors used were a hot-wire detector and a nitrogen-phosphorus detector.

The model was solved for combustion of a moist carbon monoxide opposed-jet diffusion flame. The reaction set included seven elementary reactions and eight chemical species.



The forward and reverse rate coefficients were taken from Engleman¹². The concentrations of carbon monoxide and water in the fuel stream were 36.2 percent and 3.0 percent, respectively, the diluent being nitrogen, while the oxidizing stream contained 19.1 percent oxygen in nitrogen. The initial guess employed for the solution of the differential equations used in the model was the solution of the equivalent Burke-Schuman flame (infinitely fast reactions assumed). This approach provided the basic profiles of CO, O₂, CO₂, and temperature. The temperature profile calculated matched the measured profile (after correcting measured values for radiation heat losses) in maximum temperature (approximately 1540 Kelvin) quite well, but the rest of the temperatures tended to be 200 - 300 Kelvin too high in the model (except where the flame zone transition to inlet gases occurred, of course). The predicted versus measured profiles for CO, CO₂, O₂, H₂, and H₂O were in very good agreement at selected points in the flame, but in other locations deviated

significantly. The interpretation of this fact is that the free radical concentrations were far above those predicted by the equilibrium calculations in the model which tended to alter the reactant profiles. The measured reaction zone thickness, which the authors state is a key parameter in the prediction of the formation of trace species in this type of flame, was in close agreement with that predicted. It was noted that water decomposes in the fuel-rich region, and the so-formed free radicals and H_2 molecules diffuse into the fuel-lean side of the flame where, in a very narrow region, water is formed again. The predicted peak values of the free radicals varied from 1000 to 3000 parts per million, existing mainly on the fuel-lean portion of the flame zone. No measurement of the actual free radical concentrations were carried out, although as stated above, it was inferred that they generally were higher than predicted, as evidenced by the measured values of the major species. In general, the authors felt that there was sufficient agreement between predicted and measured characteristics of the flame to claim the model a success.

The model was applied to the prediction of nitric oxide levels resultant from the addition of small quantities of ammonia to the flame. The comparisons from this effort indicated varied dependent upon to which flow (fuel or oxidizer) the ammonia was added. First, addition of ammonia to the fuel would cause the pyrolysis reactions to dominate and the garnered information pertained primarily to those reactions. Second, addition of ammonia to the oxidizer would focus the information on those reactions dealing with the oxidation process rather than pyrolysis. In the first set of tests the theoretical and measured profiles of NO, especially as a function of the concentration of ammonia in the fuel showed poor agreement. In the second set of tests, good agreement between the experimental and computer simulated values was found. This is interpreted to indicate that if some kinetic information in the reaction set representing the formation of NO were in error, it is in the reactions that become important under fuel-rich conditions, thus, the pyrolysis reactions.

*Kinetic Investigation of the Third-order Rate Processes between $K + O_2 + M$ by Time-

resolved Atomic Resonance Absorption Spectroscopy¹⁶, published in 1982 by David Husain and John M. C. Plane, compared rate constants for this reaction obtained from the pulsed photochemical method following the flash photolysis of KI vapor to those reported by Kaskan and Carabetta from their atomic resonance absorption studies on premixed, fuel-lean H₂/O₂/N₂ flames. This investigation found the rate constants determined by Kaskan for potassium were three orders of magnitude too low. A prior report by these authors similarly found that the rate constants reported by Kaskan for sodium were also three orders of magnitude too low. The tests were undertaken in a very rigorous method, and three different third bodies were investigated: He, N₂, and CO₂. A table of the results for the third-order rate constants (k/cm³ molecule⁻² sec⁻¹) for

(K^o, Na^o) + O₂ + M follows:

<u>M</u>	<u>K^o (753-873 K)</u>	<u>Na^o (724-844 K)</u>
He	1.3x10 ⁻³⁰ (784 K)	(6±1)x10 ⁻³¹
N ₂	2.2x10 ⁻³⁰ (784 K)	(1±0.2)x10 ⁻³⁰
CO ₂	5.0x10 ⁻³⁰ (784 K)	2x10 ⁻³⁰
(H ₂ + N ₂ + H ₂ O)**	1.02x10 ⁻³⁰	8.2x10 ⁻³⁴

** Kaskan's flame

David E. Jensen, in 1982, published the paper "Alkali-metal Compounds in Oxygen-rich Flames: A Reinterpretation of Experimental Results"¹⁶. Jensen reviewed principally the work of three teams of investigators who had previously published research on premixed oxygen-rich H₂/O₂/N₂ flames. These investigators were Kaskan and Carabetta, McEwan and Phillips, and Husain and Plane (W. E. Kaskan, 10th Int. Symp. Combustion (The Combustion Institute, Pittsburgh, 1965), p 41; R. Carabetta and W. E. Kaskan, J. Phys. Chem., 1968, 72, 2483; M. J. McEwan and L. F. Phillips, Trans. Faraday Soc., 1966, 62, 1717; D. Husain and J. M. C. Plane, J. Chem. Soc., Faraday Trans. 2, 1982, 78, 1631 and 1175.). Kaskan had at his disposal rate coefficients for the formation of the superoxides of both sodium and potassium that were in error

by three orders of magnitude. Both Kaskan and Carabetta and McEwan and Phillips introduced some errors into the conclusions drawn from their work by utilizing too low alkali metal concentrations and by not recognizing some inherent bias in techniques used to calculate the concentrations of some of the chemical species in the flames. Husain and Plane provided evidence supporting Jensen's interpretation of the earlier work.

The researchers studying these flames have variously considered compounds formed in significant proportions to be the hydroxides, AOH, the monoxides, AO, and the superoxides, AO₂. One difficulty associated with this work, however, is that the nature of the compounds formed had generally been inferred from dependencies of depletions of free alkali atom concentrations upon flame composition and temperature rather than established by direct observation. The evidence for formation of hydroxides appears strong because of the self-consistency of interpretations invoking their presence and because flame determinations of hydroxide bond energies agree with the results of independent experiments. Evidence for formation of AO₂ is less convincing, partly because the measurements performed on alkali-seeded oxygen-rich flames for certain parameters present greater experimental difficulties than do the corresponding determinations performed on fuel-rich flames. The earlier experiments were also interpreted based upon reaction rate data which was later seen to be in error.

Jensen took Kaskan's data from the potassium experiments and assumed that the only alkali species present in significant quantities were K^o and KOH. He then took the OH concentrations and increased them by 50% to bring them "into line with a preferred value for the oscillator strength of the appropriate OH band". After calculations based upon recent (and more accurate kinetic data), Jensen compared the predicted results to the experimental results and found good agreement. Thus the experimental data reported by Kaskan for potassium could be quantitatively interpreted on the basis of the up-to-date kinetic work on the reactions



and



without the need for inclusion of any compound other than the hydroxide.

The reinterpretation of the sodium experiments of Kaskan met with greater difficulty. When the same techniques mentioned above were applied to the sodium flame data, the predicted sodium concentrations [Na] were found to be too low near the main reaction zone and too high further downstream. Inclusion of NaO_2 in the model reportedly gave even worse agreement. Kaskan reported measured OH concentrations to be higher in cooler flames, which is contrary to expectations. Jensen took this discrepancy as justification to increase the measured values for [OH] at all points by a factor of two. He also reduced the forward and reverse rate coefficients for



by a factor of 2.5 (within the uncertainty bounds). The predictions were recalculated, and this time good agreement was achieved. Almost in passing, Jensen notes that this model could not be applied to McEwan and Phillip's data due to a lack of data correlating [OH] at atmospheric pressure to [OH] at other pressures. He does state that they had assumed that



was balanced in their flames, which led them to the conclusion that NaOH was not the main compound formed and that significant proportions of NaO_2 must be present. He concludes that the reaction would not be balanced, that NaOH would be the dominant species, and that their conclusion is thus false. The imbalance of this reaction is also taken to imply that attempts to apply the Li°/Na° comparison method for measuring radical concentrations in this type of flame, will result in erroneous data.

Summarizing, Jensen felt that his interpretation of the results of these experiments on sodium and potassium in oxygen-rich $H_2/O_2/N_2$ flames removes the conflict between the rate

coefficients for the superoxide formations obtained by Husain and Plane and the original apparent values derived by the previously mentioned investigators. Husain and Plane's work yielded revised values for Na-O₂ and K-O₂ bond energies and reaction rate coefficients. He suggests that further experiments of widely varying temperature and composition be undertaken to more rigorously test his hypotheses. Additionally, in such work it would be necessary to determine flame radical concentrations with great precision and highly desirable to observe compounds directly (either by spectrophotometric means or by mass spectrometric sampling) rather than to infer their presence by indirect methods.

J. A. Silver, M. S. Zahniser, A. C. Stanton, and C. E. Kolb published the results of similar work "Temperature Dependent Termolecular Reaction Rate Constants for Potassium and Sodium Superoxide Formation"⁹ in 1984. They measured the rate constants as a function of temperature in the range of 300 to 700 Kelvin in the low pressure third order limit from 1 to 8 torr total pressure with N₂, He, and Ar as third bodies. Laser induced fluorescence was used to monitor the disappearance of Na^o or K^o as a function of O₂ and M. Their results were in agreement with those of Husain and Plane.

APPENDIX 2 Experimental Apparatus; Standard Operating Procedure

1. Burner preparation
 - 1.1 No additive
 - 1.1.1 Stand empty burner on exit end (long axis vertical).
 - 1.1.2 Insert exit end screen, 20 mesh.
 - 1.1.3 Load ceramic beads two inches deep.
 - 1.1.4 Insert 40 mesh screen.
 - 1.1.5 Load ceramic beads to 10 13/16" total depth.
 - 1.1.6 Insert 20 mesh screen.
 - 1.1.7 Insert spring
 - 1.1.8 Lubricate o-rings on brass end-plug with stopcock grease.
 - 1.1.9 Insert brass end plug.
 - 1.1.10 Insert retainer snap ring in to groove.
 - 1.1.11 Mount burner on rail and secure.
 - 1.2 With additive
 - 1.2.1 Stand empty burner on exit end (long axis vertical).
 - 1.2.2 Insert exit end screen; 20 mesh.
 - 1.2.3 Load ceramic beads two inches deep.
 - 1.2.4 Insert 40 mesh screen.
 - 1.2.5 Lubricate o-rings on brass end plug with stopcock grease.
 - 1.2.6 Load sample boat.
 - 1.2.6.1 Spread out 2.75 ± 0.25 grams of additive evenly across bottom of sample boat.
 - 1.2.6.2 Fill remainder of sample boat with ceramic beads.
 - 1.2.7 Set burner with long axis horizontal.

- 1.2.8 Raise inlet end until long axis is approximately 20° above horizontal.
- 1.2.9 Load beads to a depth of one-half inch below midpoint of screen.
- 1.2.10 Insert load sample boat and hold in place against screen. Top of boat should have one inch clearance.
- 1.2.11 Holding sample boat long axis parallel to long axis of burner, add additional ceramic beads to cover sample boat and screen.
- 1.2.12 Raise inlet end until long axis is about 45° above horizontal.
- 1.2.13 Load remainder of ceramic beads to a total fill depth of 11 inches.
- 1.2.14 Insert 20 mesh screen.
- 1.2.15 Manipulate burner and screen as required to obtain secure screen placement perpendicular to long axis with a minimum of loose beads.

Note: Avoid raising inlet end of burner higher than 45° from horizontal and minimize vibration of burner. This is especially important in cases where the additive is a fine, or free-flowing powder. It is not desirable to allow the additive to escape the sample boat.

- 1.2.16 Insert spring.
- 1.2.17 Insert brass end plug
- 1.2.18 Insert retainer snap ring into groove.
- 1.2.19 Secure burner onto mounting rail.
2. System Operation
 - 2.1 Start up.
 - 2.1.1 Turn on spectrometer to standby mode.
 - 2.1.2 Turn on exhaust system and open inlet gate above burners.
 - 2.1.3 Turn on Burner cooling water.
 - 2.1.4 Set O₂ and N₂ flows to air side burner.

- 2.1.5 Set N_2 and H_2 flows to full side burner.
- 2.1.6 Ignite flame.
- 2.1.7 Turn on electric heater(s) and adjust.
- 2.1.8 Set translating slit width.
- 2.1.9 Observe burner temperatures (two locations).
- 2.1.10 Adjust electric heater(s) as needed for proper balance of internal and exit temperatures.
- 2.1.11 Check air side and fuel side gas flows.
- 2.1.12 Check spectrometer.
 - 2.1.12.1 Switch from standby to on mode.
 - 2.1.12.2 Set wave number to 3400 cm^{-1} .
 - 2.1.12.3 Set micrometer to 0.300 inch (3.00 tenths of inch).
 - 2.1.12.4 Observe maximum intensity displayed by recorded pen position.
- 2.1.13 Evaluate overall system function. If satisfactory, proceed to 2.2.
- 2.2 Scanning
 - 2.2.1 Check gas flows and note any deviations; adjust if necessary.
 - 2.2.2 Check and Record temperatures.
 - 2.2.3 Set micrometer position.
 - 2.2.4 Adjust paper to proper location reference to recorder pen.
 - 2.2.5 Set cm^{-1} selector to 3800 cm^{-1} .
 - 2.2.6 Depress recorder pen.
 - 2.2.7 Start Scan.
 - 2.2.8 Stop scan at 3000 cm^{-1} .
 - 2.2.9 Raise recorder pen.
 - 2.2.10 Repeat steps 2.2.3 through 2.2.9 for three additional scans.
 - 2.2.11 Run chart paper ahead to new location.

- 2.2.12 Repeat steps 2.2.3 through 2.2.9 for four additional scans.
- 2.2.13 Repeat 2.2.1 through 2.2.12 as required for completion of test matrix.
- 2.2.14 Set spectrometer to standby mode.

2.3 Shut down

Note: This is a minimum duration shut down procedure acceptable for burner temperatures of 300°C or less. If burner temperature is between 300°C and 400°C at start of shut down, increase waiting periods in 2.3.5 and 2.3.9 by five additional minutes each. If burner temperature is greater than 400°C, perform steps 2.3.6 through 2.3.9 two times before proceeding to step 2.3.10, as well as increasing the waiting periods as mentioned previously.

- 2.3.1 Reduce electric heaters to 50% of present settings.
- 2.3.2 Turn off H₂ and O₂ flows.
- 2.3.3 Turn off spectrometer.
- 2.3.4 Remove recorded scans from spectrometer; put lab notebook and scans in proper storage.
- 2.3.5 Wait five minutes.
- 2.3.6 Reduce electric heaters to 50% of present settings.
- 2.3.7 Reduce N₂ flows to 50% of present value.
- 2.3.8 Reduce cooling water to 50%.
- 2.3.9 Wait five minutes.
- 2.3.10 Turn off electric heaters.
- 2.3.11 Turn off N₂ flows.
- 2.3.12 Monitor burner temperature until cooled to 50°C or less.
- 2.3.13 Turn off cooling water.
- 2.3.14 Allow apparatus to cool for one additional hour if disassembly is required.

2.3.15 Inspect all gas cylinders to ensure closed and secure.

2.3.16 Turn off exhaust system.

APPENDIX 3 SOP Comments (Numbers in parentheses are from operating procedure)

1.0 Burner Preparation: Only one burner is described here - The elongated burner wrapped with heating coils for additive evaporation. There are two other burners which were utilized in the research, but did not require any "preparation", as such, - just an initial set up and securing to the mounting rail.

1.1 No Additive

Screens: (1.1.2, 1.1.4, 1.1.6) Screens are cut from wire cloth stock of the proper mesh of stainless steel. The diameter should be slightly larger than the internal diameter of the burner to aid in maintaining proper placement of the screen. Screens should be kept in good shape. No plugged holes are allowed, and screens should be replaced if oxidation or loss of physical dimensions becomes a problem.

Loading Ceramic Beads: (1.1.3, 1.1.5) Once the volume or weight of beads required has been determined by trial and error with repeated screen placement and removal, etc., the technical should develop a technique for rapid premeasurement of the necessary quantity of beads. I find that a volume measurement with a graduated cylinder is adequate. Generally, if one is setting up the burner for a "no additive" run, the previous configuration contained an additive. Complete removal of all beads from the previous run is required. Beads used in a "no additive" run can be used over if the supply is limited, either for a subsequent "no additive" run, or for use with additives. The used beads should be stored separately with proper labels indicating history.

Lubrication: (1.1.8) Before any operation of burner prep or disassembly, remove all traces of lubricant from the gas inlet end. Lubricant on the ceramic beads will contaminate them, as it will screens or any other of the internal pieces.

1.2 With additives

Screens: (1.2.2, 1.2.4, 1.2.14) See comments under 1.1 No additive.

Ceramic Beads: (1.2.3, 1.2.6.2, 1.2.9, 1.2.11, 1.2.13) See comments above under 1.1 No additives. Also, some judgement calls will be required here to decide what beads are suitable for use or reuse with additives. All of the beads from any additive run should be segregated from beads used with other additives or without additives at all. They can be reused for subsequent runs with the same additive, provided the beads are not clumped together, etc., and provided that residues from the initial experiment will not react during storage to form another compound that could confuse results (for instance: beads that are covered initially with potassium will be found to potassium hydroxide on them after a storage period in humid air. These would probably be more suitable for a subsequent KOH run instead of another K^o run.)

Lubricant: (1.2.5) See comments under 1.1 No additive.

Final Screen Placement: (1.2.15) KO₂ is especially of concern since it is fine and free flowing and can likely be poured out of the sample boat if the burner is tilted up too high. This out-of-position KO₂ may then be blown towards the flame by drag forces from the moving gases.

2.0 System Operation: This section assumes that each subsystem has been set up and checked out, and is ready to run. These subsystems are described elsewhere and include: exhaust system, gas flow and metering system, burners, electric heating system, optic system, cooling water system, and spectrometer.

2.1 Start up

Exhaust System: (2.1.2) The exhaust system should always be functioning before any gas flow is commenced at any step of experimentation or set up.

Cooling Water: (2.1.3) The cooling system should function well even at low water flows. The purpose of the cooling system is to protect the o-ring seal on the brass end plug. The water itself will have an inlet temperature of 20°C to 25°C and the outlet temperature should be kept below 50°C for safety reasons. Generally, 5 cm³/sec of water should be adequate for burner

temperatures below 300°C. Flows of 10 cm³/sec should be adequate for burner temperatures between 300°C and 600°C. Lower flows may be utilized if the outlet water temperature and brass end plug temperature do not exceed 50°C. In case of loss of cooling water, a burner shut down should be implemented but the cool-down should not be rushed, as breakage of the ceramic materials may occur. A moderate flow of N₂ (equal to same flow as used during experimental runs) will provide some cooling. If brass end plug temperature becomes too high the o-rings may deteriorate causing difficulty in disassembly, but no serious equipment damage should result. Use caution when working around high temperature materials at all times.

Caution: The burner heating elements carry large currents and voltages. Electric shock may result if water is allowed to contact any of the exposed wiring or to contact the burner insulation. Immediately shut off and disconnect power to heating elements in case of cooling system leakage or water spillage in vicinity of burners. Water contacting the heated burner will cause immediate release of steam and sever damage to brittle components (mullite tube, ceramic cement, ceramic wire insulation).

Oxygen Flow: (2.1.4) High concentrations (>21%) of oxygen can cause serious fire and explosion hazards.

Hydrogen Flow: (2.1.5) High concentrations of hydrogen (>4%) can cause serious fire and explosion hazards.

Flame ignition: (2.1.6) Match holders for lighting gas pilot lights of gas ranges, water heaters, and furnaces are readily available. The match holder should be 6 inches or more in length. Light the flame as soon as possible after commencing hydrogen flow. An increased hydrogen flow will aid in initial ignition; 25% increase in H₂ should be sufficient. Light the flame from the lower side of the burner gap. Reduce the hydrogen flow to nominal setting after ignition.

Electric Heaters: (2.1.7, 2.1.10) Electric heating elements are used to provide a more uniform temperature gradient through the ceramic bead bed, and to elevate the bead temperature as

desired for sample evaporation. Two separate sections of heating coils are used: The flame end section, and the central additive section. The power to these sections is controlled independently. To avoid condensation of additive in the exit end of the burner, the temperature of the flame end section should be kept higher than the additive section. When possible, a constant temperature difference between additive section and flame end section should be maintained throughout a given experimental run, and in a repeat with or without additive. The heaters may be used to preheat the burner if desired, either with or without gas flow. The burner will self-heat with a burning flame, with the temperature being highest of course on the flame end. This flame end temperature rises quickly at first and will keep rising for a period in excess of two hours. The rate of increase falls off with time. The temperatures cannot be controlled independently of this self-heating phenomenon and must always be controlled in conjunction with it. Do not heat the burners at an excessive rate of rise, as this will also cause thermal shock that can cause damage to the equipment.

Spectrometer: (2.1.12) The spectrometer check out is also a check out of the entire experimental apparatus. Try to determine at this point if the flame signal is steady, the maximum intensity is reasonable and located at a typical micrometer position. See if the flame edges are where they should be and that total flame width is normal. Debug the system if any anomalies show up at this point. Factors to examine: gas flows, burner alignment, burner gap, burner location, optic system components set properly, spectrometer settings normal, temperature profile of burner.

2.2 Scanning

Gas Flows: (2.2.1) Gas flows will deviate upon occasion, in either an increasing or decreasing directional. Small variations in gas flow will alter the flame intensity, so it is very important to check, verify, or adjust the flow settings throughout the experimental runs. Each deviation or adjustment required should be recorded for input in interpreting experimental data.

Temperatures: (2.2.2) Temperatures are tracked at two positions in the burner; near the flame

end, and in the midpoint of the additive region. The thermocouple sensing end lies against the Inconel 600 burner tube, on the exterior surface. When eight scans have been completed, immediately read the temperature indicated on the display for that location. Record the value and location. Relocate the thermocouple to the other position and carry out other activities while the thermocouple comes to equilibrium. Usually one to two minutes is required. Before proceeding with the next eight scans, read and record the temperature at this location. The temperatures obtained (i.e. at 5" and 8") will be the final temperatures for run number X, and the starting temperatures for run number X + 1.

Scan Duration: (2.2.7 to 2.2.8) The recording of the signal on any scan from 3800 cm^{-1} to 3000 cm^{-1} at 1000 cm^{-1} per minute takes less than one minute to complete. During this time, the technician should always pay close attention to the scan trace being recorded, as it will be his window on the status of the entire system. Also, occasional problems with the spectrometer/recorder may develop, and early detection results in minimum loss of data.

2.3 Shut Down: No additional comments.

Appendix 4 Heat transfer calculations; thermocouple errors.

The following calculations are based upon methods supplied in "Heat Transmission" Third Edition, by William H. McAdams, 1954; McGraw-Hill Chemical Engineering Series¹⁰. The question being asked is "Does the wall thermocouple temperature give an accurate indication of the gas temperature at those same locations?"

Page 293 (McAdams): "Vershoor and Schuit (Verschoor, H., and G. C. A. Schuit, "Appl. Sci. Research, A2, 97-119 (1950)) obtained data for heating of air in tubes containing glass beads, lead and steel balls, crushed pumice, and terrana tablets. The values of K_a computed from the data were correlated by

$$K_a/k_g = 1.72(k_g/k_p)^{0.28} + 0.1(aD_i)^{0.5}(G_p/\mu a)^{0.69} \quad \text{EQN 11-19.}$$

within 16 percent. For spherical particles, this gives

$$K_a/k_g = 1.72(k_g/k_p)^{0.28} + 0.071(D_p G_p/\mu)^{0.69}/((D_p/D_i)^{0.5}(1-\epsilon)^{0.19}) \quad \text{EQN 11-20.}$$

The variables are defined as :

K_a = apparent thermal conductivity of a fluid-solid system, Btu/(hr)(sq ft)(deg F per ft)

k_g = true thermal conductivity of gas, Btu/(hr)(sq ft)(deg F per ft)

k_p = true thermal conductivity of solids, Btu/(hr)(sq ft)(deg F per ft)

D_p = diameter of particle, feet

D_i = diameter of tube, feet

G_p = superficial mass velocity of the gas, i.e., the mass rate of flow divided by the cross of the empty tube, pounds/(hr)(sq ft)

μ = viscosity of gas, lb/(hr)(ft)

a = surface area of packing per unit volume of packed bed, sq ft/(cubic ft)

ϵ = average fraction void in bed, dimensionless

For the experimental system employed, the known values of the variables were :

$$k_g = 0.0438 \quad (\text{McAdams page 458})$$

$k_s = 2.0$	(Coors Ceramics data)
$D_p = 0.0052$	(measured)
$D_1 = 0.1719$	(measured)
$\mu = 0.0215$	(McAdams page 469)
$\varepsilon = 0.413$	(calculated from measured weight of beads, known volume of tube, and Mullite density reported by Coors)

$$G_o = (m_{H_2} + m_{N_2})/A$$

$$m_{H_2} = \text{mass flow rate of hydrogen} = 5.2 \text{ l/min} = 0.0614 \text{ lb/hr}$$

$$m_{N_2} = \text{mass flow rate of nitrogen} = 4.1 \text{ l/min} = 0.6779 \text{ lb/hr}$$

$$A = \text{tube cross sectional area} = 0.0232 \text{ sq ft}$$

$$G_o = 31.87 \text{ lb/(hr)(sq ft)}$$

Substituting the known values into EQN 11-20 and solving for K_a gives :

$$K_a = 0.2845$$

The temperature gradient is described by:

$$\delta v \delta x = (K_w/G_o c_p) ((\delta^2 v \delta r^2) + (1 \delta v r \delta r) + (\delta^2 v \delta x^2)) \quad \text{EQN 11-11}$$

If axial conduction is neglected, $\delta^2 v \delta x^2$ disappears from EQN 11-11, which then becomes integrable for constant wall temperature and uniform mass velocity. The integrated expression for rodlike flow, with an appropriate change of variable, gives:

$$(t_w - t_2)/(t_w - t_1) = 0.692 \exp(-23.1X) + 0.131 \exp(-122X) + 0.0535 \exp(-300X) \quad \text{EQN 11-12}$$

in which

$$X = K_a L / c_p G_o D_1^2 \quad \text{EQN 11-13}$$

For values of X greater than 0.04, or for $(t_w - t_2)/(t_w - t_1)$ less than 0.28, only the first term of EQN 11-12 need be employed for accuracy within 1 percent.

Additional variables to be defined:

t_w = temperature at wall, degrees Fahrenheit

t_1 = temperature at inlet, deg F

t_2 = temperature at outlet, deg F

c_p = specific heat of fluid at constant pressure, Btu/(lb)(deg F)

L = length of exchanger or packed bed, feet

As noted in the text of the "experimental procedure" section of this thesis (page 25), the gas temperature was desired to be within 5 degrees Celsius of the wall temperature to accept the wall temperature as an accurate indication of the gas temperature.

Solving equations 11-12 and 11-13 for the following case:

$t_w = 572^\circ\text{F}$ (300°C)

$t_1 = 72^\circ\text{F}$ (22°C)

$t_2 = 567^\circ\text{F}$ (297°C)

$c_{pH_2} = 3.5$ (McAdams page 464)

$c_{pN_2} = 0.26$ (McAdams page 464)

$c_{pAvg} = 0.5291$ (calculated)

$$(t_w - t_2)/(t_w - t_1) = (572 - 567)/(572 - 72) = 5/500 = 0.01$$

Since this value is less than 0.28, only the first term of EQN 11-12 was employed.

$$0.01 = 0.629 \exp(-23.1X)$$

$$X = 0.179$$

This value is greater than 0.04, which verifies the use of first term only.

Now, solving EQN 11-13

$$L = 0.313 \text{ feet} = 3.76 \text{ inches}$$

Thus, if the tube wall is at 300°C for a length of 3.76 inches prior to the location of temperature

measurement, the gas temperature will be at 297°C at that location. The gas temperature would be 295°C after 3.13 inches of length. It takes the final 17% of the tube length to obtain the final 1% of the temperature increase within this region investigated.

Wall temperature measurements made for a typical run are tabulated below:

Thermocouple Location Scale (Inches)	Indicated Temperature (degrees C)
-3	25**
-2	55**
-1	90**
0	125
1	175
2	225
3	260
4	290
5	305
6	305
7	300***
8	305

** Indicates estimated values. The wall temperature was not measured at these three locations, but was assumed to decrease linearly from the temperature at 0 inches to the edge of the cooling coils at -3 inches.

*** Thermocouple temperature measurements were rounded to the nearest 5 degrees Celsius. The actual difference in temperatures between locations 7 inches and 6 or 8 inches could have been less than one degree C (i.e., 302.4°C at 7 in., 302.6°C at 8 in.).

This case is not so straight forward as the problem worked, because the wall temperature is not constant at 300°C. At the burner inlet, it was approximately 75°C too low at 2 inches and 125°C too low at 1 inch. To answer the question more accurately, the gas temperature versus wall temperature and tube length problem was broken into one inch segments, and solved as above.

Thermocouple Location Scale (Inches)	Indicated Wall Temperature (degrees C)	Gas Temperature Calculated (degrees C)
-3	25	25
-2	55	49
-1	90	81
0	125	116
1	175	163
2	225	212
3	260	250
4	290	282
5	305	300
6	305	304
7	300	301
8	305	304

This analysis indicates that wall temperatures reported at locations of 6 inches and greater would accurately reflect the gas temperature, but at the 5 inches location, wall temperature appears to

exceed gas temperature by 5 degrees Celsius. The worst case temperature error encountered was for a wall temperature of 25°C at -3 in., increasing to 350°C at 5 inches and beyond. The wall temperature exceeded the gas temperature by 6°C at 5 inches; 1°C , at 6 inches.

The additive evaporation boat temperature was assumed equal to that of the surrounding gas/packed bed. The boat was 2.5 inches long by 0.5 inch wide, oriented with its long axis parallel to the tube axis, and located near the tube midplane between 3.5 and 6 inches on the thermocouple scale. In the worst case example, cited above, its temperature varied end-to-end by 44°C - from 305°C at 3.5 in. to 349°C at 6 inches. The temperature at 6 inches was used to correlate vapor pressure in the potassium additive experiments; at 5 inches, in the potassium superoxide experiments.

The previous calculations contribute to answering the question of whether the wall temperature accurately reflected the bed temperature, and hence, the gas temperature. However, the burner was not operated in an equilibrium state, that is, the temperature of the burner increased during an experimental run. Perhaps a more fundamental question to be posed then, would be what happens to the packed bed and gas temperature as the burner wall temperature increases at the rates of increase employed in this experimentation? This is especially important since the concentration of additive in the gas stream is dependent upon the additive temperature, which is equal to the boat temperature, which is equal to the temperature of the surrounding gas and packed bed temperature. Thus we seek to determine the additive temperature as a function of wall temperature and time. The following calculations will serve to answer this question.

McAdams page 41 : Fig. 3-8.(not reproduced here) Gurney-Lurie chart (Gurney, H.P., and J. Lurie, Ind. Eng. Chem., 15, 1170-1172 (1923) for long cylinder; values of Y , the dimensionless ratio of temperature differences $(t_w - t)/(t_w - t_b)$; X , the dimensionless term $(k\theta/dc_p(r_m^2))$; and m , the dimensionless term (k/hr_m) .

Variables to be defined:

t_s = temperature of surroundings (wall), deg F

t_0 = original uniform (base) temperature of solid (packed bed), deg F

t_n = temperature at surface for $n=1$, deg F

t = temperature at position n at time T , deg F

k = thermal conductivity of solid, Btu/(hr)(sq ft)(deg F per ft)

Θ = time from start of heating, hours

d = density of packed bed, pounds/cubic foot

c_p = specific heat of solid, Btu/(lb)(deg F)

r_m = normal distance from midplane to surface, feet

h = coefficient of heat transfer between surroundings and surface, Btu/(hr)(sq ft)(deg F)

n = position ratio (r/r_m)

r = radius, normal distance from midplane to point in body, feet

Solution:

First, calculate m : Since the wall temperature is established by the heating wire, the external heat transfer coefficient is infinite.

$$k = K_w, \text{ and } r_m = 0.0859 \text{ ft.}$$

$$m = K_w/(\infty)(r_m) = 0$$

Second, calculate X , with $k = K_w$, $d = 102.6$, $c_p = 0.21$, $r_m = 0.0859$, for various values of Θ .

$$X = 0.298 \text{ for } \Theta = 0.1667 \text{ hr (10 minutes)}$$

$$X = 0.596 \text{ for } \Theta = 0.3334 \text{ hr (20 min.)}$$

$$X = 0.894 \text{ for } \Theta = 0.5001 \text{ hr (30 min.)}$$

Third, refer to Gurney-Lurie chart for values of Y , as indicated below.

Fourth, calculate temperatures at specified locations in packed bed versus time for given temperature of burner wall.

At this point, some discussion is required to explain the procedures to accomplish the third and fourth steps. Y is a function of X , m , and n . X and m were calculated above. The values of n available on the chart are 0, 0.2, 0.4, 0.6, 0.8, and 1. These values represent positions within the packed bed expressed as a ratio of (normal distance from midplane to point)/(normal distance from midplane to surface), or the fractional radial distance from center of the packed bed towards the outer surface. $n = 0$ is the midplane location, $n = 0.5$ would be one half the way out, and $n = 1$ is the location of bed/tube-wall interface. The top of the additive boat was located approximately at the midplane location ($n = 0$). The bottom of the boat was located approximately at the $n = 0.5$ location.

For a given value of m , there is a family of six lines representing the n locations. Four of these families are graphed, each one corresponding to a different value of m ; $m = 0$, $m = 0.5$, $m = 1$, and $m = 2$. The procedure that was followed involved determining graphically a value of Y at X for each n value at $m = 0$. Thus six values of Y were determined, one for each of the six locations within the packed bed to be modeled, for each value of X (X varied with Θ - time of exposure).

	Values	Values	Values
Values	of Y	of Y	of Y
of n	(10 min)	(20 min)	(30 min)
0.0	0.30	0.057	0.01
0.2	0.275	0.050	0.009
0.4	0.23	0.045	0.0075
0.6	0.16	0.028	0.005
0.8	0.08	0.015	0.0025
1.0	0.0	0.0	0.0

Substituting 100°C for wall temperature, and 25°C for initial temperature yields:

	Temperature	Temperature	Temperature
Values	Degrees C	Degrees C	Degrees C
of n	(10 min)	(20 min)	(30 min)
0.0	77.5	95.7	99.3
0.2	79.4	96.3	99.3
0.4	82.8	96.6	99.4
0.6	88.0	97.9	99.6
0.8	94.0	98.9	99.8
1.0	100	100	100

Substituting 200°C for wall temperature, and 25°C for initial temperature yields:

	Temperature	Temperature	Temperature
Values	Degrees C	Degrees C	Degrees C
of n	(10 min)	(20 min)	(30 min)
0.0	147.5	190.0	198.3
0.2	151.9	191.3	198.4
0.4	159.8	192.1	198.7
0.6	172.0	195.1	199.1
0.8	186.0	197.4	199.6
1.0	200	200	200

Substituting 300°C for wall temperature, and 25°C for initial temperature yields:

Values	Temperature Degrees C	Temperature Degrees C	Temperature Degrees C
of n	(10 min)	(20 min)	(30 min)
0.0	217.5	284.3	297.3
0.2	224.4	286.3	297.5
0.4	236.8	287.6	297.9
0.6	256.0	292.3	298.6
0.8	278.0	295.9	299.3
1.0	300	300	300

The $n = 0$ location is always the position of minimum predicted temperature. In all three cases (wall temperature = 100°, 200°, 300°C; initial bed temperature = 25°C), the temperature increase $(t-t_0)$ at each location was a specific percentage of the initial temperature difference, (t_w-t_0) , for the specified duration of exposure. This table gives the values for

$100(t-t_0)/(t_w-t_0)$:

Values	10 minutes	20 minutes	30 minutes
of n	(percent)	(percent)	(percent)
0.0	70.0	94.1	99.1
0.2	72.5	95.1	99.1
0.4	77.1	95.5	99.2
0.6	84.0	97.2	99.5
0.8	92.0	98.5	99.7
1.0	100	100	100

The additive boat (positioned between $n = 0.0$ and 0.5) temperature increase was 70 - 80 percent of the initial wall-to-midplane temperature difference over the first 10 minute exposure. It can be shown that the average temperature increase at $n = 0.0$ for any 10 minute increment is linear with respect to the temperature difference between the wall and the temperature at $n = 0$ at the start of that time increment. Consequently the average temperature rise rate at $n = 0$ is fixed for a given temperature difference. Alternatively, the temperature difference is fixed for a given average temperature rise rate at $n = 0$.

The percentage data in the above table is correlated at $n = 0.0$ in time by

$$(100 - \%) = \exp(-0.1407T) ,$$

where T is expressed in minutes, over the range studied of zero to 30 minutes. Solving for $T =$ one minute, $\% = 13$. That is, the temperature increase at $n = 0.0$ is equal to 13 percent of the temperature difference between $n = 0.0$ and the wall ($n=1$), in any one minute increment.

The rate of temperature increase, R (deg C/min), is equal to $0.13(t_w-t)$. By equating the rate of temperature increase at the wall to the rate of temperature increase at $n = 0$, the differential temperatures remain fixed. Thus, we can ascribe a temperature difference to any temperature increase rate by the relation

$$0.13(t_w-t) = R ,$$

or, $(t_w-t) = 7.69(R)$, where t = temperature at $n = 0$, and R = the rate of temperature increase at both $n = 0$ and $n = 1$ (the wall). For $R = 1$, $(t_w-t) = 7.7^\circ\text{C}$; for $R = 2$, 15.4°C . The average rate of temperature increase for potassium additive experiments was 1.2°C per minute, indicating the average midplane temperature (and hence, the additive temperature), was approximately 9° Celsius below the measured wall temperature.

One other problem that needs to be addressed is correction of the pyrometer temperature values for heat losses from the thermocouple. The case studied was for a thermocouple inclosed in a protective tube, as was used in the present research. The quasi-empirical equation given

below corrects for conduction losses in a shielded (low radiative loss system) thermocouple inserted varying distances into the area to be sensed.

McAdams page 265: Rizika and Rohsenow (Rizika, J. W., and W. M. Rohsenow, Ind. Eng. Chem., 44, 1168-1171 (1952)) derived an equation for calculating the temperature t_g of a fluid from the temperature t_p of a thermocouple in a protecting tube immersed a distance x_i in the fluid:

$$(t_p - t_a)/(t_g - t_p) = \cosh(a_p x_i) - 1 + (h_p/h_a)^{0.6} \sinh(a_p x_i) \quad \text{EQN 10-5}$$

where

t_a = temperature of ambient air, deg Fahrenheit

t_p = temperature of pyrometer (thermocouple) in protective tube, deg F

t_g = actual temperature of area to be sensed, deg F

h_p = heat transfer coefficient from high temperature heat source
(gas/wall) to thermocouple, Btu/(hr)(sq ft)(deg F)

h_a = heat transfer coefficient from thermocouple to air

a_p = dimensional term = $(h_p b/kS)^{0.6}$, feet⁻¹

x_i = distance inserted into high temperature gas, feet

$b = \pi d_{OD}$ = circumference of protective tube, feet

d_{OD} = outside diameter of protective tube, feet

$d_{ID} = (d_{OD} - 2t_w)$ = inside diameter of protective tube, feet

t_w = wall thickness of protective tube, feet

k = thermal conductivity of protective tube, Btu/(hr)(ft)(deg F per ft)

$S = (\pi d_{OD}^2/4) - (\pi d_{ID}^2/4)$ = cross sectional area of protective tube, sq ft

For the particular case of our experimental apparatus,

$t_a = 72$ (measured)

$h_p = 2$ (contact heat transfer coefficient)

$h_a = 2$ (coefficient for convective heat transfer)

$x_i = 5/12, 6/12, \text{ or } 8/12$ (depending on thermocouple location)

$k = 10.2$ (McAdams page 447)

$d_{OD} = 0.0125$ (inch) (measured, 1/8 inch tube)

$d_{OD} = 0.0104$ (conversion of units, inches to feet)

$th_w = 0.028, 0.035$ (inch) (standard wall thicknesses, 304 stainless steel tube)

$th_w = 0.0023, 0.0029$ (conversion of units, inches to feet)

$d_{ID} = 0.0058, 0.0046$ (calculated)

$b = 0.0327$ (calculated)

$S = 5.93E-5, 6.87E-5$ (calculated)

$a_p = 108.2, 93.3$ (calculated)

Substituting these values into EQN 10-5, and setting $x = 5/12$,

for $t_p = 662^\circ\text{F}$ (350°C),

$t_b = 662^\circ\text{F}$ (350°C), 662°F (350°C).

For $t_p = 212^\circ\text{F}$ (100°C),

$t_b = 212^\circ\text{F}$ (100°C), 212°F (100°C).

Setting $x = 6/12$,

for $t_p = 662^\circ\text{F}$ (350°C),

$t_b = 662^\circ\text{F}$ (350°C), 662°F (350°C).

For $t_p = 212^\circ\text{F}$ (100°C),

$t_b = 212^\circ\text{F}$ (100°C), 212°F (100°C).

Setting $x = 8/12$,

for $t_p = 662^\circ\text{F}$ (350°C),

$t_b = 662^\circ\text{F}$ (350°C), 662°F (350°C).

For $t_p = 212^\circ\text{F}$ (100°C),

$t_b = 212^\circ\text{F}$ (100°C), 212°F (100°C).

The conclusions to be drawn from all of these calculations are:

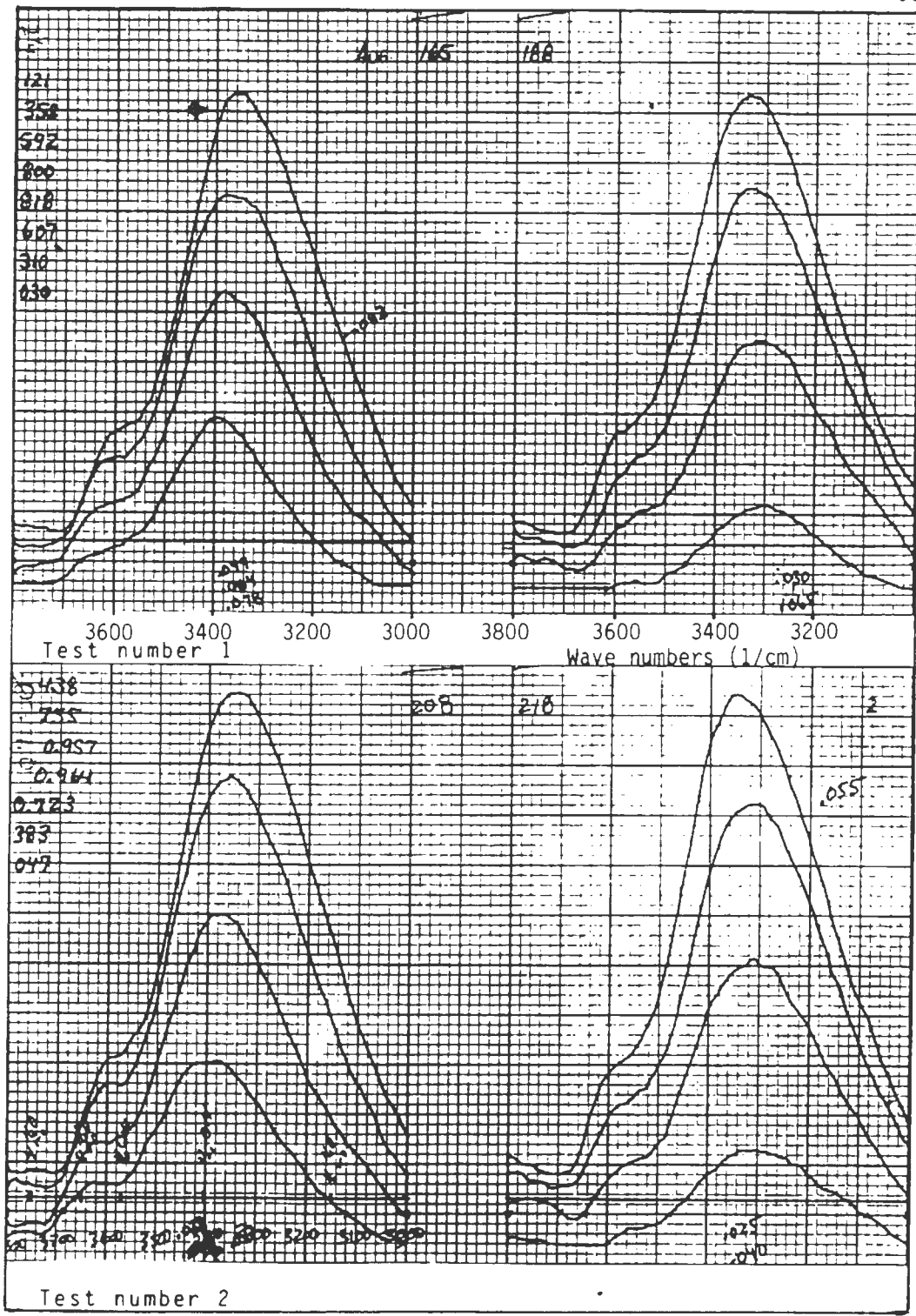
1. Thermocouple measurements accurately reflect wall temperatures .
2. Gas temperatures on exit of the burner are equal to wall temperatures at 7.75 or 8 inches
3. Additive temperatures average 10°C below wall temperatures at 5 or 6 inches.

APPENDIX 5 Experimental settings, temperatures, data, and spectra scans.

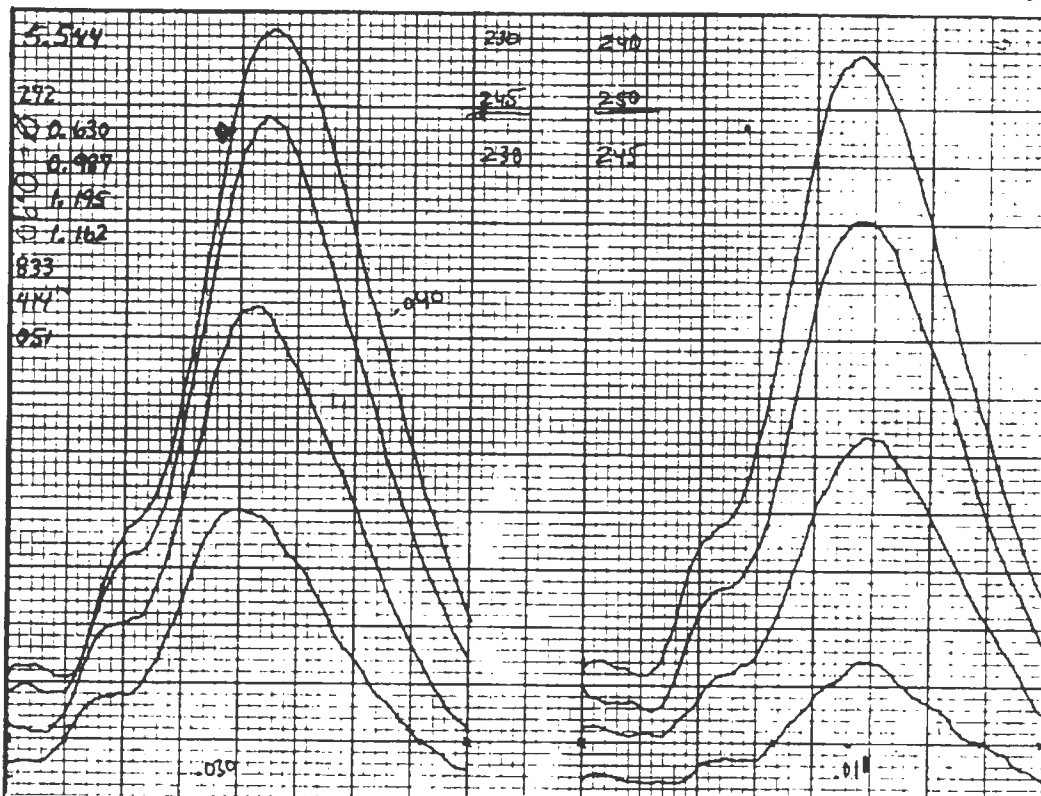
FUEL SIDE HEATED							
SPECTROPHOTOMETER						FUEL/AIR	
SETTINGS						(actual)	
TEST NO.	GAIN	TIME	SCAN	SLIT	SETTING	FUEL/AIR	FLAME
		PERIOD (SEC)	SPEED CM-1/MIN	WIDTH	INITIAL	(stoich) "PHI"	ADDITIVE
1	200	18	1000	0.25	1.95	1.21	NONE
2	200	18	1000	0.25	1.95	1.08	NONE
3	200	18	1000	0.25	1.95	0.98	NONE
4	200	18	1000	0.25	1.95	1.21	NONE
5	200	18	1000	0.25	1.95	1.21	NONE
6	200	18	1000	0.25	1.95	1.08	NONE
7	200	18	1000	0.26	1.95	0.98	NONE
8	200	18	1000	0.25	1.95	1.21	NONE
9	200	18	1000	0.25	1.95	1.08	NONE
10	200	18	1000	0.25	1.95	0.98	NONE
11	200	18	1000	0.25	1.95	1.21	NONE
12	200	18	1000	0.25	1.95	1.08	NONE
13	200	18	1000	0.25	1.95	0.98	NONE
14	200	18	1000	0.25	1.95	1.21	NONE
15	200	18	1000	0.25	1.95	1.08	NONE
16	200	18	1000	0.25	1.95	0.98	NONE
17	200	18	1000	0.25	1.95	1.21	NONE
18	200	18	1000	0.25	1.95	1.21	K
19	200	18	1000	0.25	1.95	1.08	K
20	200	18	1000	0.25	1.95	0.98	K
21	200	18	1000	0.25	1.95	1.21	K
22	200	18	1000	0.25	1.95	1.08	K
23	200	18	1000	0.25	1.95	0.98	K
24	200	18	1000	0.25	1.95	1.21	K
25	200	18	1000	0.25	1.95	1.08	K
26	200	18	1000	0.25	1.95	0.98	K
27	200	18	1000	0.25	1.95	1.21	K
28	200	18	1000	0.25	1.95	1.08	K
29	200	18	1000	0.25	1.95	0.98	K
30	200	18	1000	0.25	1.95	1.21	K
31	200	18	1000	0.25	1.95	1.08	K
32	200	18	1000	0.25	1.95	0.98	K
33	200	18	1000	0.25	1.95	1.21	K
34	200	18	1000	0.25	1.95	1.08	K
35	200	18	1000	0.25	1.95	0.98	K
36	200	18	1000	0.25	1.95	1.21	NONE
37	200	18	1000	0.25	1.95	1.21	NONE
38	200	18	1000	0.25	1.95	1.21	NONE
39	200	18	1000	0.25	1.95	1.08	NONE
40	200	18	1000	0.25	1.95	0.98	NONE
41	200	18	1000	0.25	1.95	1.21	NONE
42	200	18	1000	0.25	1.95	1.08	NONE
43	200	18	1000	0.25	1.95	0.98	NONE
44	200	18	1000	0.25	1.95	1.21	NONE
45	200	18	1000	0.25	1.95	1.08	NONE
46	200	18	1000	0.25	1.95	0.98	NONE

	FUEL	SIDE	HEATED			
BURNER TEMPERATURE						
(DEGREES CELSIUS)						
TEST	INITIAL	INITIAL	FINAL	FINAL	AVERAGE	AVERAGE
NUMBER	TEMP	TEMP	TEMP	TEMP	TEMP	TEMP
	AT 6"	AT 7.75"	AT 6"	AT 7.75"	AT 6"	AT 7.75"
1	155	180	175	195	165	188
2	200	210	215	225	208	218
3	230	240	245	250	238	245
4	255	255	265	260	260	258
5	135	155	150	175	143	165
6	155	185	170	195	163	190
7	175	200	180	215	178	208
8	190	215	200	220	195	218
9	200	225	210	225	205	225
10	210	230	220	240	215	235
11	225	240	235	245	230	243
12	240	245	250	255	245	250
13	255	255	265	265	260	260
14	265	270	275	275	270	272
15	280	280	300	300	290	290
16	300	305	325	325	312	315
17	325	330	345	350	335	340
18	090	120	110	145	100	133
19	120	155	135	170	128	163
20	145	175	170	200	158	188
21	175	200	195	210	185	205
22	200	220	210	225	205	223
23	210	230	225	240	218	235
24	225	245	230	245	228	245
25	230	245	235	250	232	248
26	240	255	250	255	245	255
27	250	260	260	260	255	260
28	265	270	275	275	270	272
29	275	280	290	305	282	292
30	295	315	305	320	300	318
31	310	315	315	315	313	315
32	315	320	325	330	320	325
33	325	330	330	335	328	333
34	330	340	340	350	335	345
35	340	350	345	350	343	350
36	080	105	105	130	092	118
37	115	145	130	170	122	158
38	275	280	270	290	272	285
39	280	300	280	295	280	298
40	300	325	310	335	305	330
41	100	120	125	150	113	135
42	130	155	150	175	140	165
43	155	180	180	200	168	190
44	190	205	205	220	198	213
45	215	225	225	235	220	230
46	225	240	235	250	230	245

FUEL SIDE HEATED									
INTEGRATED SPECTRAL AREA									AREA
TEST	SCAN	SCAN	SCAN	SCAN	SCAN	SCAN	SCAN	SCAN	CALC'D
NO.	1	2	3	4	5	6	7	8	1-8
1	0.121	0.358	0.592	0.800	0.818	0.607	0.310	0.030	3.651
2	0.171	0.438	0.755	0.957	0.964	0.723	0.383	0.047	4.474
3	0.272	0.630	0.987	1.195	1.162	0.833	0.414	0.051	5.586
4	0.125	0.352	0.610	0.801	0.855	0.696	0.392	0.064	3.918
5	0.081	0.260	0.500	0.670	0.711	0.555	0.281	0.020	3.101
6	0.141	0.390	0.670	0.874	0.882	0.649	0.335	0.031	4.000
7	0.270	0.588	0.939	1.150	1.095	0.781	0.376	0.031	5.273
8	0.113	0.302	0.535	0.719	0.762	0.603	0.338	0.031	3.434
9	0.153	0.389	0.684	0.893	0.911	0.707	0.372	0.038	4.178
10	0.264	0.586	0.920	1.151	1.095	0.795	0.390	0.047	5.278
11	0.109	0.298	0.538	0.730	0.772	0.604	0.332	0.040	3.449
12	0.171	0.420	0.715	0.929	0.968	0.760	0.410	0.052	4.459
13	0.236	0.566	0.909	1.140	1.119	0.837	0.440	0.049	5.333
14	0.093	0.289	0.525	0.722	0.810	0.685	0.400	0.064	3.611
15	0.151	0.404	0.688	0.912	0.972	0.786	0.459	0.077	4.479
16	0.235	0.545	0.901	1.141	1.170	0.912	0.494	0.082	5.520
17	0.099	0.302	0.536	0.751	0.849	0.731	0.457	0.086	3.835
18	0.125	0.346	0.563	0.717	0.646	0.409	0.146	0.000	2.955
19	0.226	0.487	0.759	0.865	0.741	0.464	0.183	0.000	3.756
20	0.359	0.695	0.976	1.056	0.869	0.522	0.190	0.000	4.707
21	0.166	0.371	0.597	0.723	0.654	0.447	0.183	0.003	3.163
22	0.249	0.494	0.780	0.908	0.812	0.527	0.228	0.011	4.052
23	0.369	0.718	1.005	1.129	0.953	0.592	0.248	0.007	5.064
24	0.180	0.408	0.623	0.770	0.721	0.492	0.230	0.010	3.459
25	0.251	0.521	0.792	0.915	0.841	0.541	0.241	0.008	4.157
26	0.350	0.690	0.997	1.105	0.950	0.599	0.236	0.007	4.978
27	0.154	0.370	0.592	0.743	0.711	0.487	0.219	0.006	3.305
28	0.225	0.486	0.748	0.890	0.827	0.545	0.231	0.008	3.994
29	0.341	0.669	1.000	1.112	0.959	0.600	0.259	0.005	5.003
30	0.169	0.378	0.629	0.783	0.769	0.541	0.236	0.009	3.545
31	0.141	0.364	0.640	0.822	0.816	0.582	0.270	0.011	3.675
32	0.263	0.588	0.914	1.130	1.031	0.671	0.279	0.010	4.915
33	0.130	0.338	0.580	0.769	0.755	0.559	0.277	0.013	3.442
34	0.193	0.466	0.730	0.911	0.880	0.625	0.296	0.019	4.146
35	0.323	0.640	0.972	1.130	1.068	0.710	0.315	0.020	5.237
36	0.140	0.358	0.588	0.714	0.651	0.421	0.191	0.006	3.093
37	0.165	0.388	0.633	0.760	0.671	0.452	0.198	0.011	3.297
38	0.149	0.385	0.677	0.853	0.837	0.622	0.332	0.039	3.926
39	0.241	0.557	0.906	1.094	1.049	0.779	0.408	0.058	5.131
40	0.356	0.756	1.125	1.324	1.196	0.822	0.394	0.042	6.057
41	0.178	0.397	0.579	0.742	0.735	0.501	0.256	0.028	3.443
42	0.322	0.553	0.799	0.988	0.848	0.592	0.285	0.040	4.454
43	0.430	0.791	1.081	1.194	1.020	0.676	0.323	0.035	5.603
44	0.226	0.460	0.690	0.842	0.791	0.572	0.289	0.046	3.941
45	0.303	0.599	0.870	1.010	0.921	0.670	0.329	0.054	4.786
46	0.420	0.770	1.113	1.220	1.071	0.719	0.351	0.042	5.774



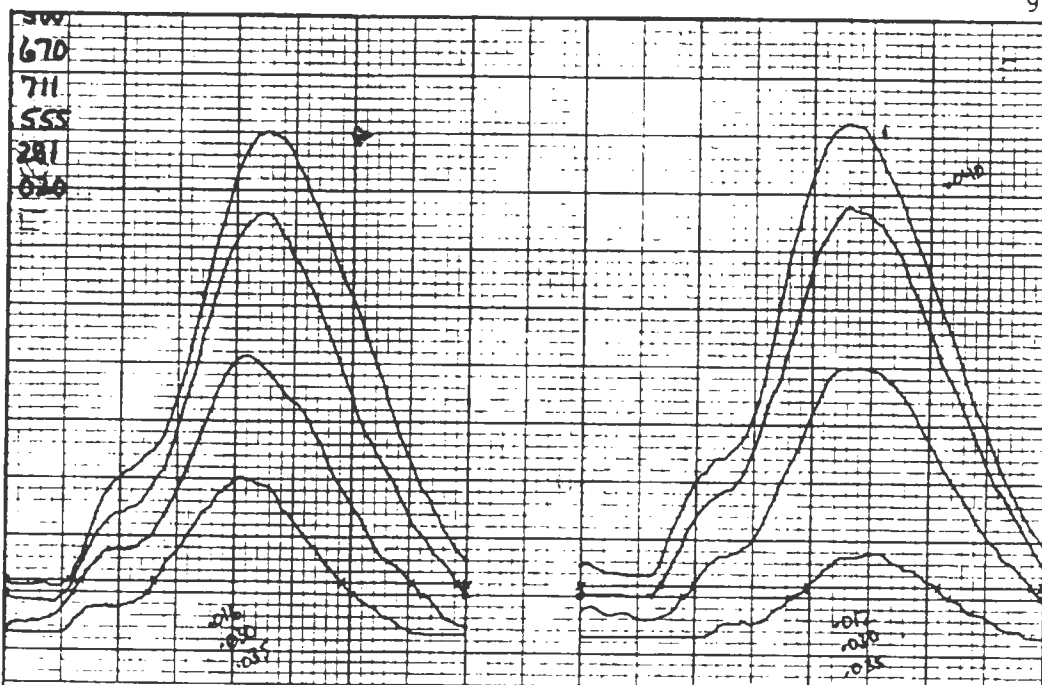
Test number 2



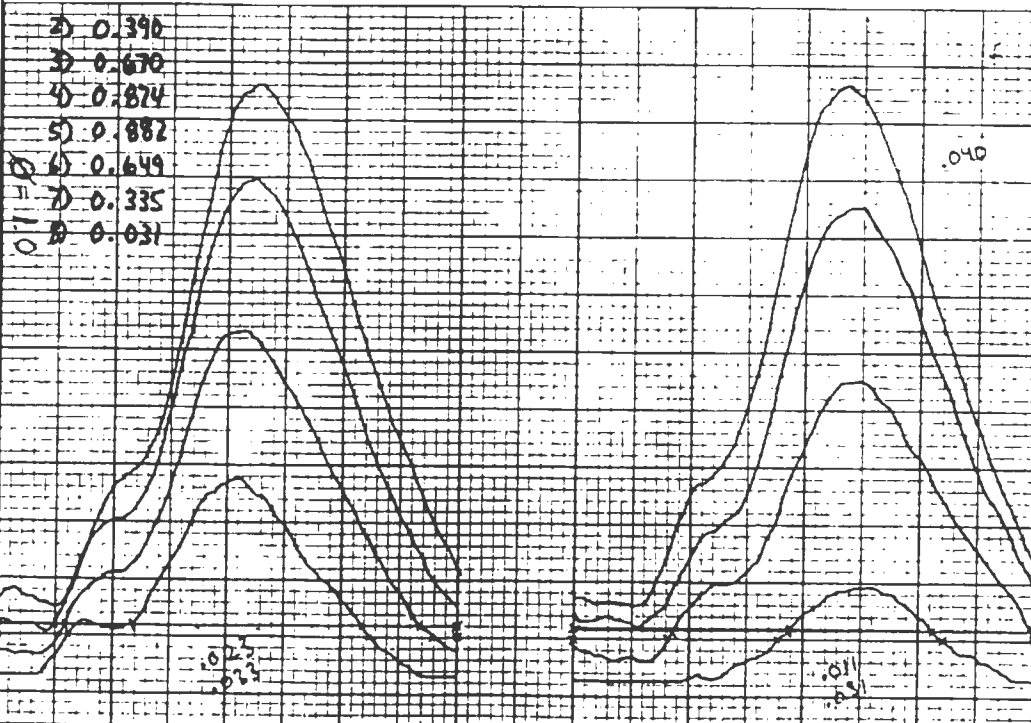
Test number 3



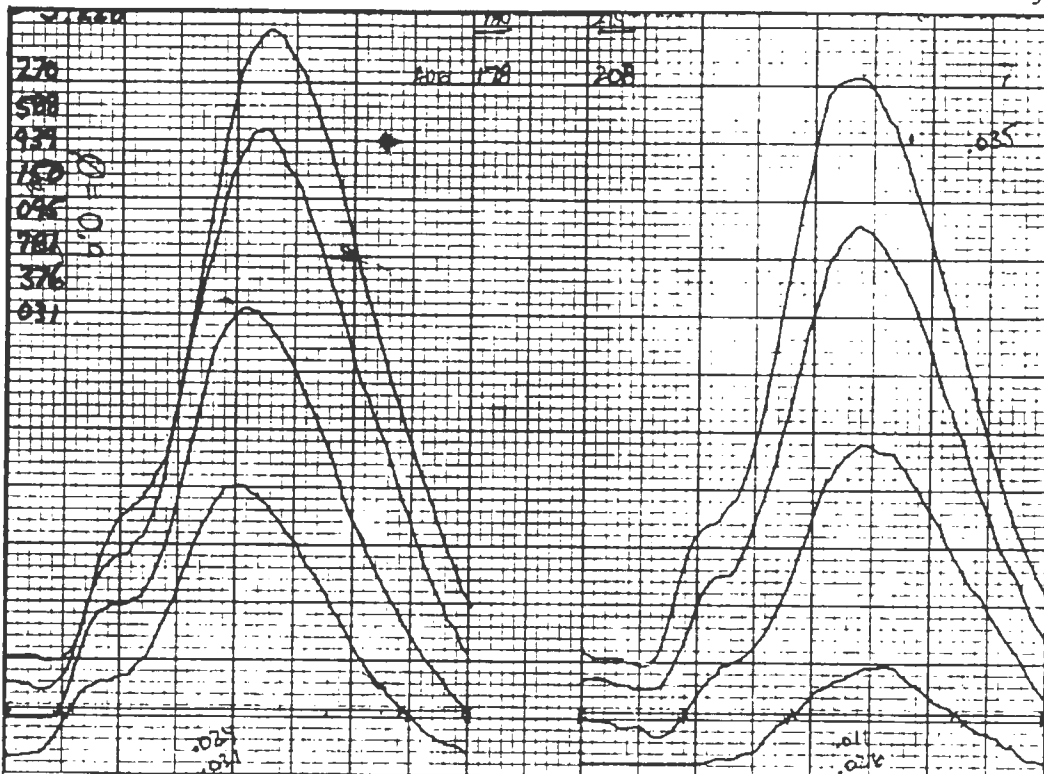
Test number 4



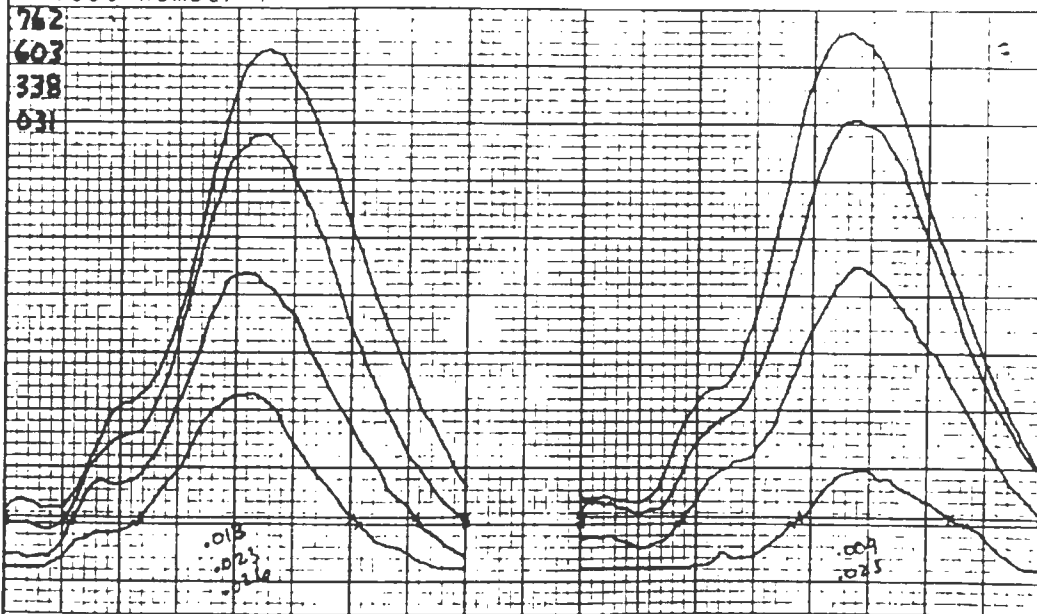
Test number 5



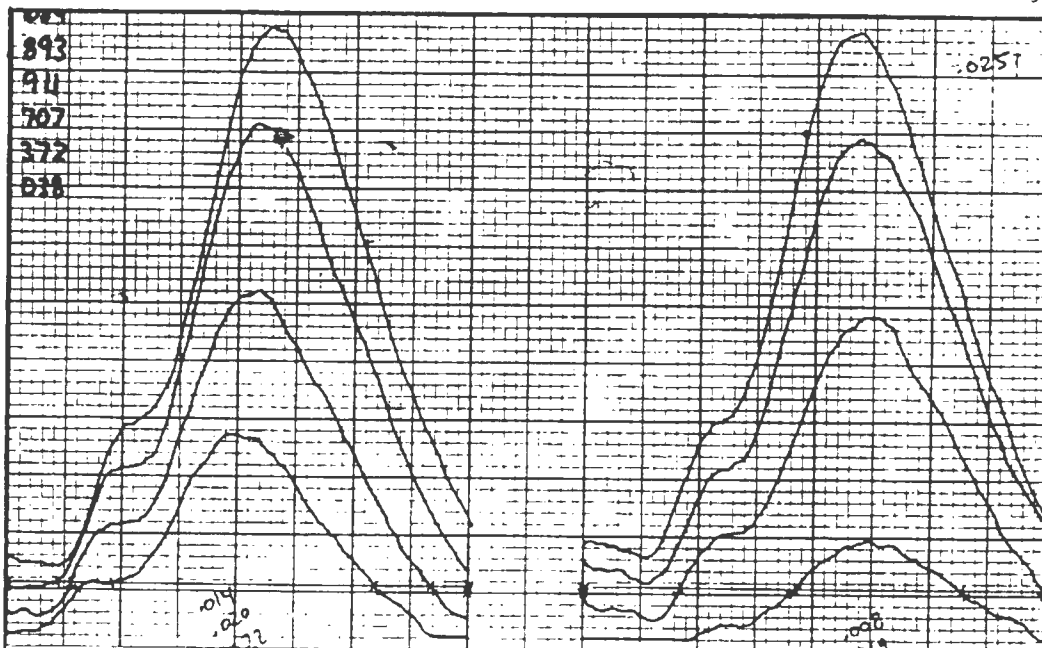
Test number 6



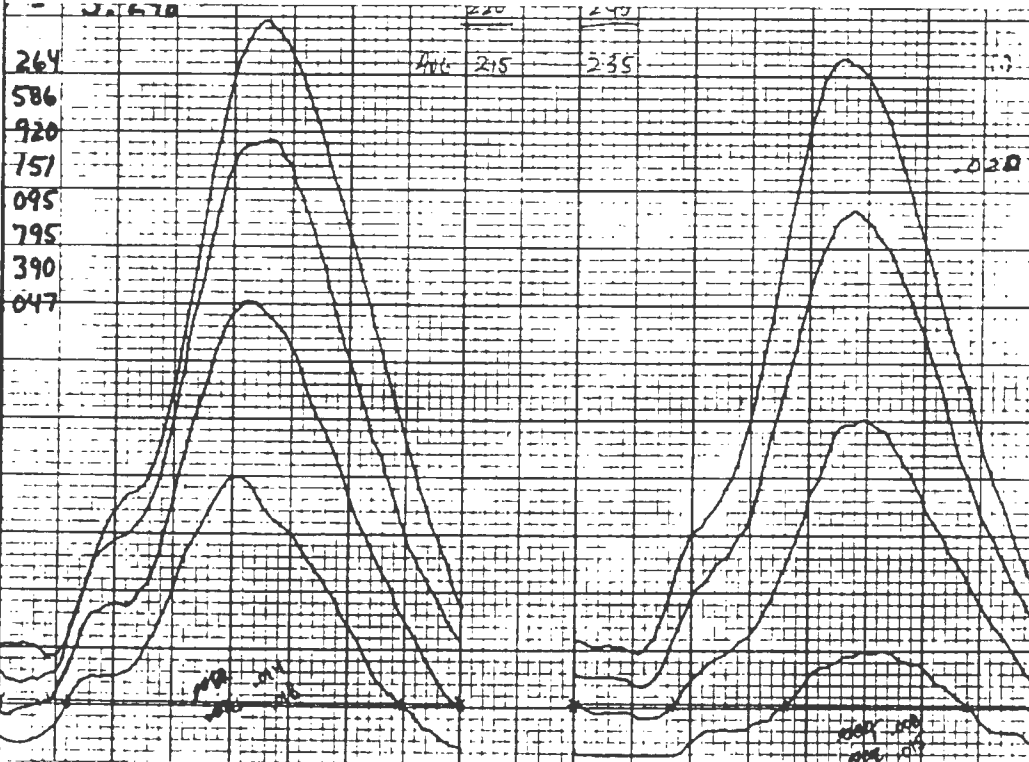
Test number 7



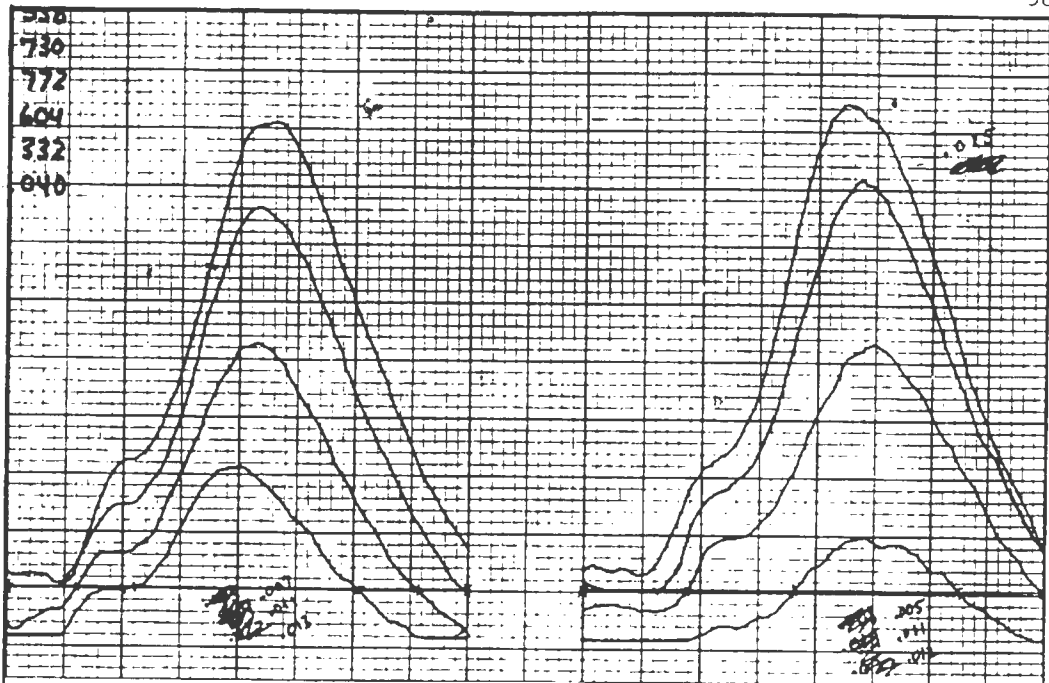
Test number 8



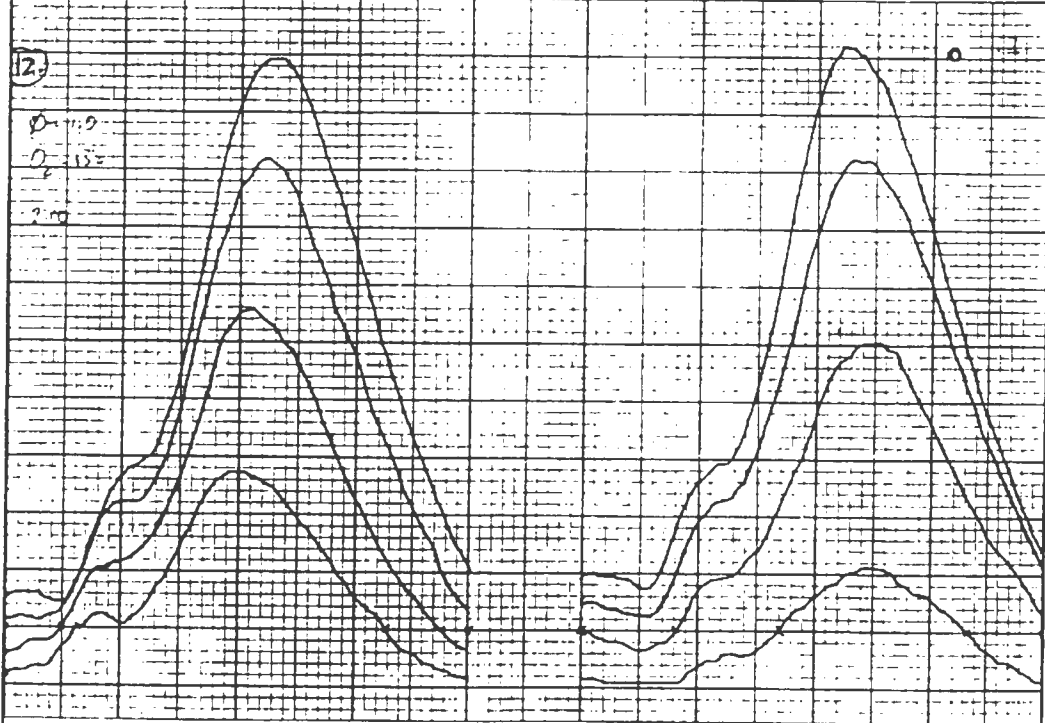
Test number 9



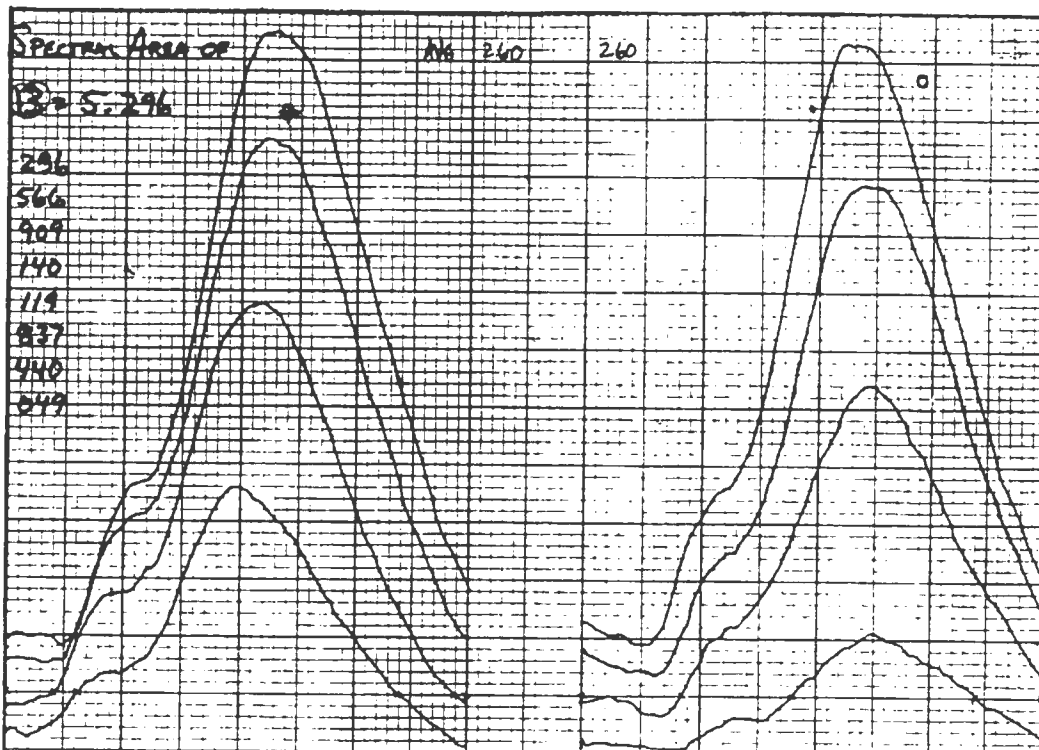
Test number 10



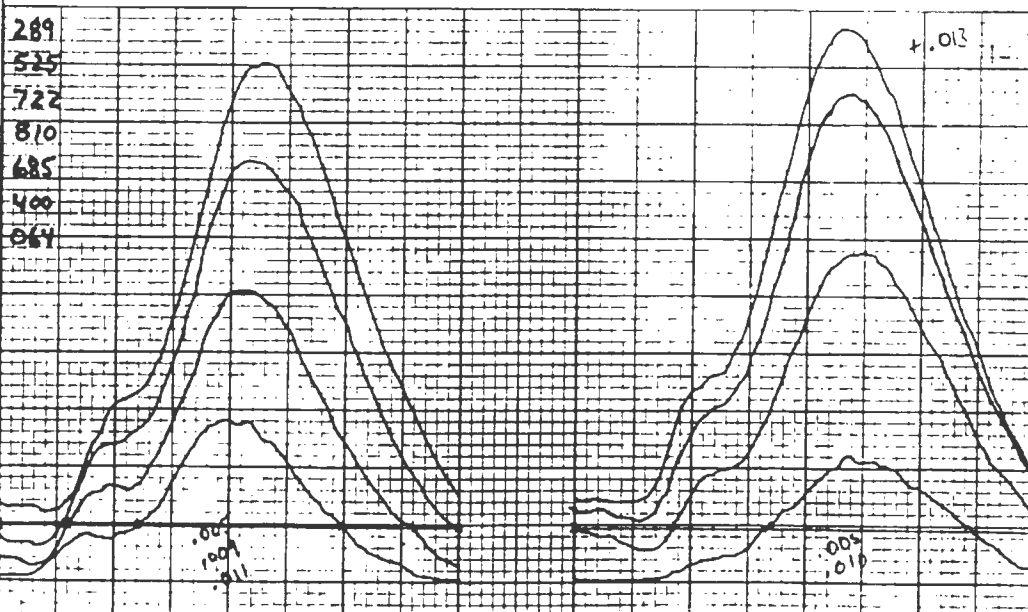
Test number 11



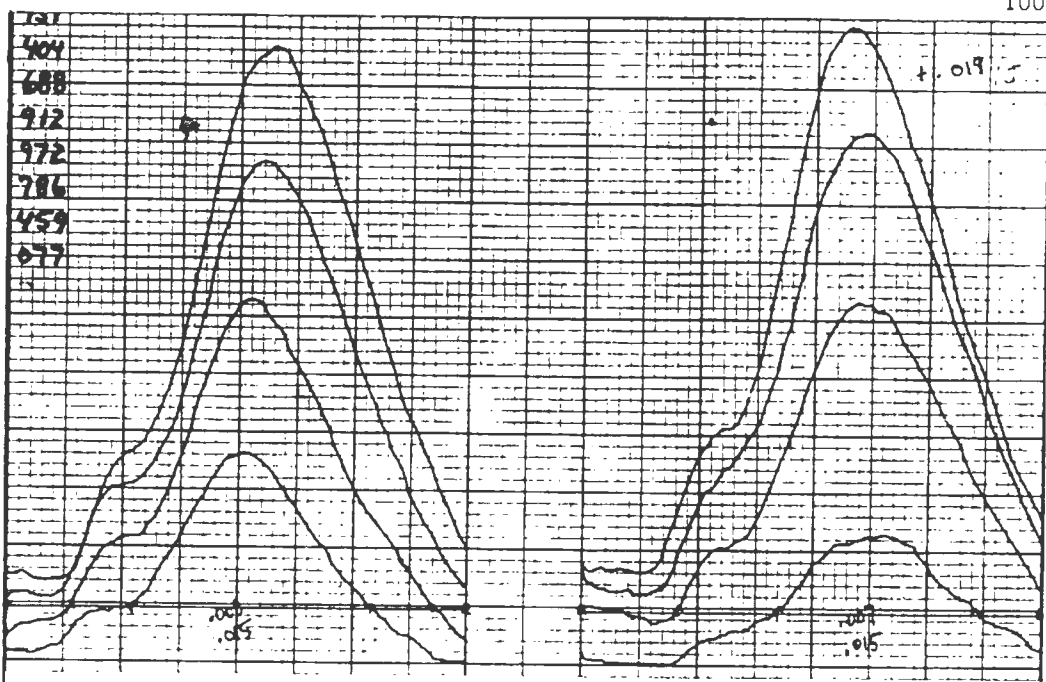
Test number 12



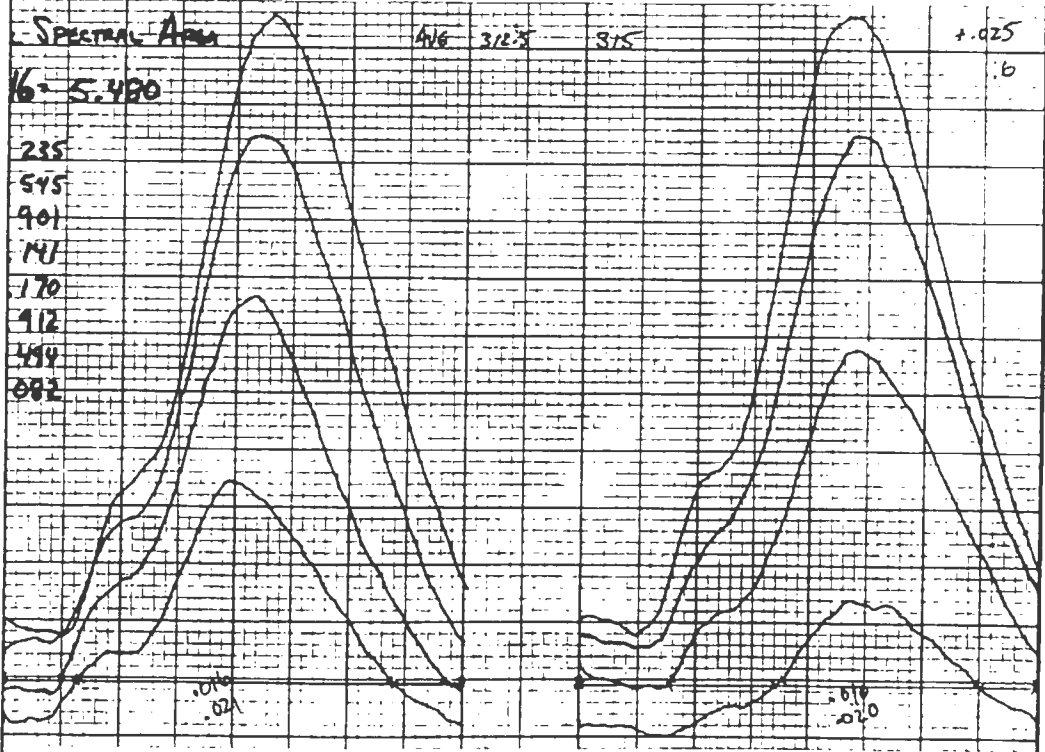
Test number 13



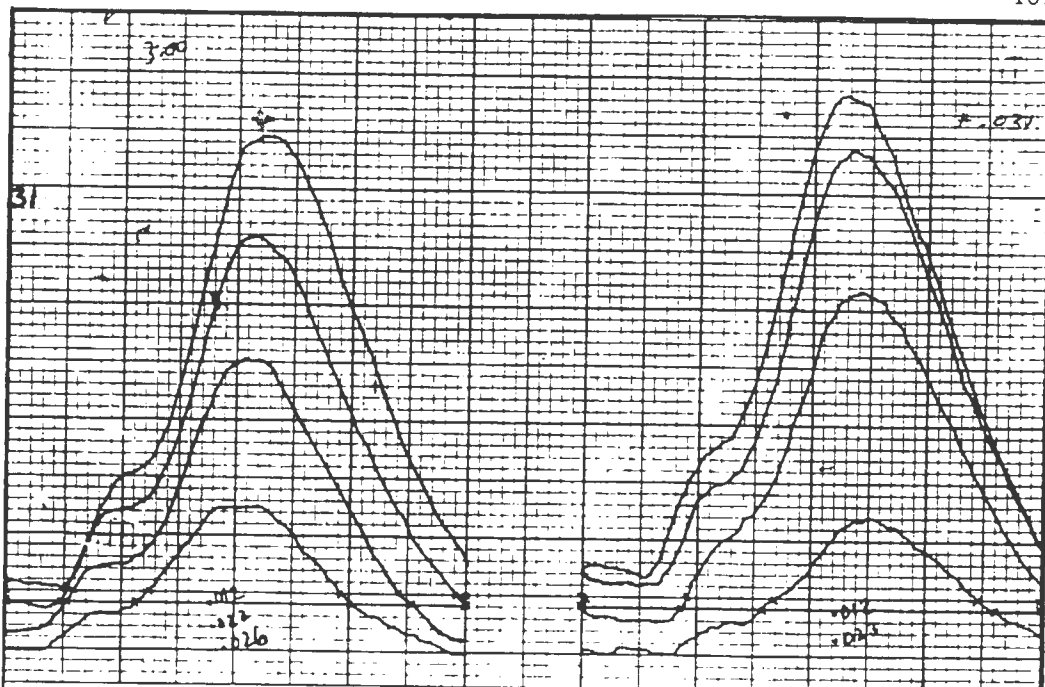
Test number 14



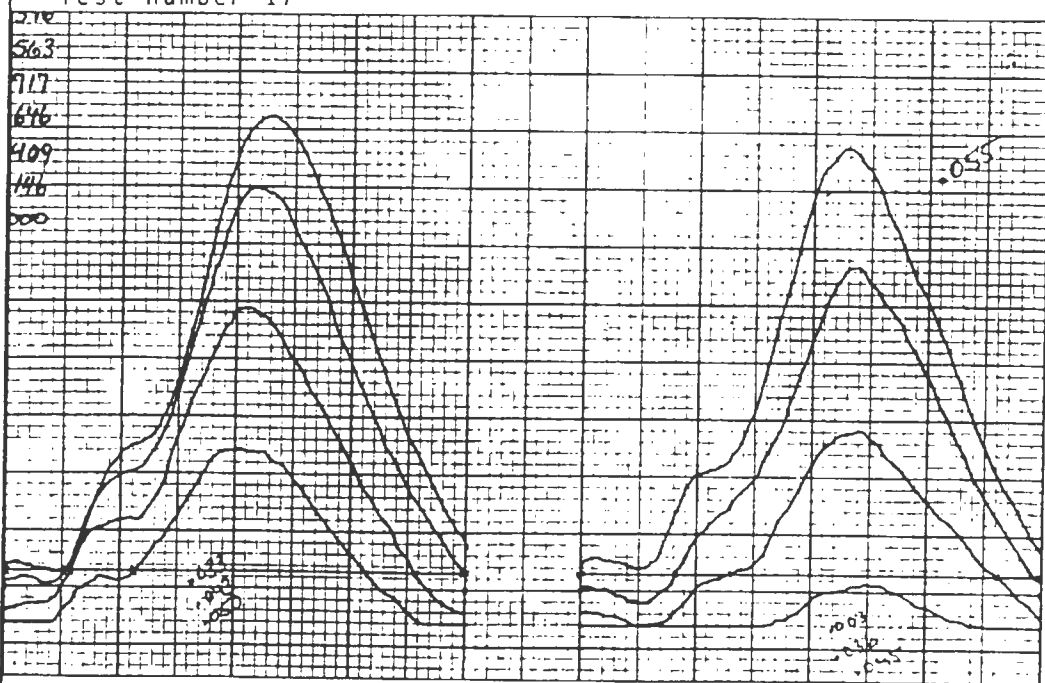
Test number 15



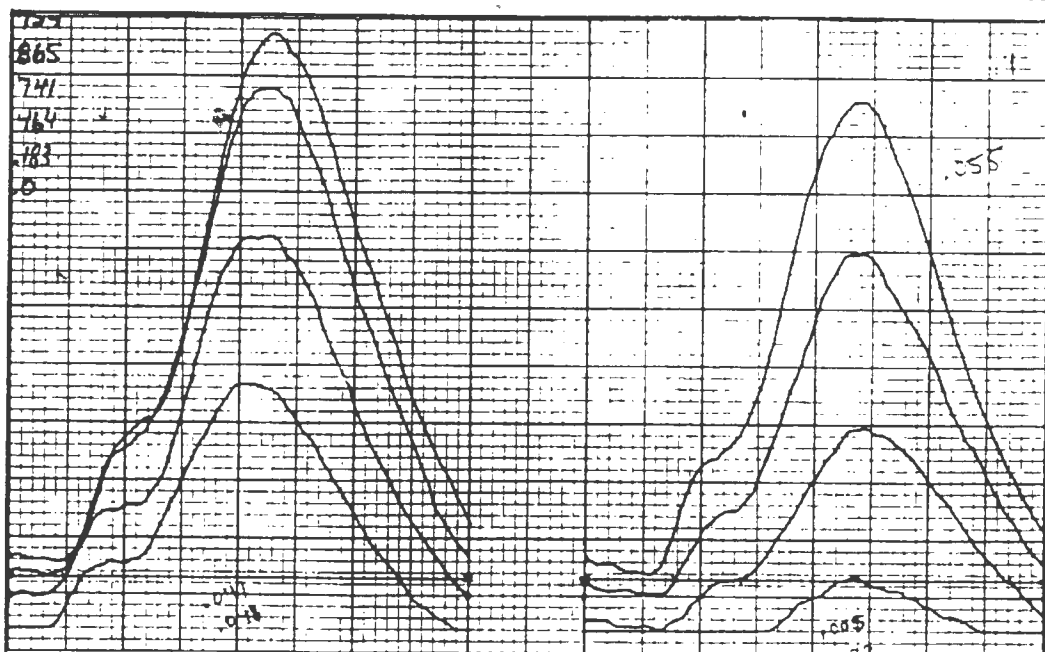
Test number 16



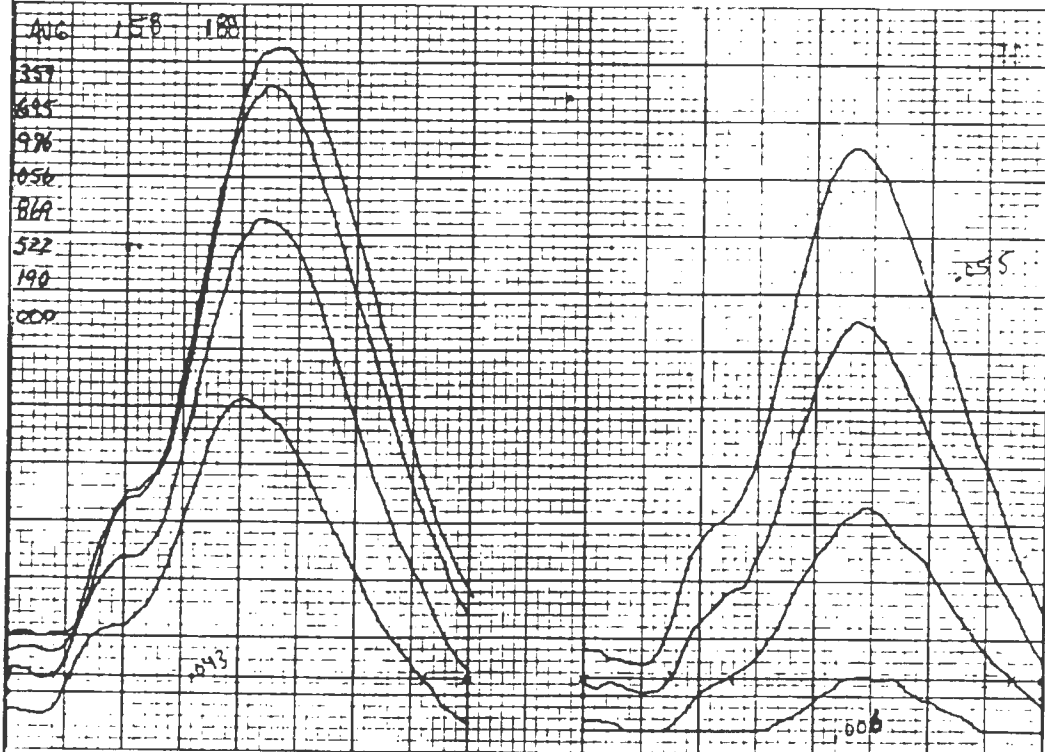
Test number 17



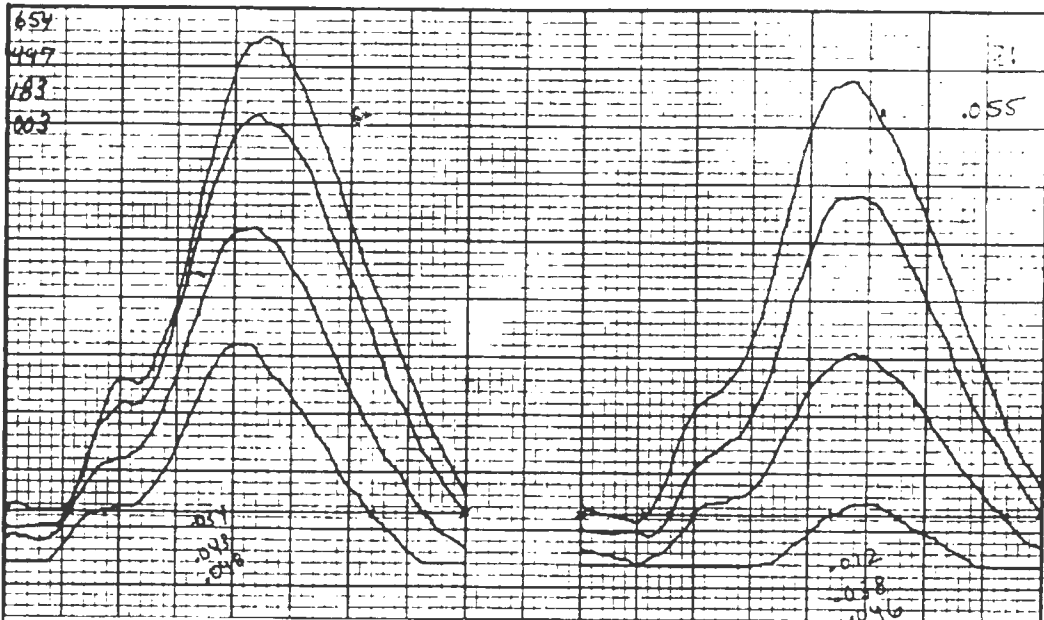
Test number 18



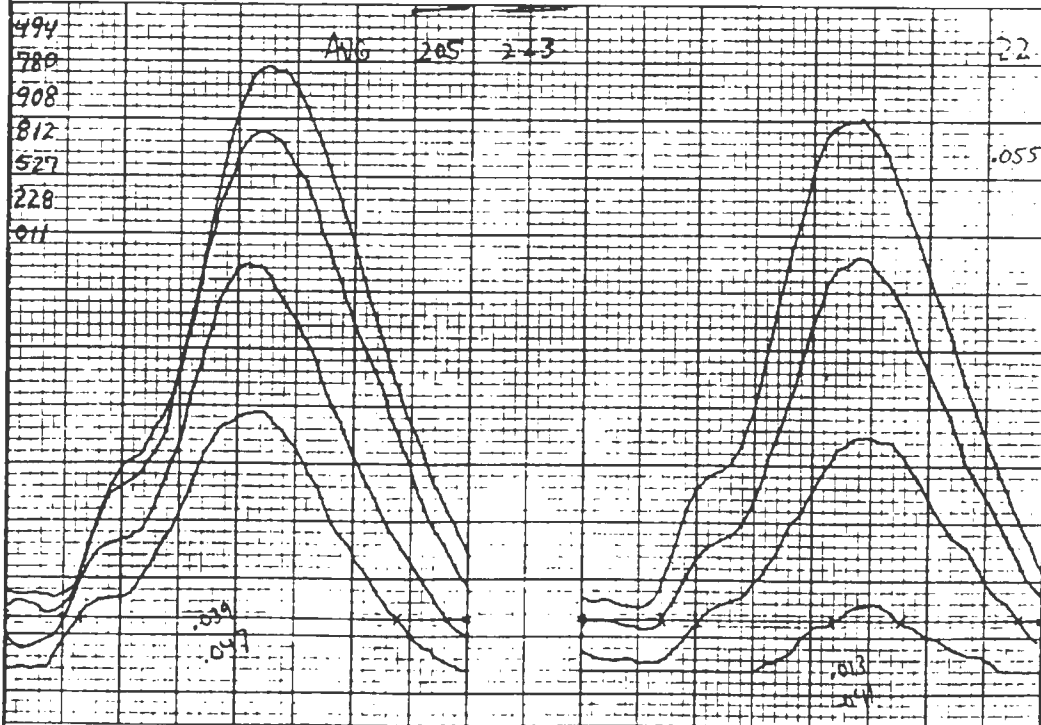
Test number 19



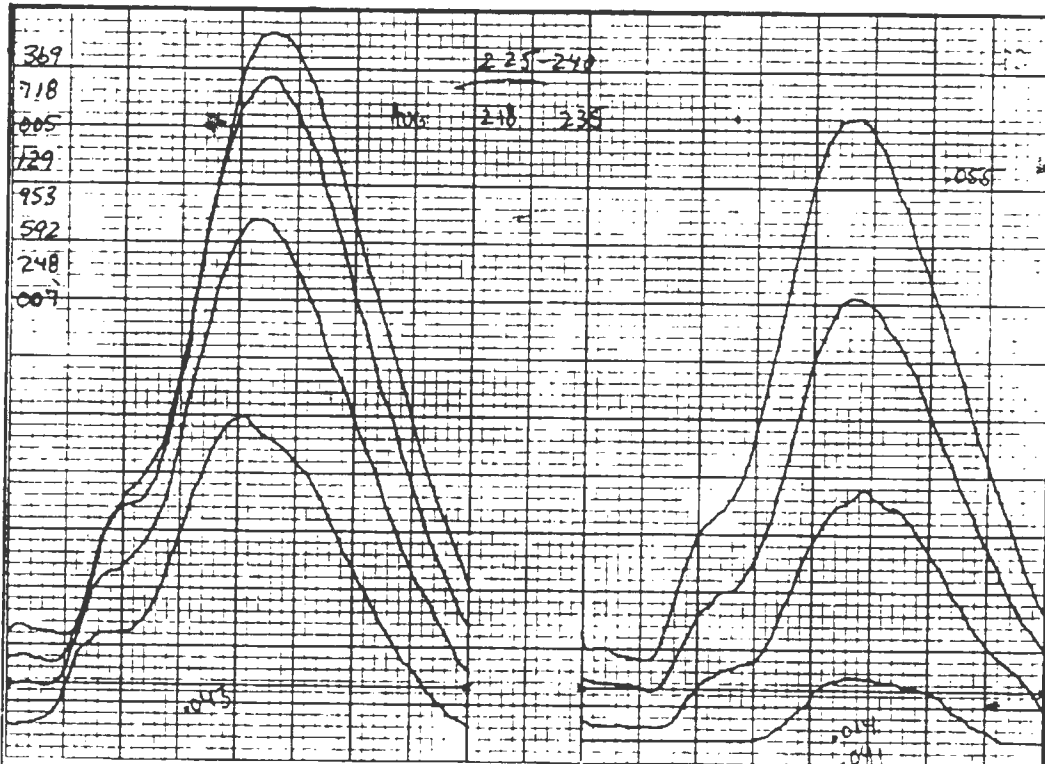
Test number 20



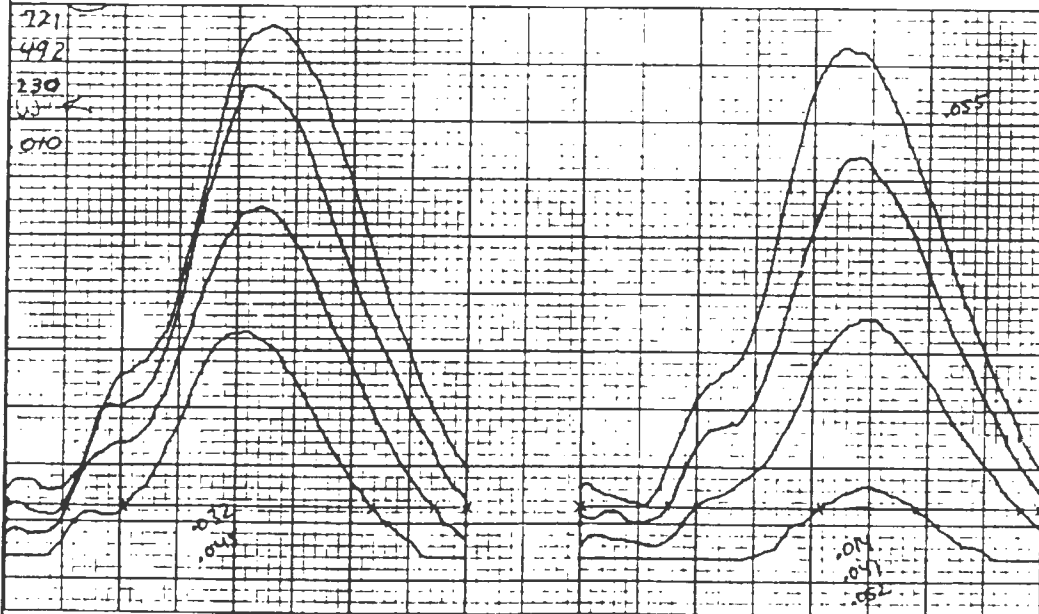
Test number 21



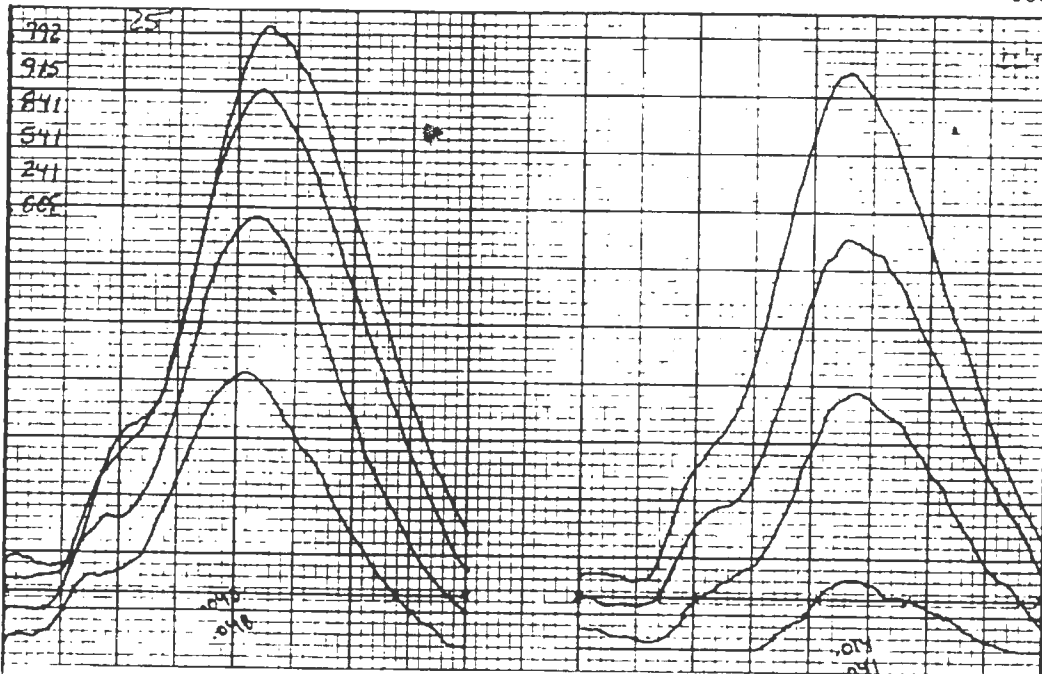
Test number 22



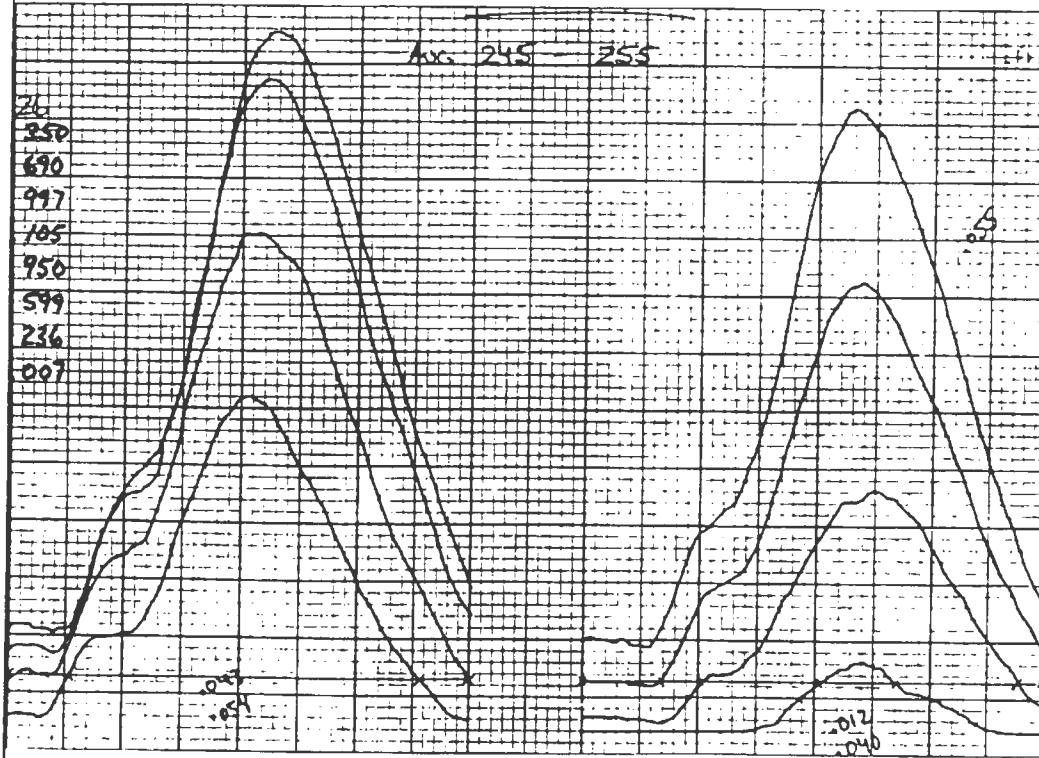
Test number 23



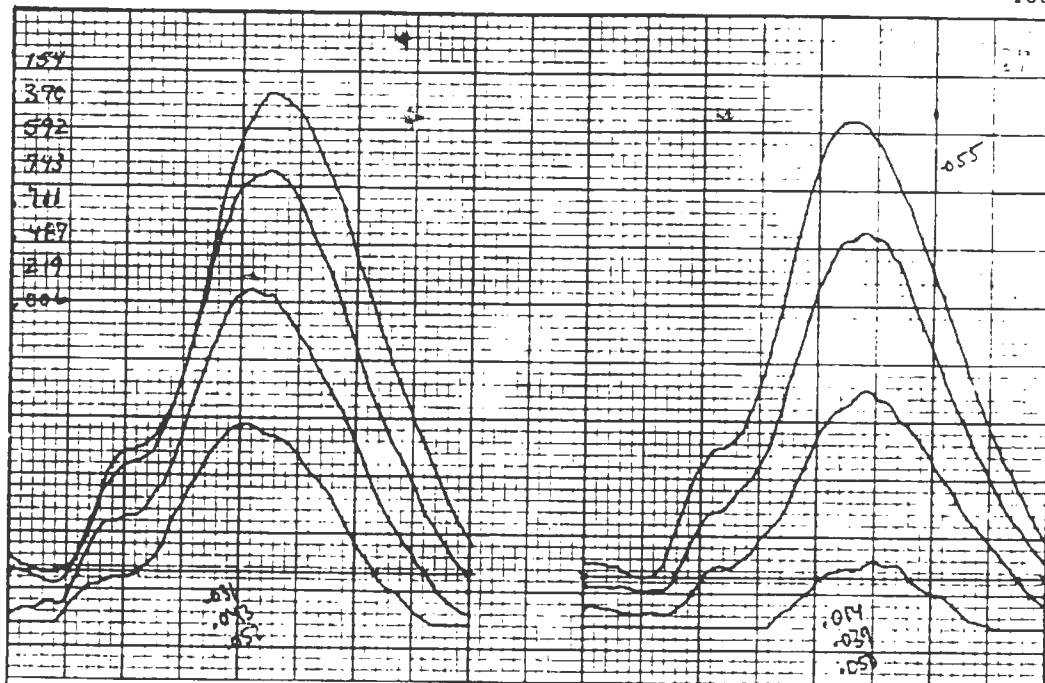
Test number 24



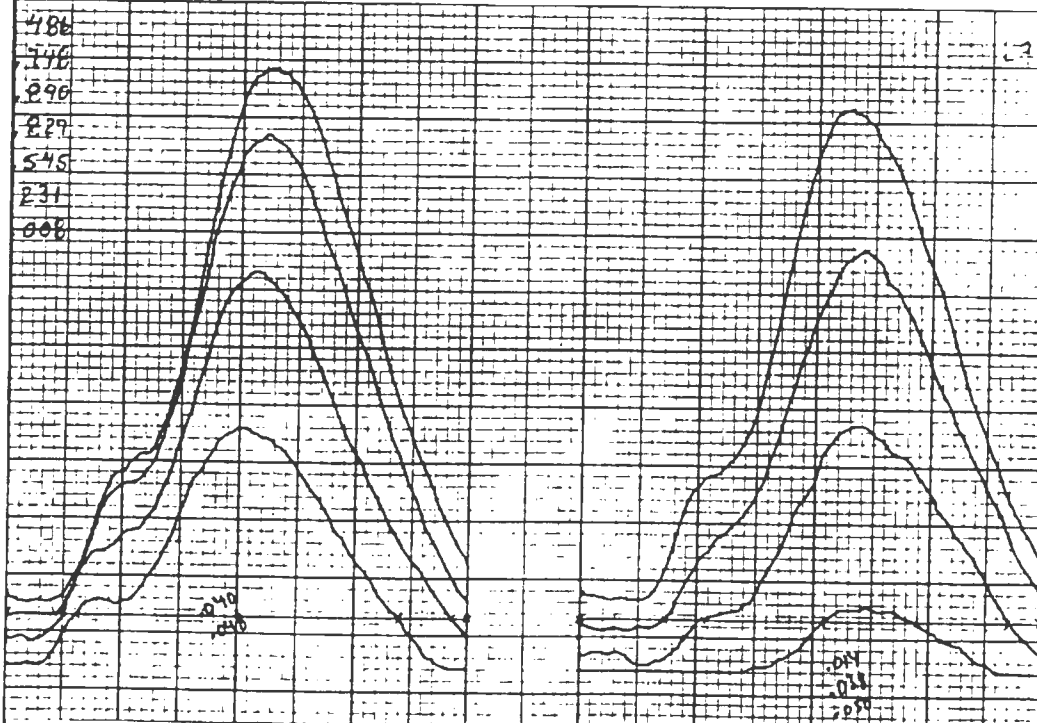
Test number 25



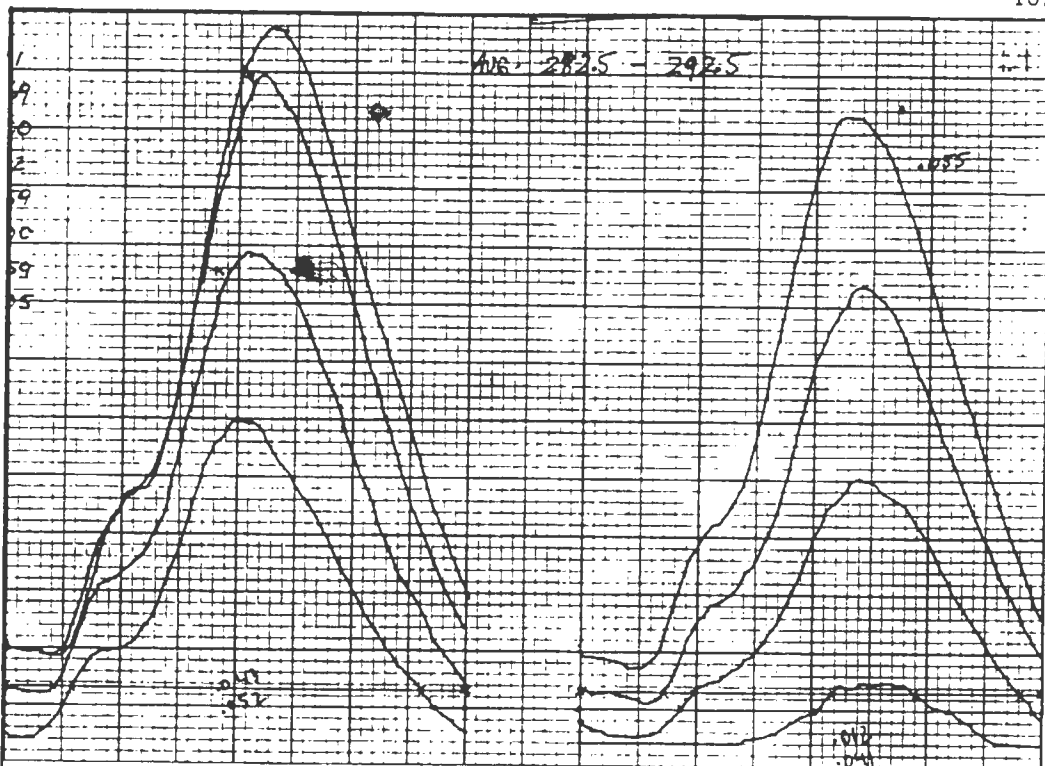
Test number 26



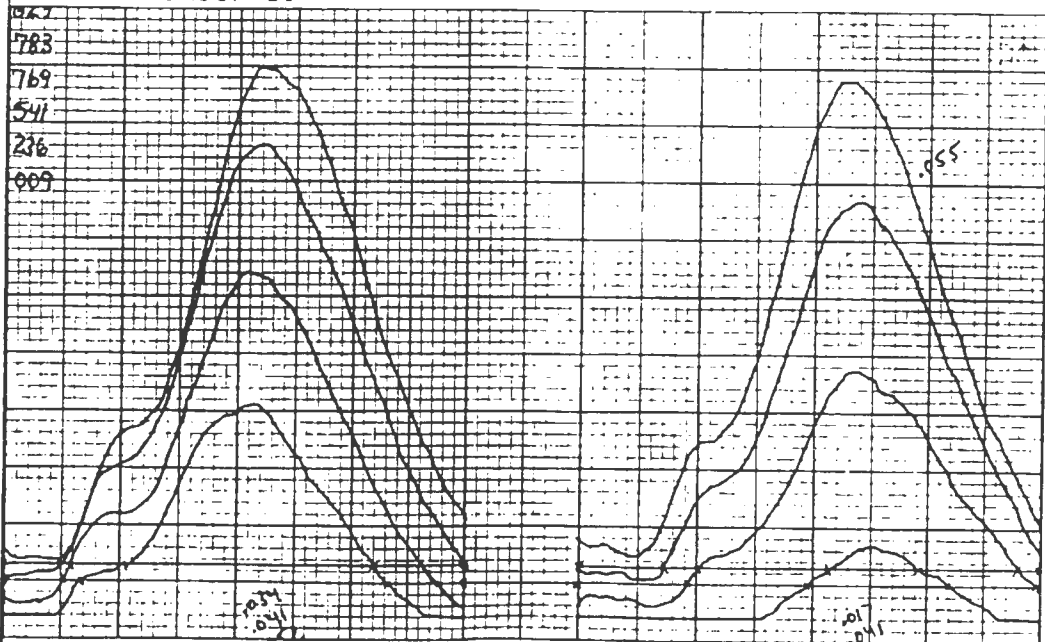
Test number 27



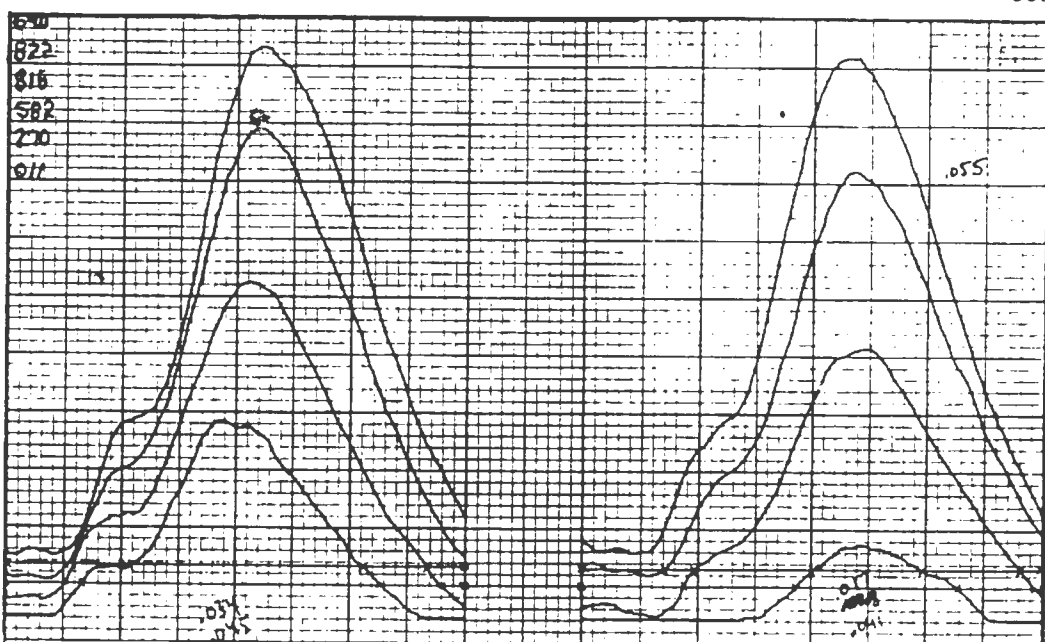
Test number 28



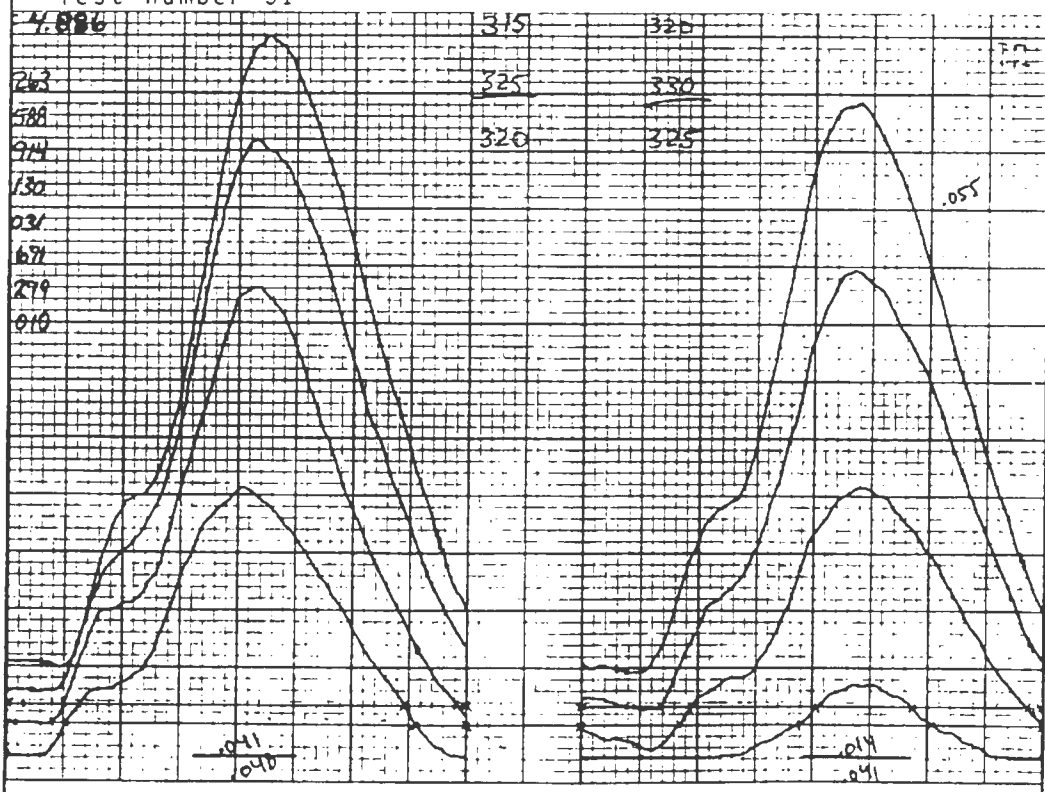
Test number 29



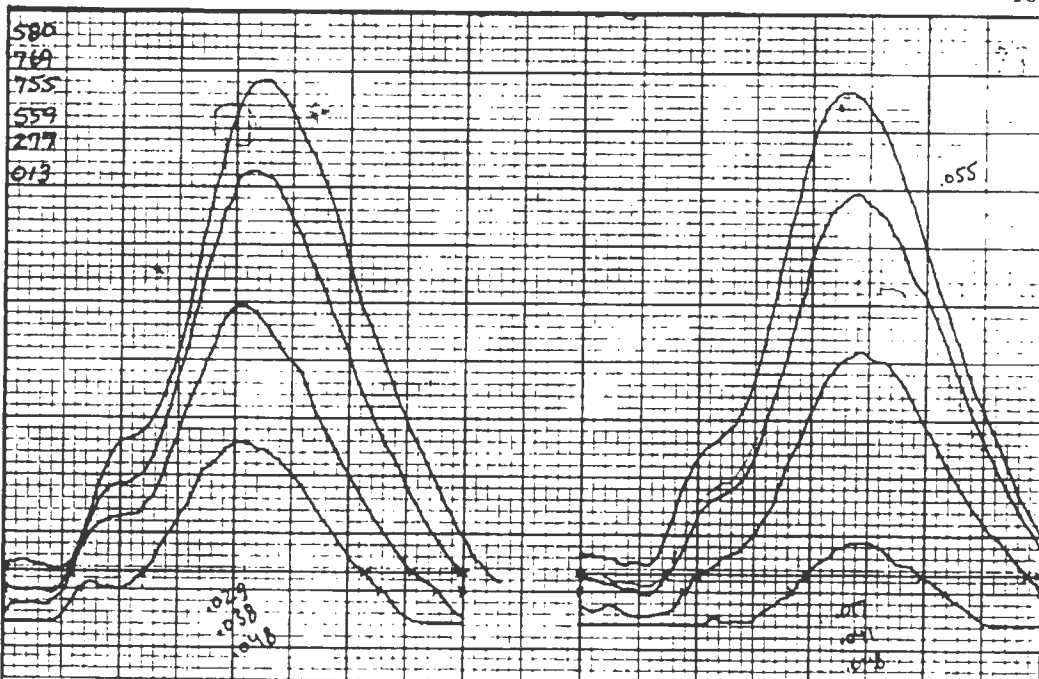
Test number 30



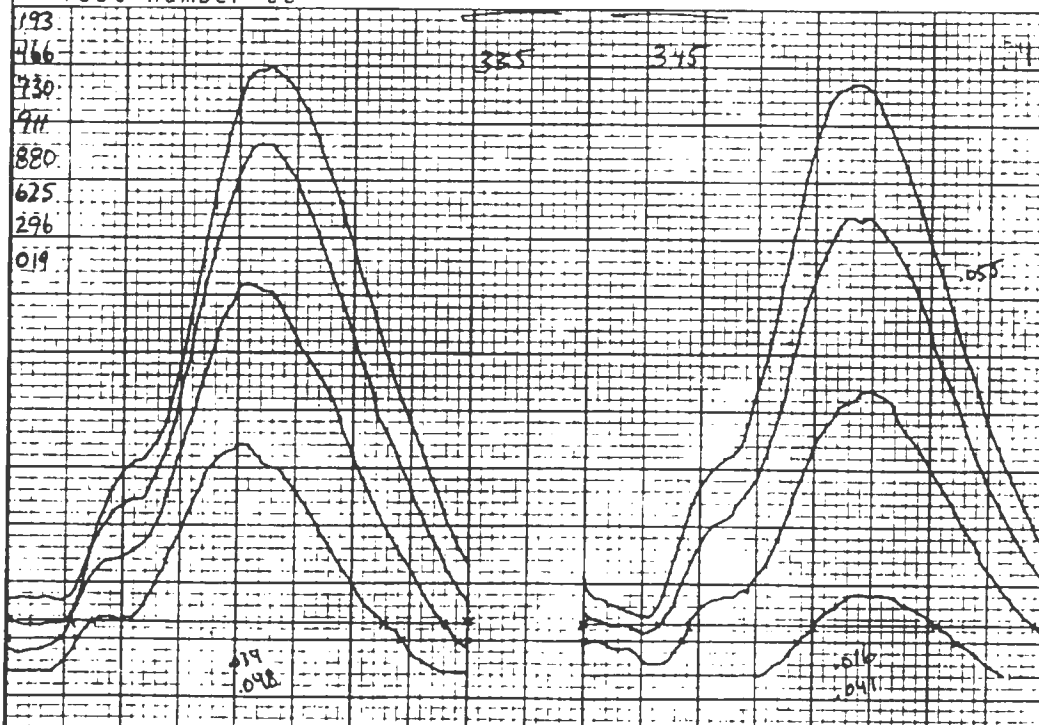
Test number 31



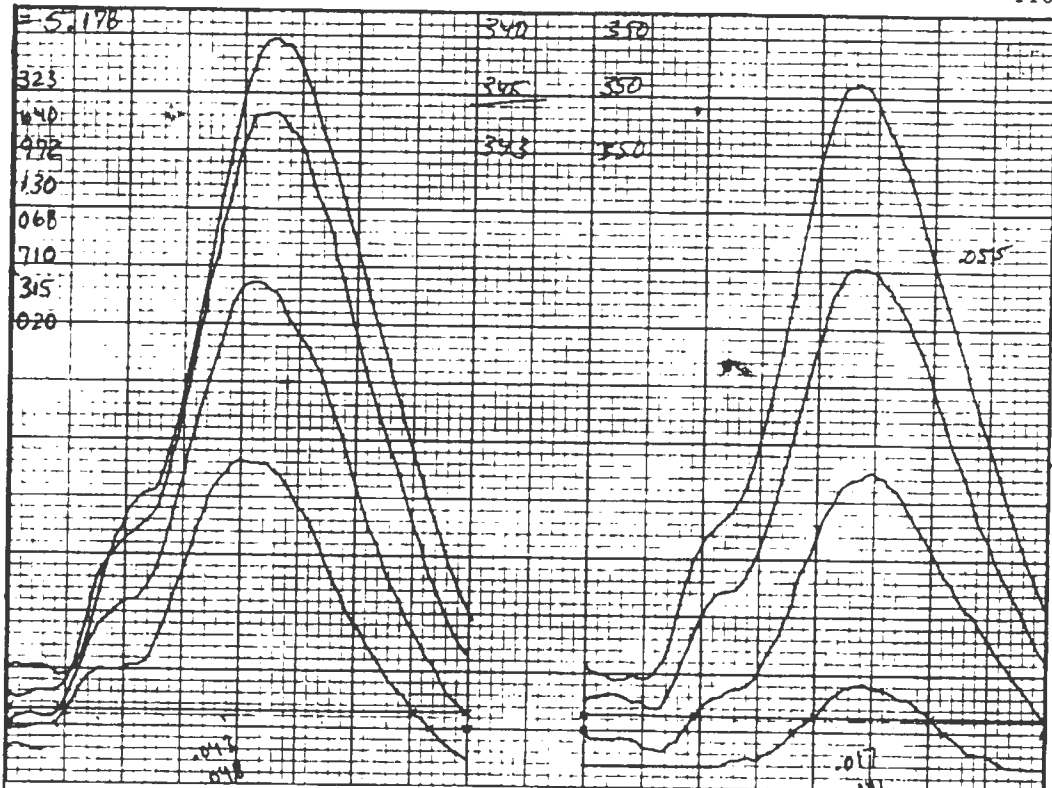
Test number 32



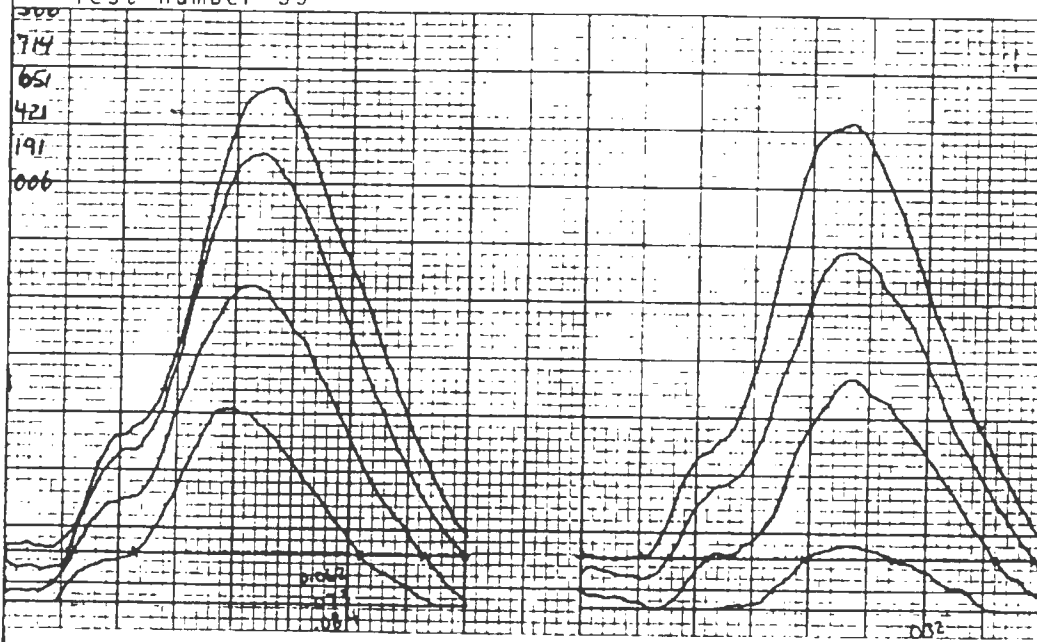
Test number 23



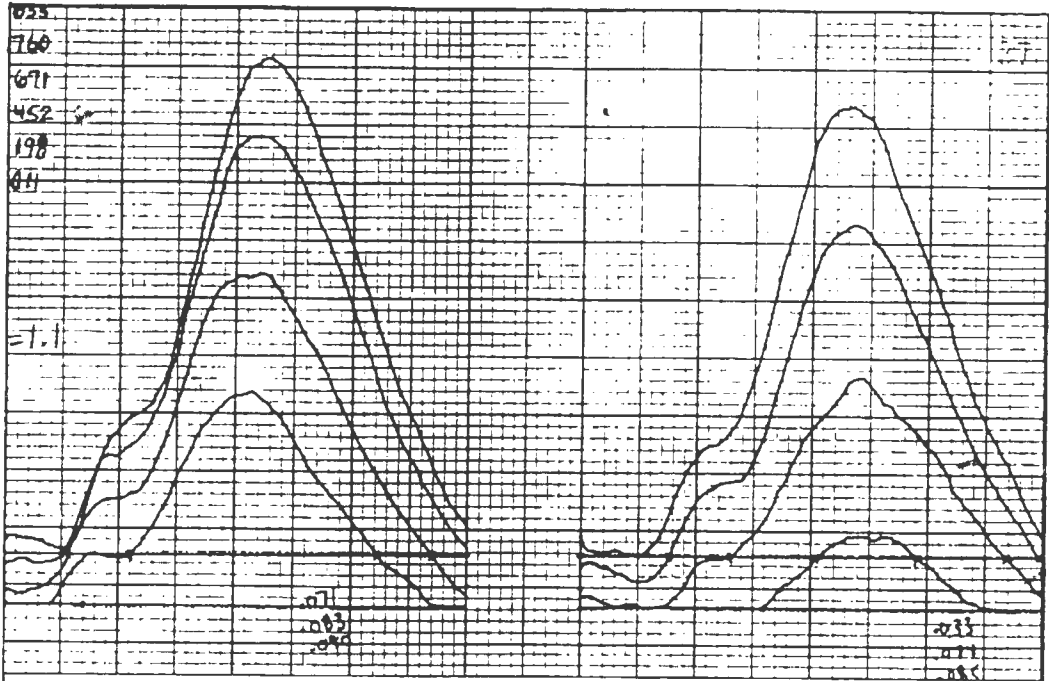
Test number 34



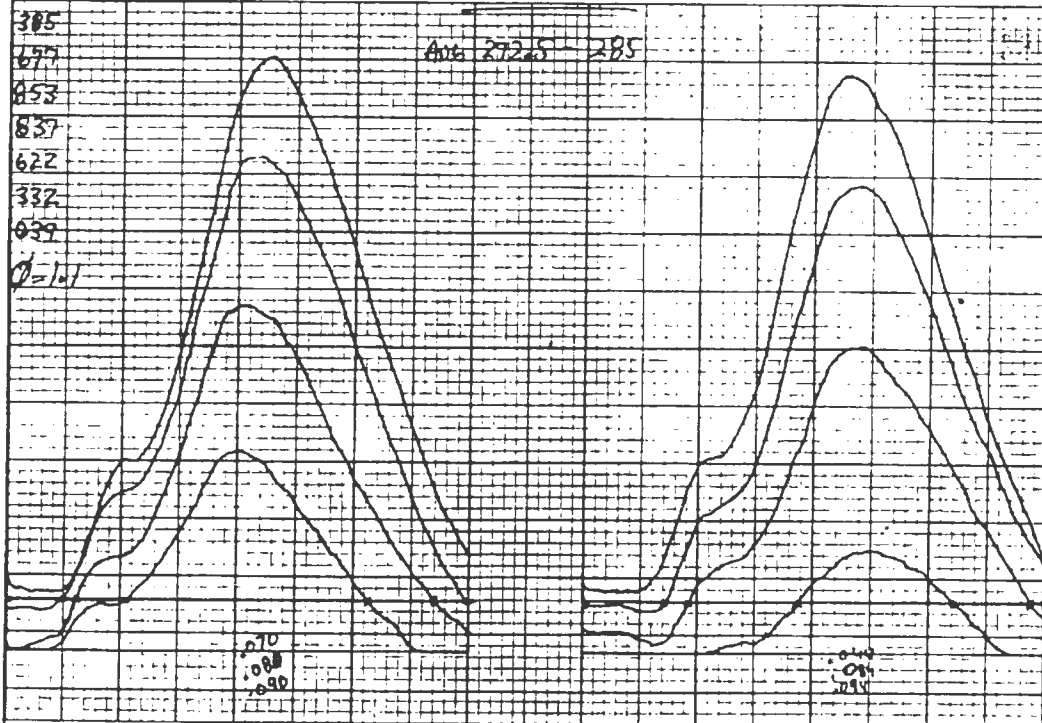
Test number 35



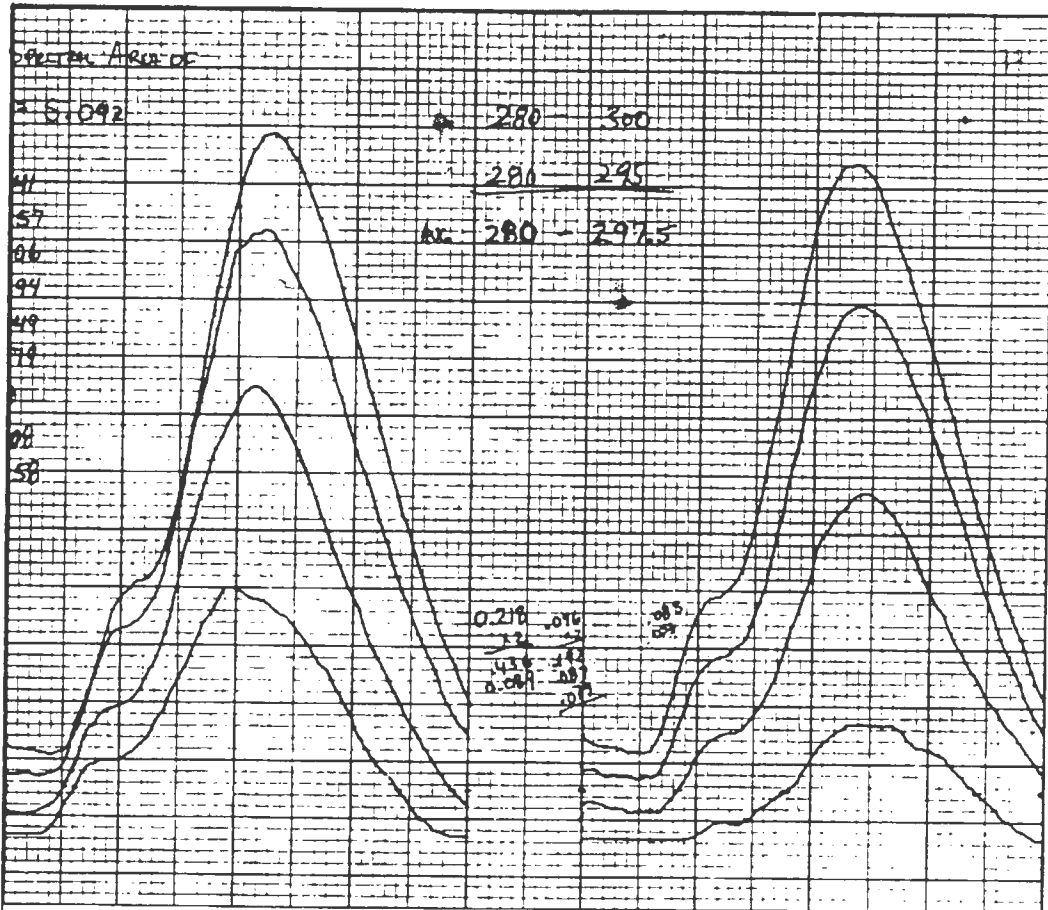
Test number 36



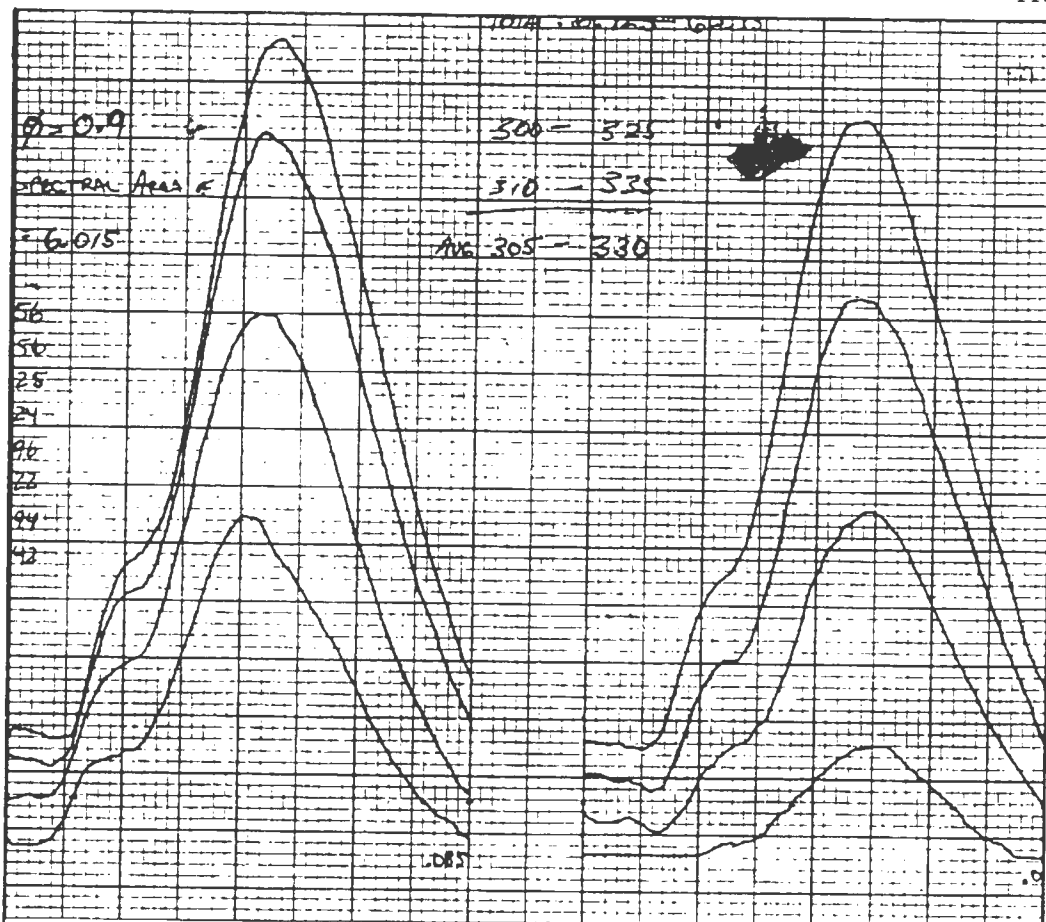
Test number 37



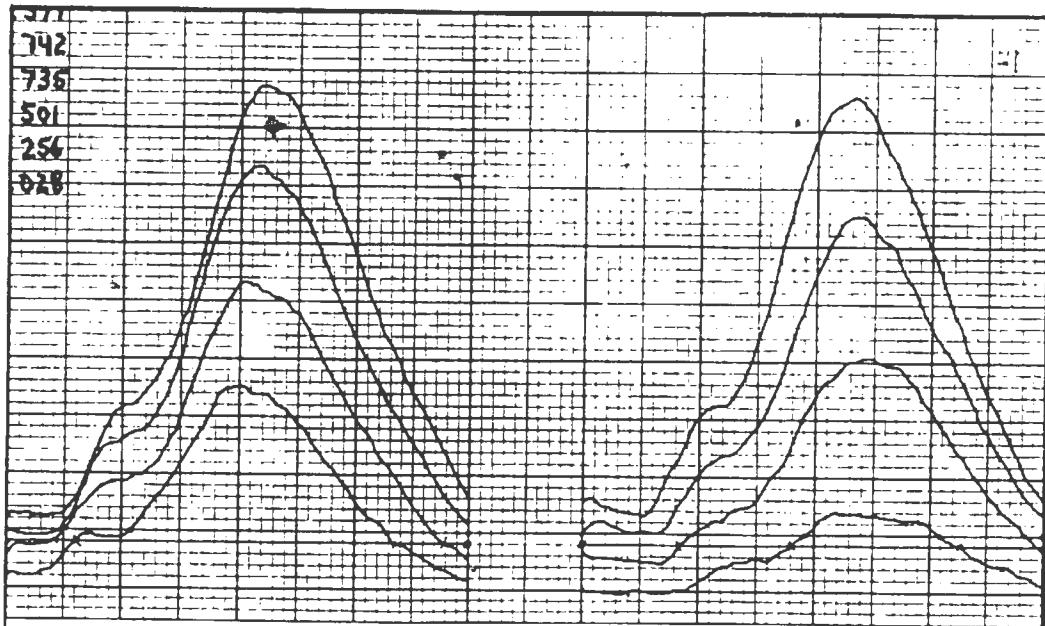
Test number 38



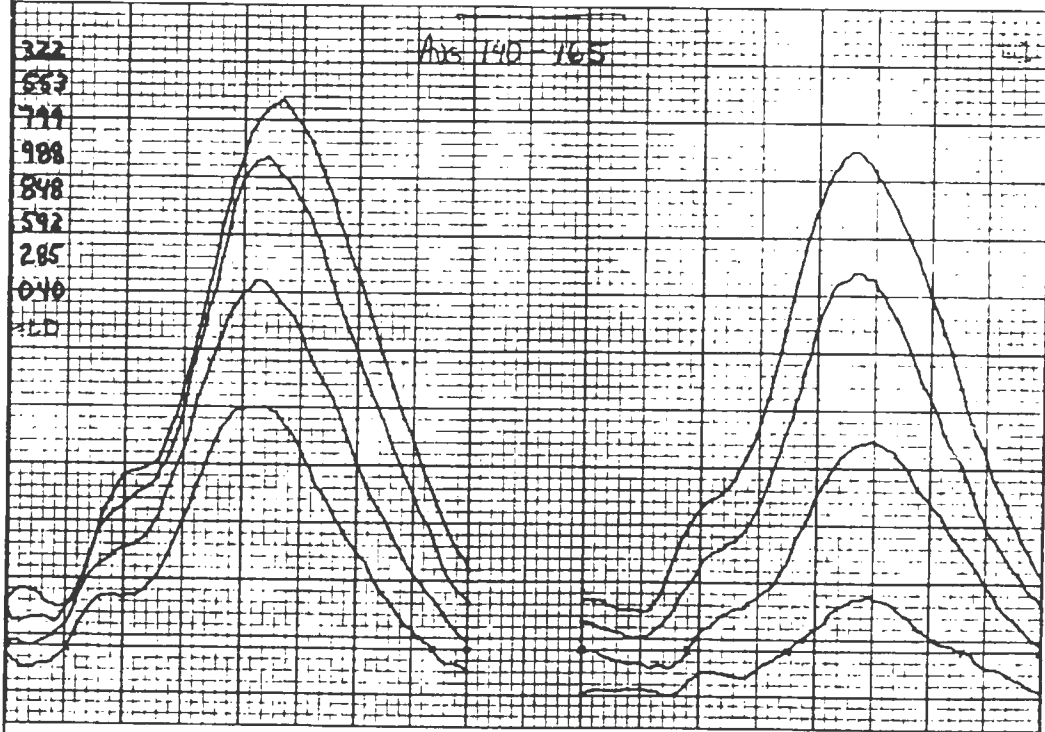
Test number 39



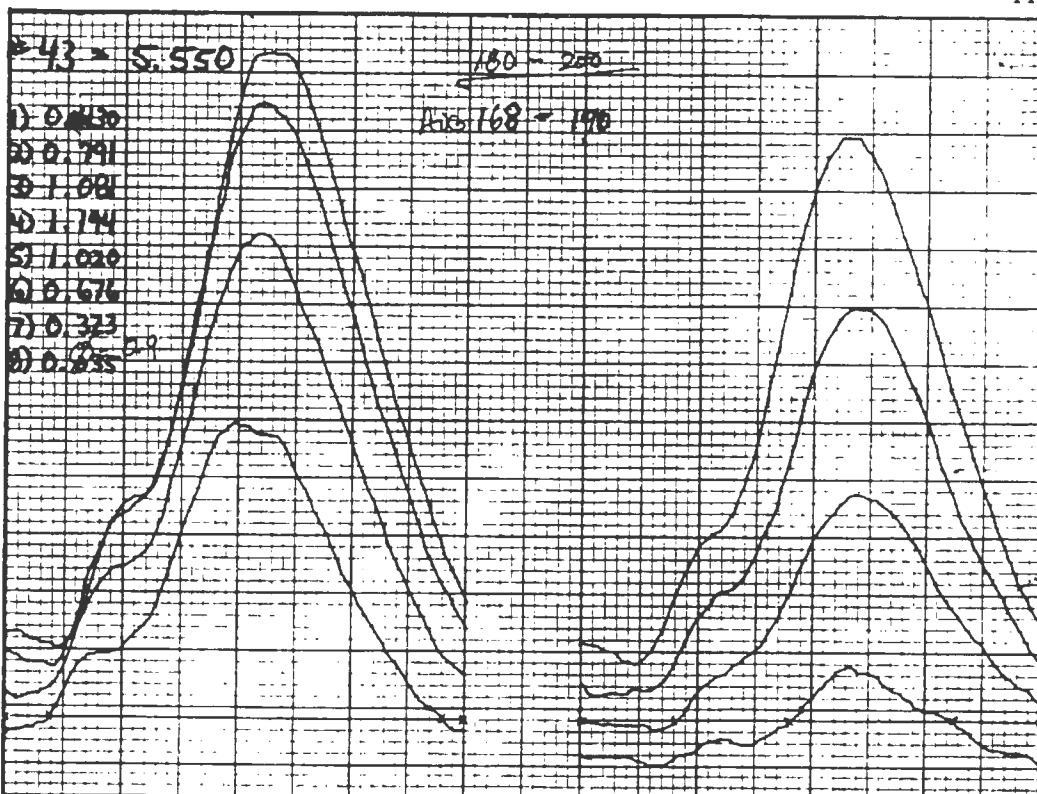
Test number 40



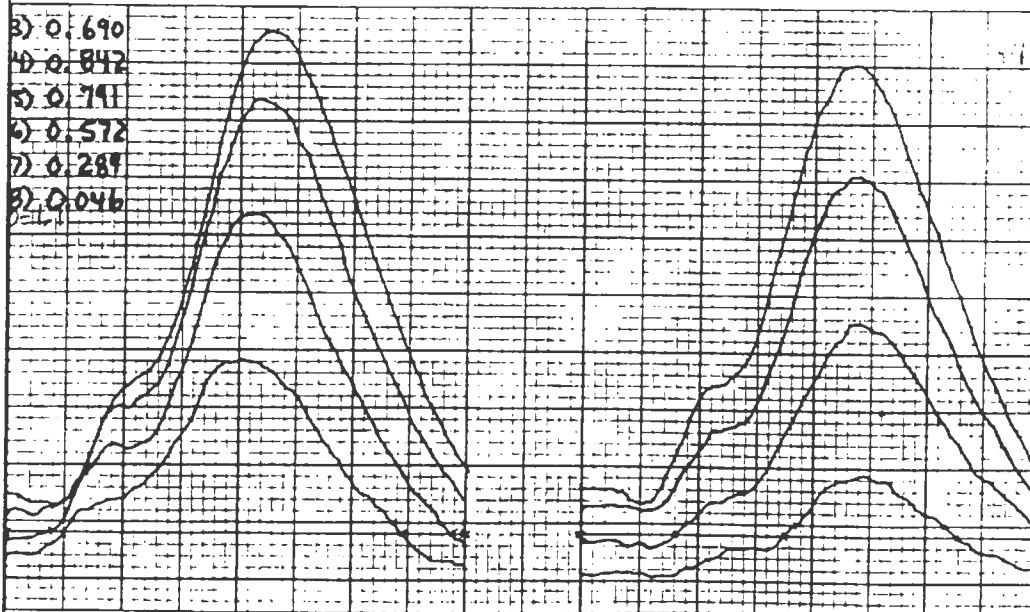
Test number 41



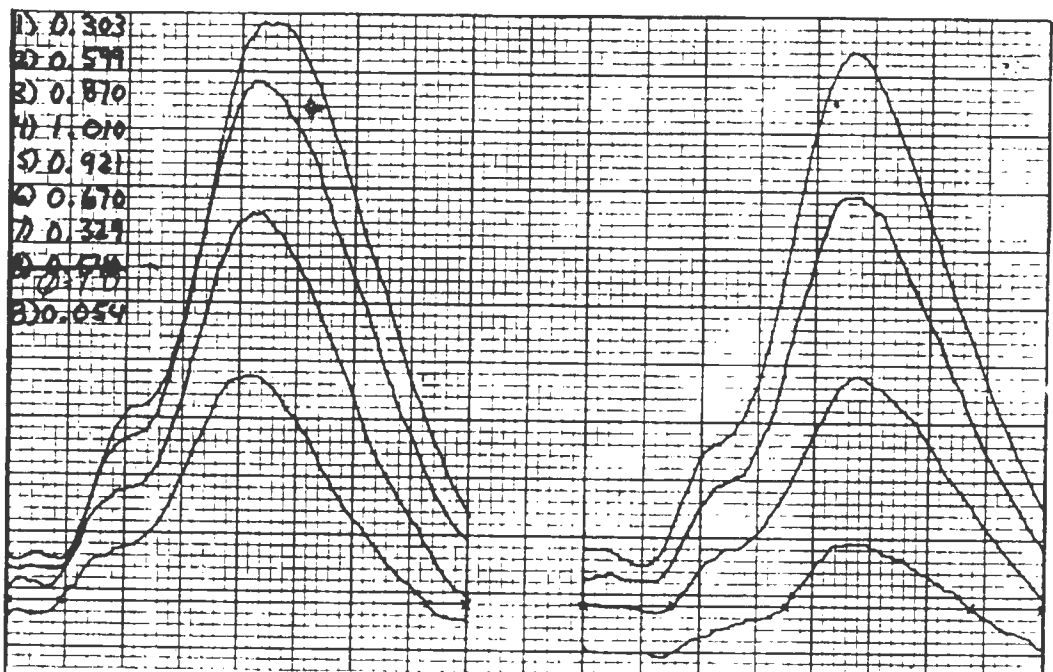
Test number 42



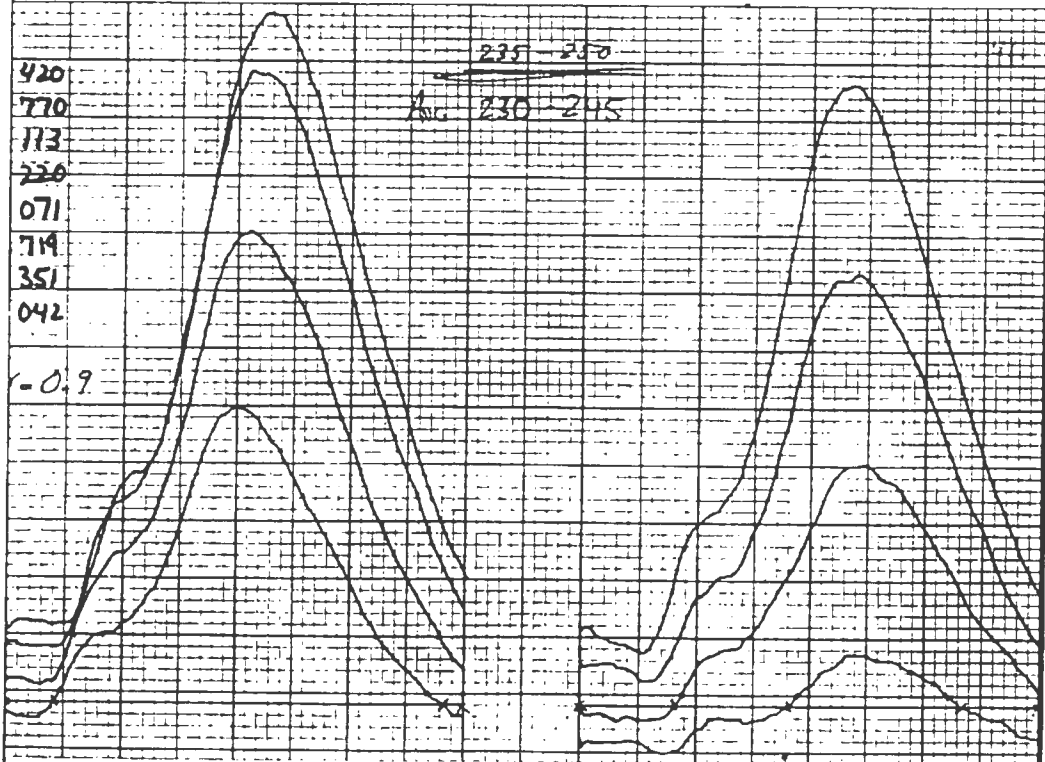
Test number 43



Test number 44



Test number 45

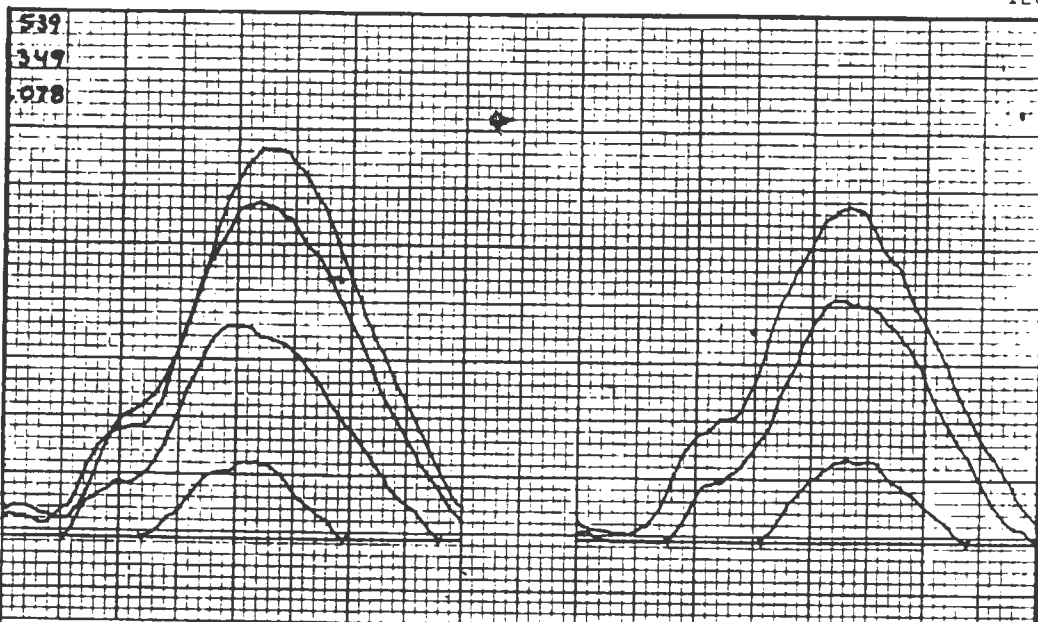


Test number 46

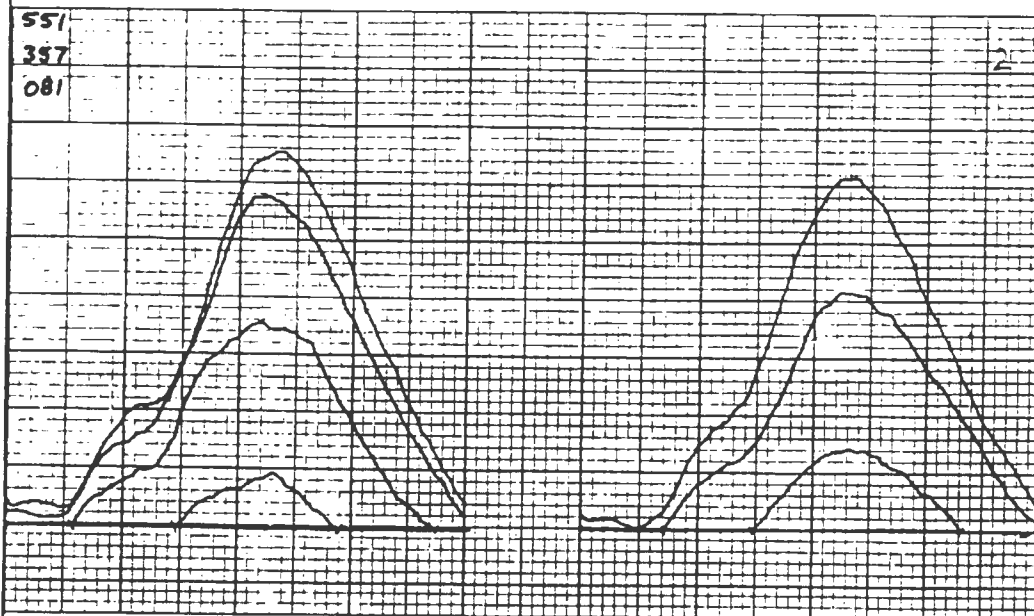
AIR SIDE HEATED							
SPECTROPHOTOMETER				FUEL/AIR			
SETTINGS				(actual)			
TEST	TIME	SCAN	SLIT	MIC	FUEL/AIR		
NO.	PERIOD	SPEED	WIDTH	SETTING	(stoich)	FLAME	
	GAIN	(SEC)	CM-1/MIN	(mm)	INITIAL	"PHI"	ADDITIVE
1	200	18	1000	0.25	2.25	1.21	KO2
2	200	18	1000	0.25	2.25	1.21	KO2
3	200	18	1000	0.25	2.25	1.21	KO2
4	200	18	1000	0.25	2.25	1.21	KO2
5	200	18	1000	0.25	2.25	1.21	KO2
6	200	18	1000	0.25	2.25	1.21	KO2
7	200	18	1000	0.25	2.25	1.21	KO2
8	200	18	1000	0.25	2.25	1.21	KO2
9	200	18	1000	0.25	2.25	1.21	KO2
10	200	18	1000	0.25	2.25	0.72	KO2
11	200	18	1000	0.25	2.25	0.72	KO2
12	200	18	1000	0.25	2.25	0.72	KO2
13	200	18	1000	0.25	2.25	0.72	KO2
14	200	18	1000	0.25	2.25	0.72	KO2
15	200	18	1000	0.25	2.25	0.72	KO2
16	200	18	1000	0.25	2.25	0.72	KO2
17	200	18	1000	0.25	2.25	0.72	KO2
18	200	18	1000	0.25	2.25	0.72	KO2
19	200	18	1000	0.25	2.25	0.72	KO2
20	200	18	1000	0.25	2.25	0.72	NONE
21	200	18	1000	0.25	2.25	0.72	NONE
22	200	18	1000	0.25	2.25	0.72	NONE
23	200	18	1000	0.25	2.25	0.72	NONE
24	200	18	1000	0.25	2.25	1.21	NONE
25	200	18	1000	0.25	2.25	1.21	NONE
26	200	18	1000	0.25	2.25	1.21	NONE
27	200	18	1000	0.25	2.25	1.21	NONE
28	200	18	1000	0.25	2.25	0.72	NONE
29	200	18	1000	0.25	2.25	0.72	NONE
30	200	18	1000	0.25	2.25	0.72	NONE
31	200	18	1000	0.25	2.25	1.21	NONE
32	200	18	1000	0.25	2.25	1.21	NONE
33	200	18	1000	0.25	2.25	1.21	NONE

		AIR	SIDE	HEATED		
BURNER TEMPERATURE						
(DEGREES CELSIUS)						
TEST	INITIAL	INITIAL	FINAL	FINAL	AVERAGE	AVERAGE
NUMBER	TEMP	TEMP	TEMP	TEMP	TEMP	TEMP
	AT 5"	AT 8"	AT 5"	AT 8"	AT 5"	AT 8"
1	105	177	110	185	108	181
2	120	210	125	225	123	218
3	125	225	140	230	133	228
4	140	230	145	245	143	238
5	145	245	150	245	148	245
6	150	245	155	270	153	258
7	155	270	195	280	175	275
8	195	280	205	295	200	288
9	205	295	220	300	213	298
10	080	170	085	175	083	173
11	085	175	090	175	088	175
12	105	205	125	225	115	215
13	125	225	130	240	128	233
14	130	240	145	245	138	243
15	150	250	155	255	153	253
16	160	255	175	260	168	258
17	177	265	180	270	179	269
18	195	295	200	300	198	298
19	205	305	210	310	208	308
20	100	190	103	190	102	190
21	103	190	115	202	109	196
22	115	202	115	210	115	206
23	115	210	122	220	119	215
24	122	220	125	220	124	220
25	125	220	130	230	128	225
26	130	230	130	237	130	234
27	130	237	140	245	135	241
28	140	245	140	250	140	248
29	140	250	150	260	145	255
30	153	270	170	275	162	273
31	170	275	175	275	173	275
32	195	300	205	302	200	301
33	205	305	225	320	215	313

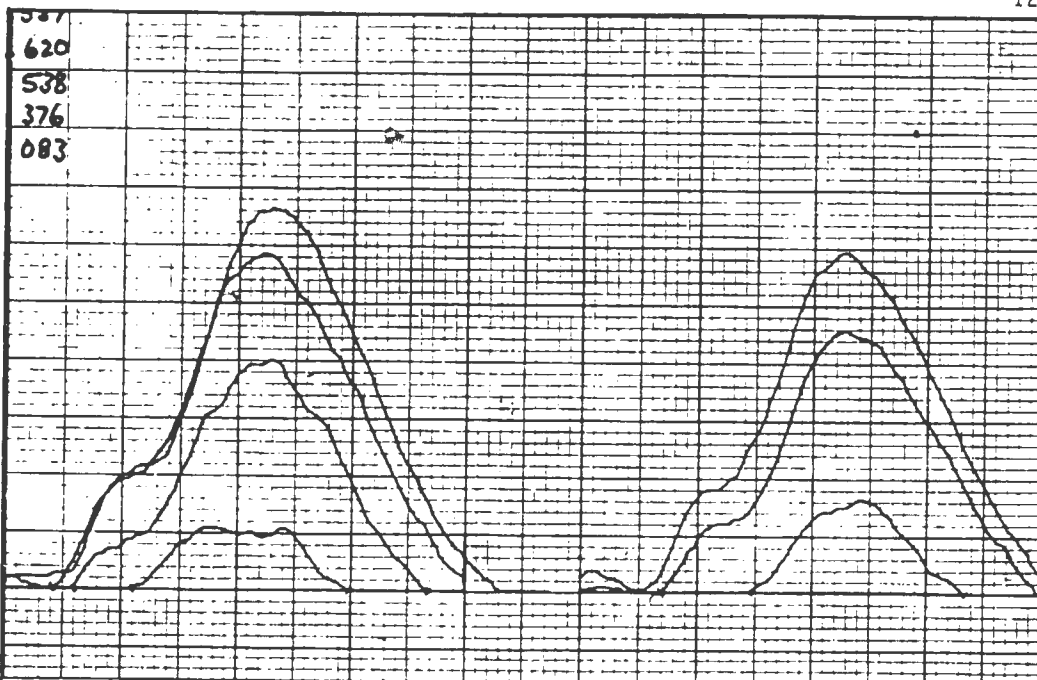
AIR SIDE HEATED								
INTEGRATED SPECTRAL AREA								
TEST	SCAN	SCAN	SCAN	SCAN	SCAN	SCAN	SCAN	AREA
NO.	1	2	3	4	5	6	7	1 - 7
1	0.068	0.312	0.561	0.649	0.539	0.349	0.078	2.535
2	0.039	0.296	0.524	0.613	0.551	0.357	0.081	2.437
3	0.063	0.309	0.537	0.62	0.538	0.376	0.083	2.498
4	0.106	0.288	0.519	0.619	0.545	0.381	0.075	2.519
5	0.076	0.261	0.489	0.58	0.503	0.336	0.066	2.297
6	0.042	0.23	0.449	0.513	0.433	0.327	0.069	2.037
7	0.02	0.229	0.472	0.559	0.511	0.372	0.089	2.229
8	0.072	0.274	0.457	0.569	0.528	0.377	0.087	2.339
9	0.066	0.245	0.43	0.563	0.52	0.361	0.08	2.241
10	0.048	0.286	0.535	0.688	0.671	0.509	0.161	2.875
11	0.06	0.266	0.521	0.69	0.68	0.52	0.15	2.865
12	0.077	0.306	0.578	0.699	0.662	0.525	0.167	2.999
13	0.061	0.288	0.56	0.716	0.681	0.525	0.17	2.982
14	0.051	0.273	0.576	0.712	0.689	0.547	0.182	3.019
15	0.07	0.298	0.58	0.735	0.702	0.545	0.18	3.095
16	0.051	0.291	0.561	0.724	0.701	0.541	0.179	3.027
17	0.039	0.281	0.55	0.71	0.703	0.539	0.171	2.971
18	0.043	0.256	0.535	0.697	0.695	0.541	0.169	2.919
19	0.038	0.265	0.531	0.698	0.704	0.548	0.177	2.941
20	0.059	0.346	0.636	0.815	0.834	0.684	0.24	3.589
21	0.058	0.33	0.635	0.83	0.869	0.705	0.259	3.671
22	0.051	0.323	0.634	0.842	0.85	0.681	0.251	3.612
23	0.054	0.312	0.611	0.829	0.851	0.71	0.257	3.598
24	0.063	0.325	0.521	0.621	0.54	0.35	0.069	2.455
25	0.068	0.313	0.537	0.609	0.561	0.395	0.089	2.551
26	0.071	0.296	0.541	0.629	0.569	3.88	0.09	4.898
27	0.055	0.303	0.548	0.625	0.569	0.391	0.091	2.563
28	0.049	0.277	0.599	0.815	0.866	0.725	0.271	3.591
29	0.04	0.285	0.6	0.813	0.861	0.749	0.289	3.618
30	0.048	0.283	0.609	0.821	0.881	0.757	0.3	3.691
31	0.072	0.289	0.539	0.64	0.603	0.429	0.1	2.657
32	0.055	0.3	0.536	0.66	0.6	0.424	0.111	2.659
33	0.054	0.285	0.524	0.649	0.62	0.474	0.135	2.716



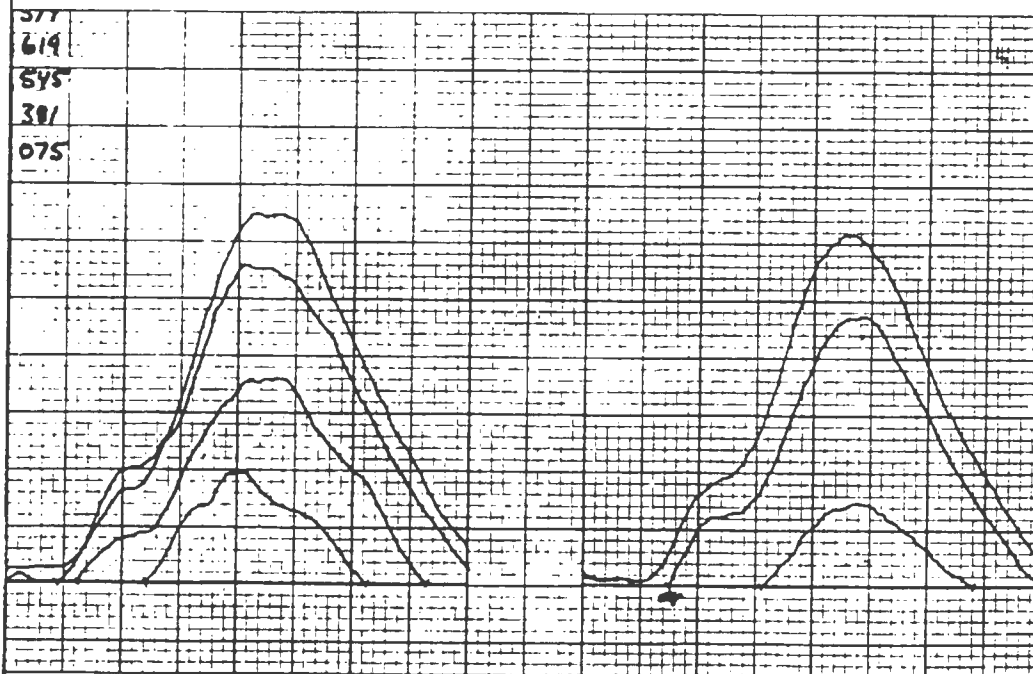
Test number 1



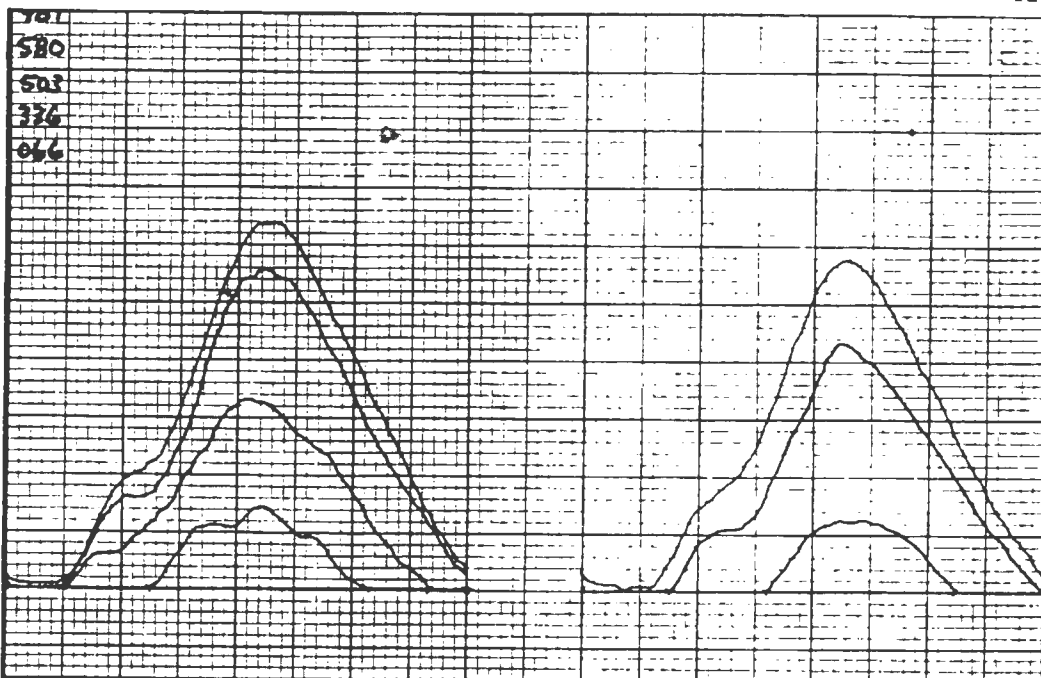
Test number 2



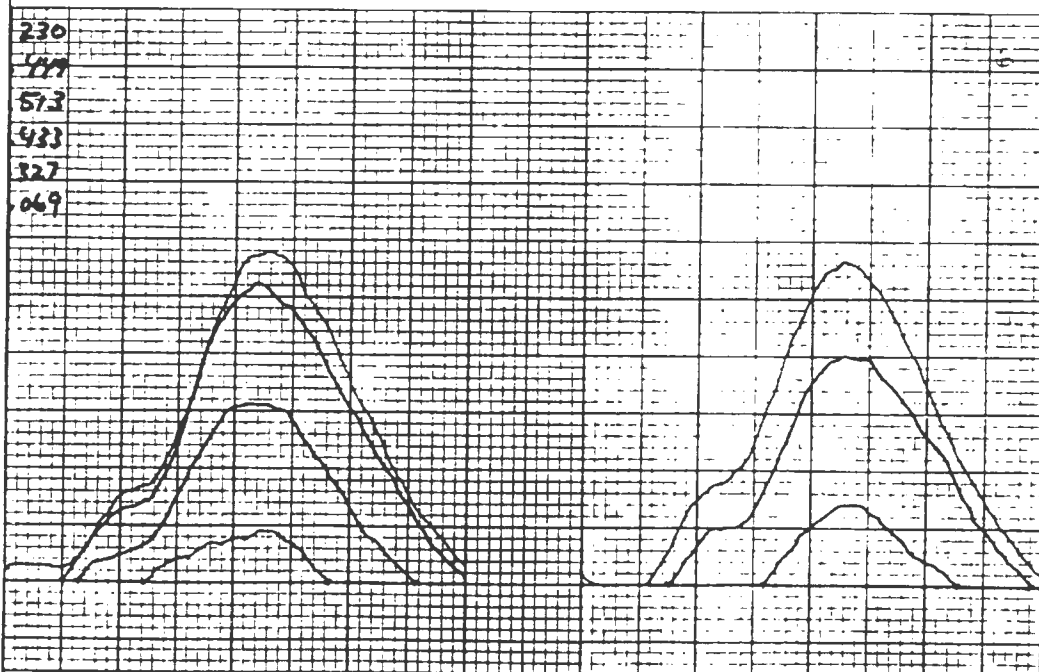
Test number 3



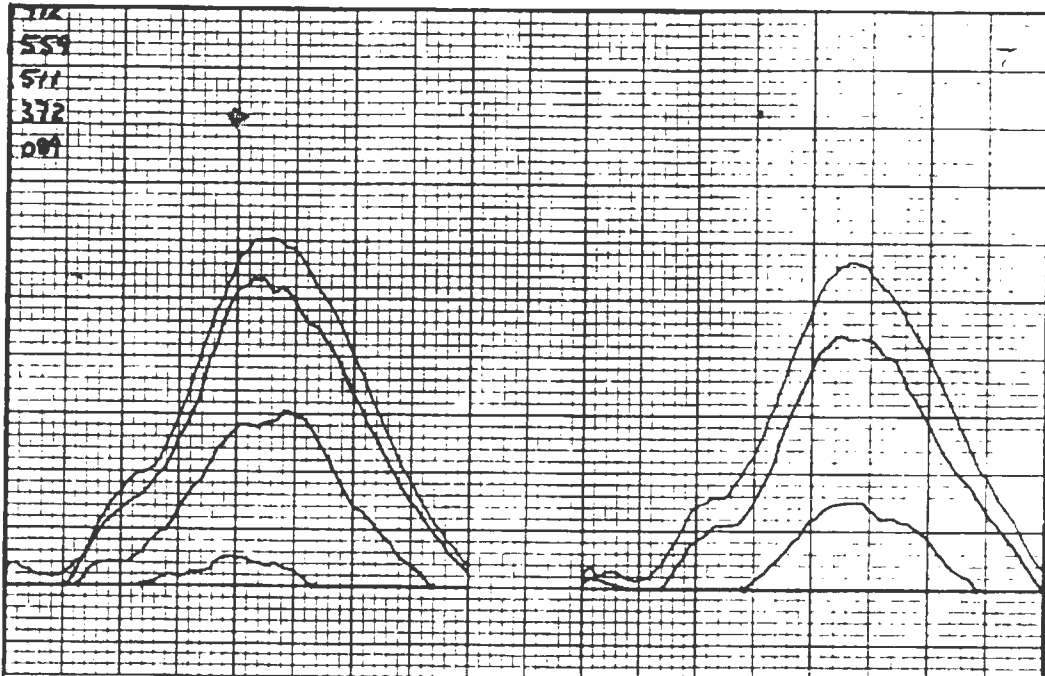
Test number 4



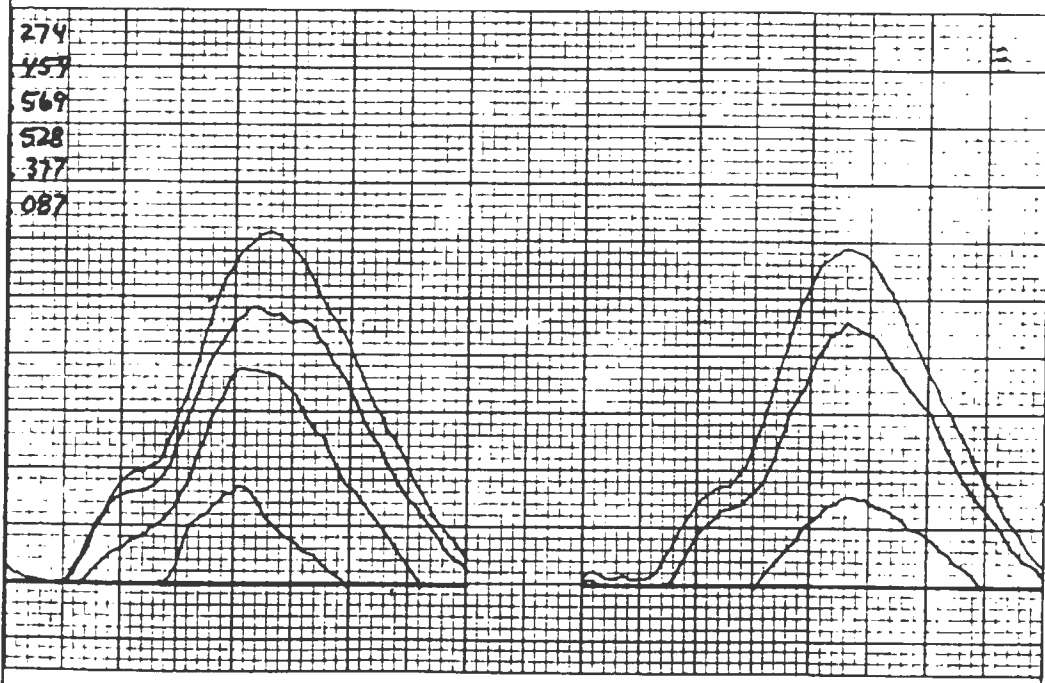
Test number 5



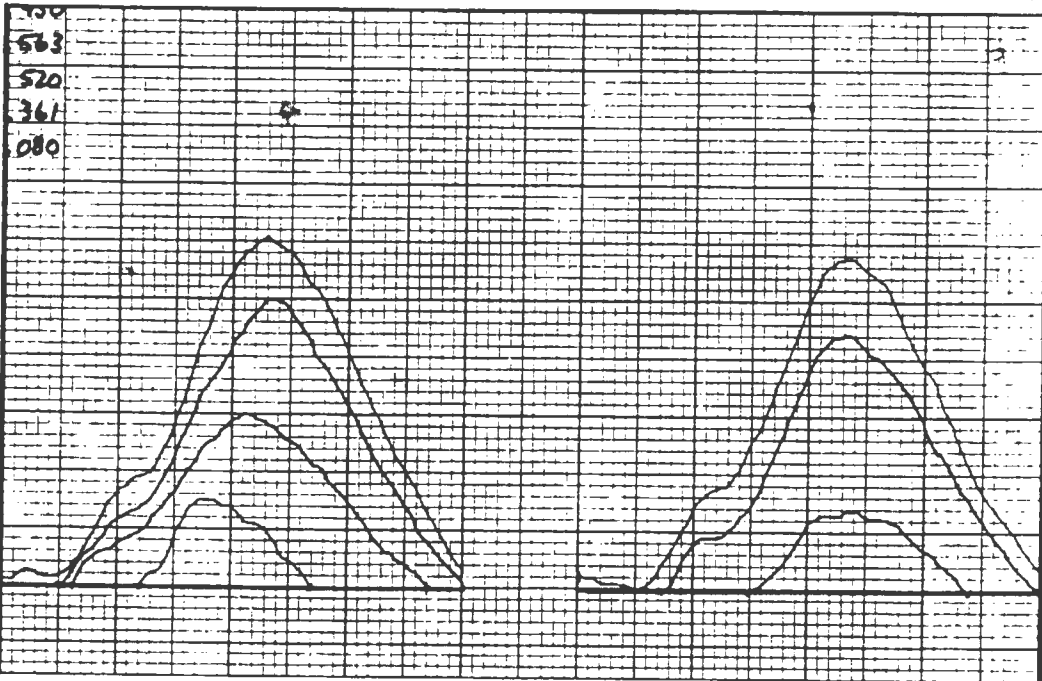
Test number 6



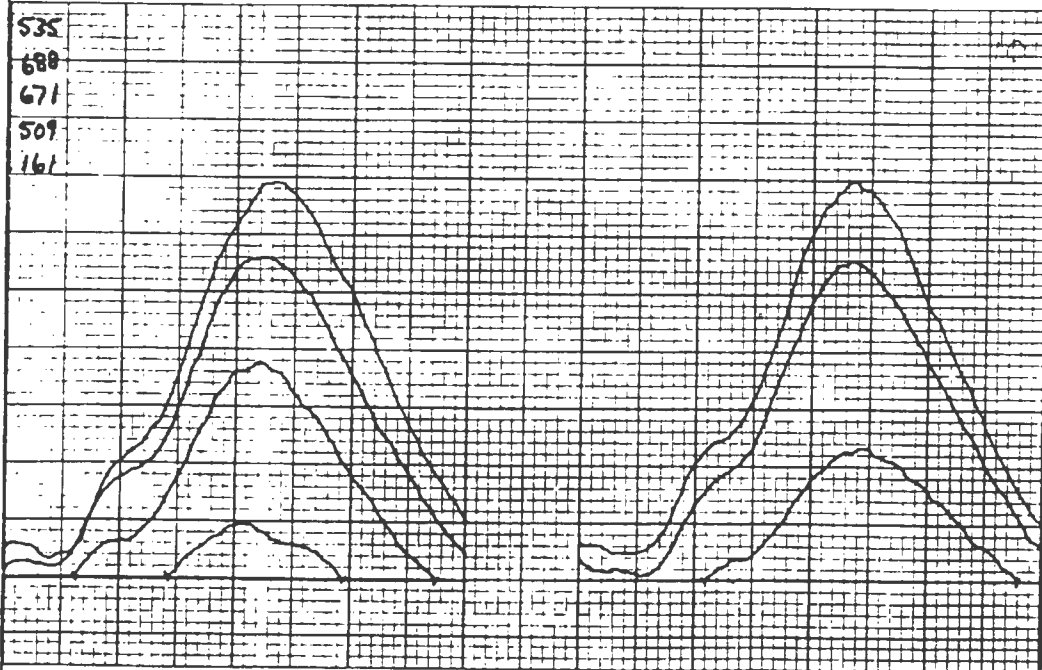
Test number 7



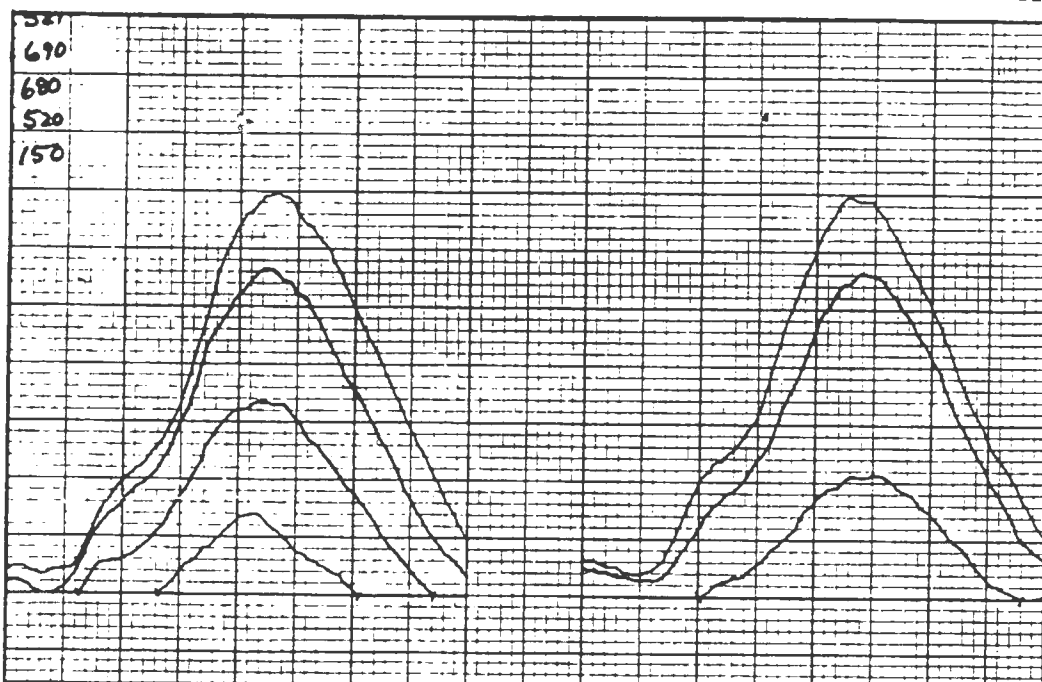
Test number 8



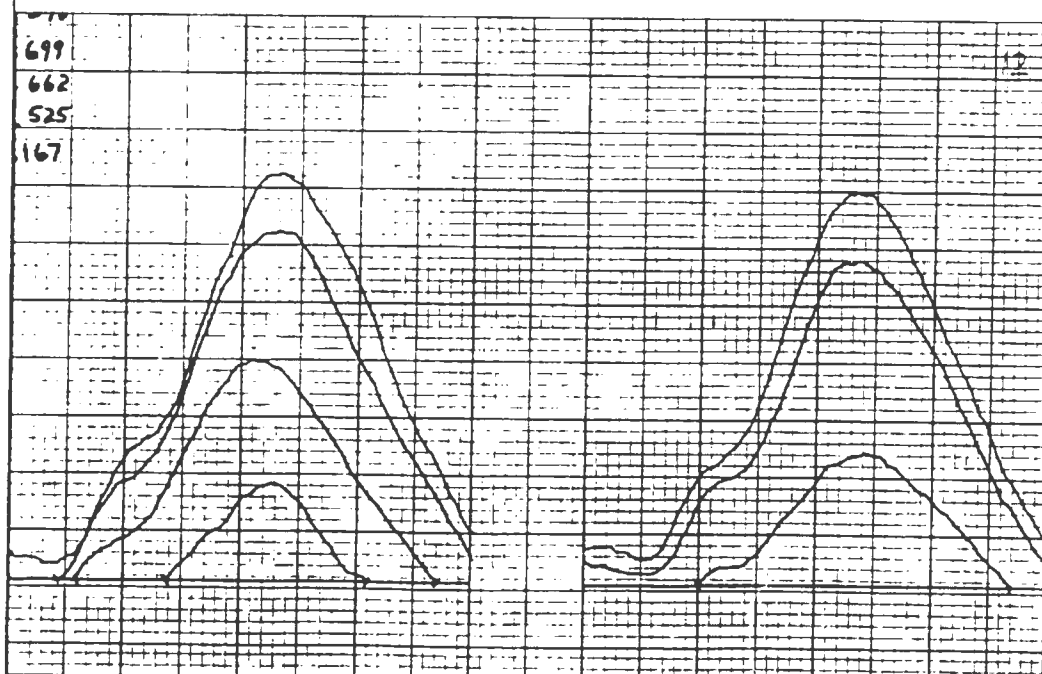
Test number 9



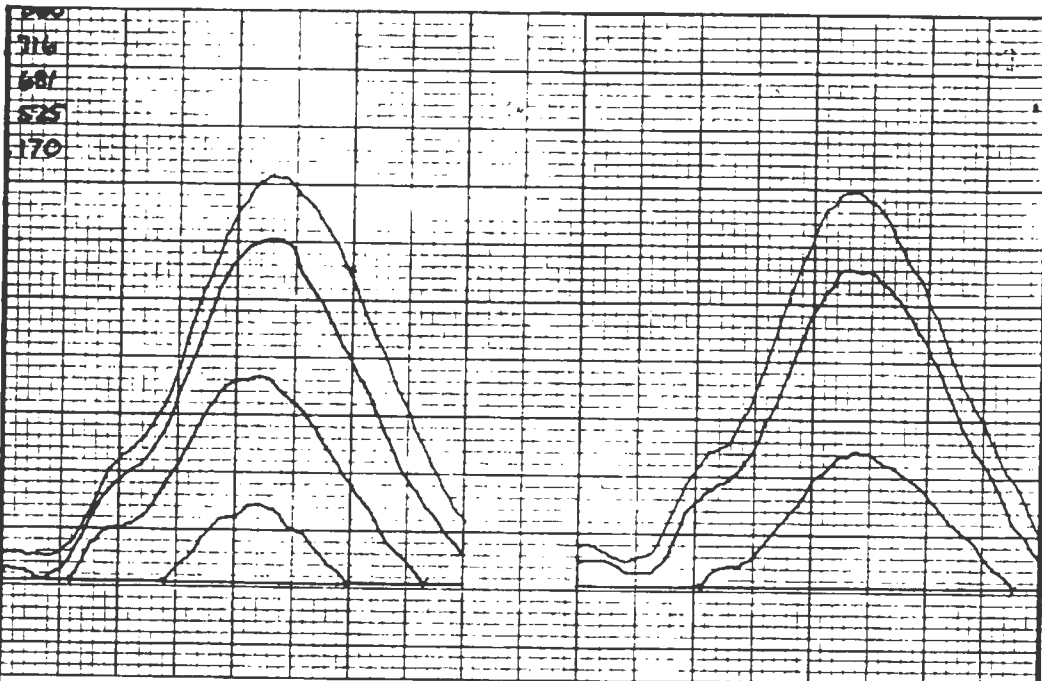
Test number 10



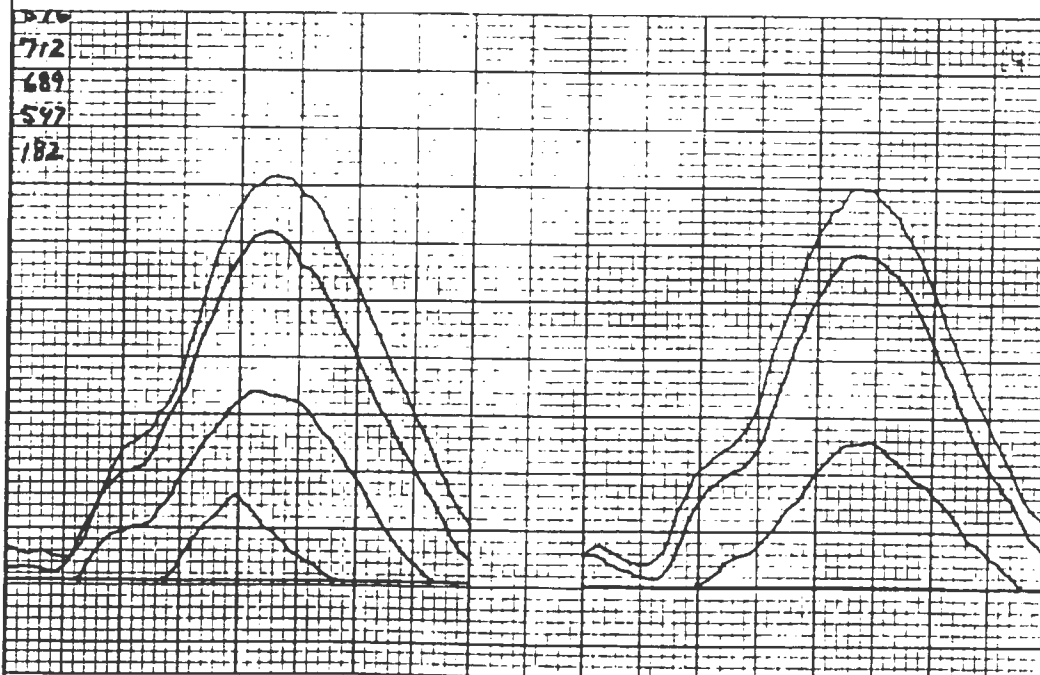
Test number 11



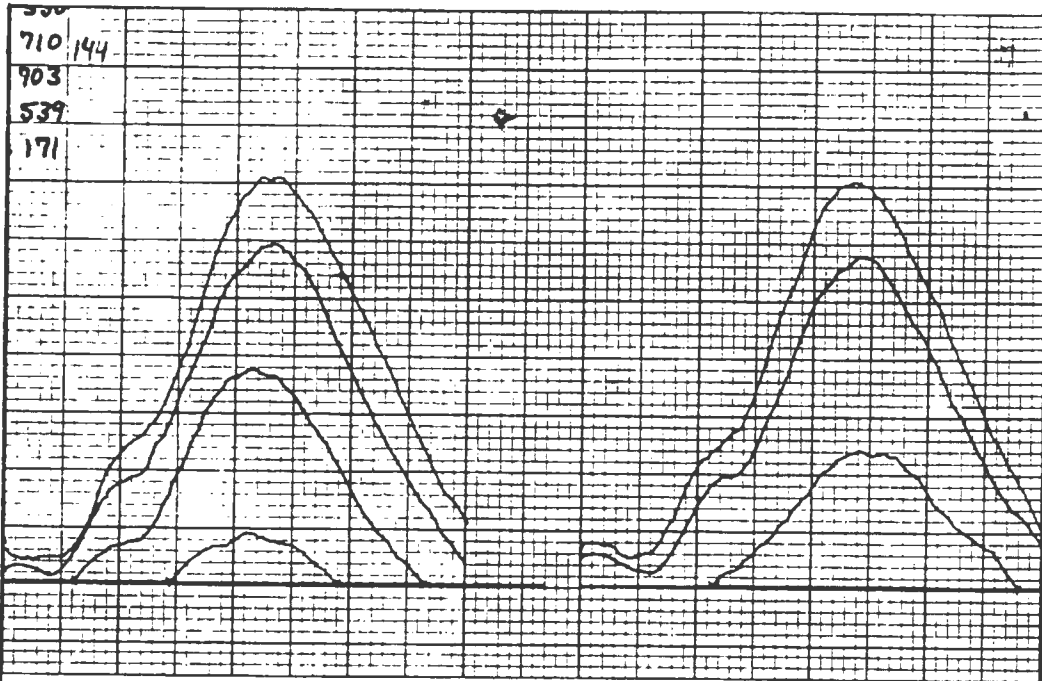
Test number 12



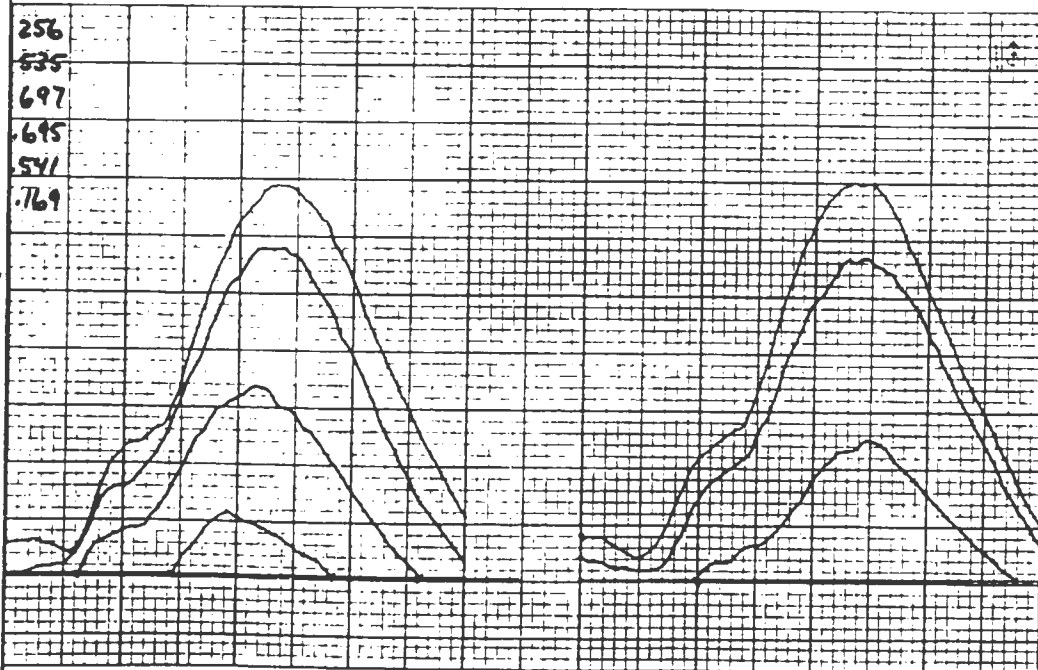
Test number 13



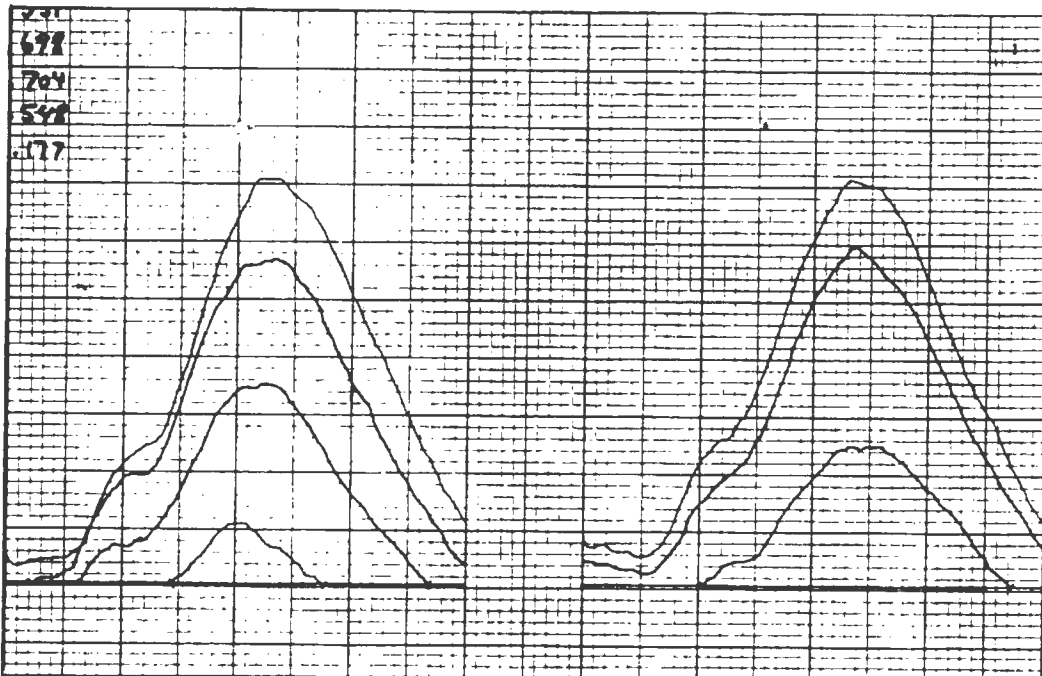
Test number 14



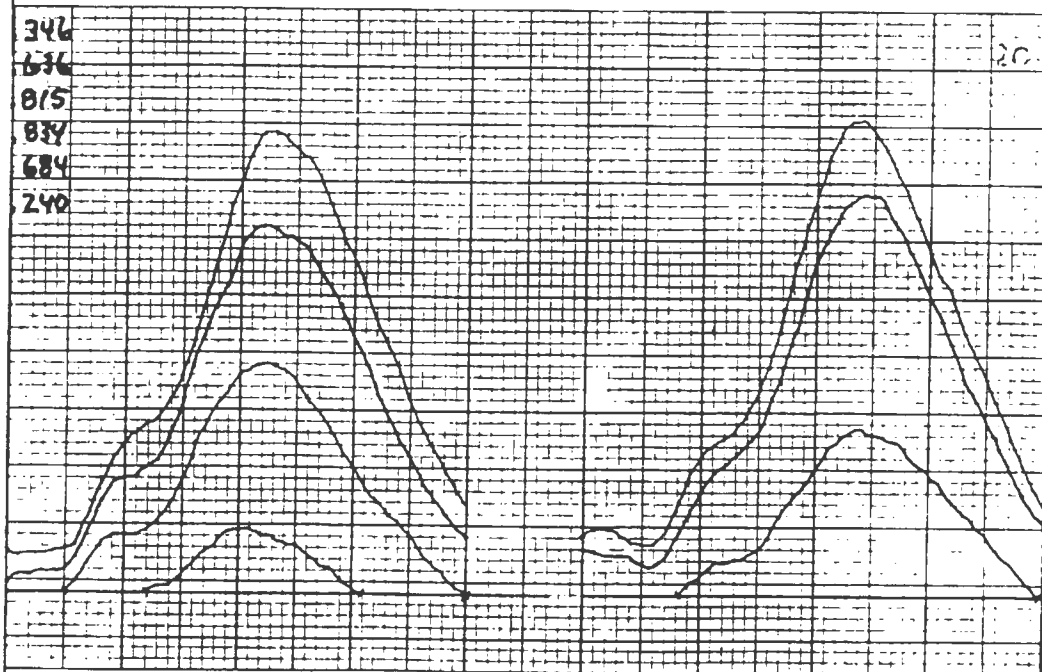
Test number 17



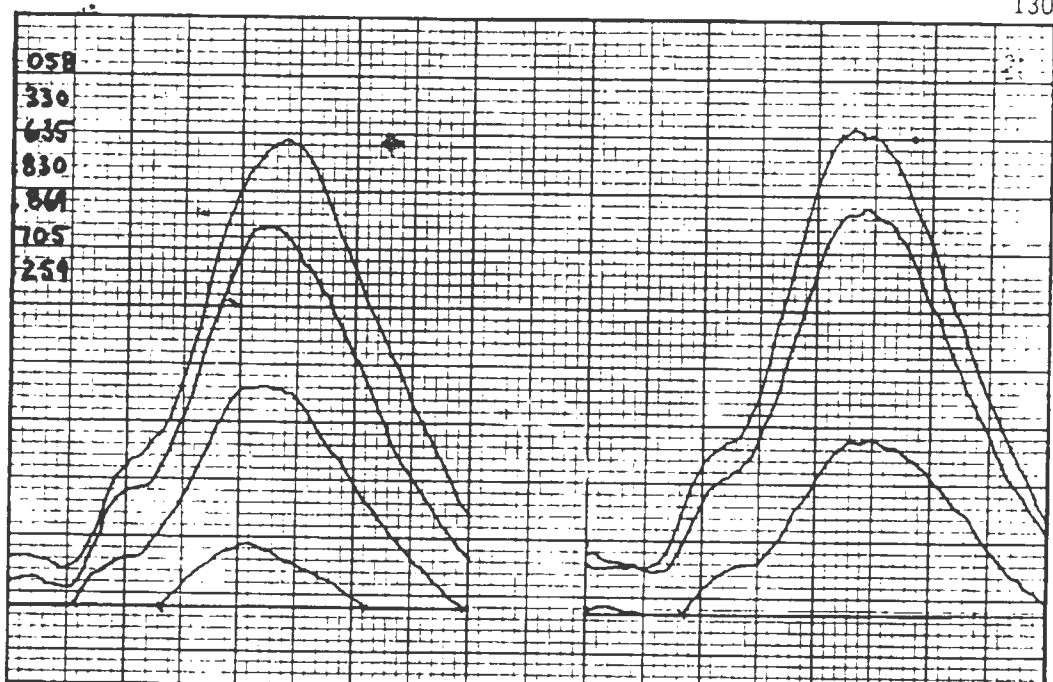
Test number 18



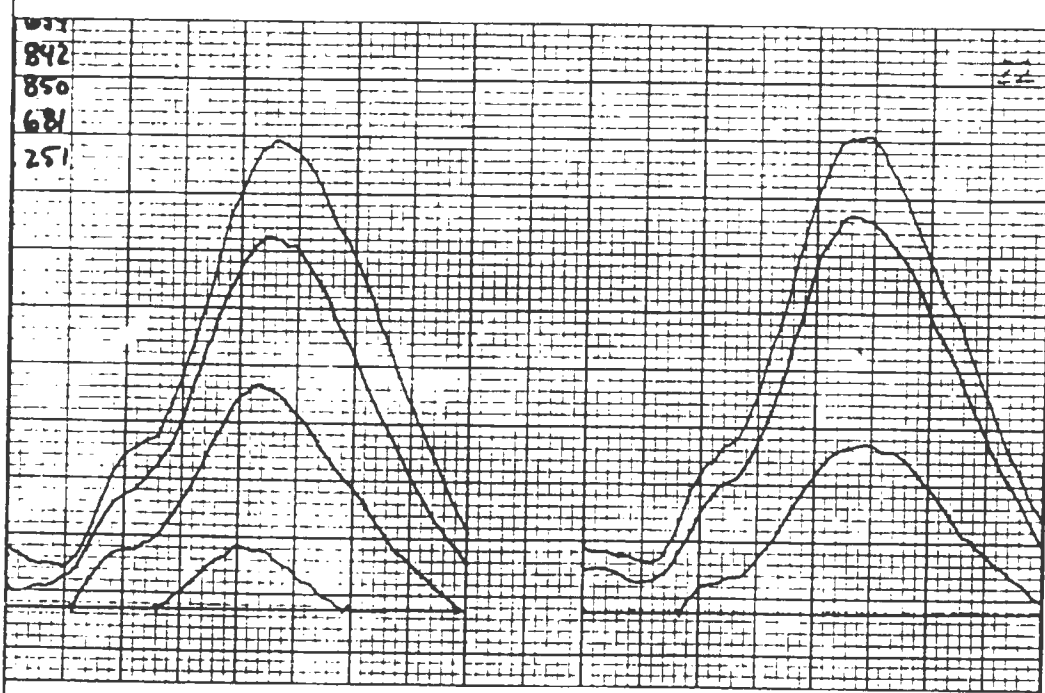
Test number 19



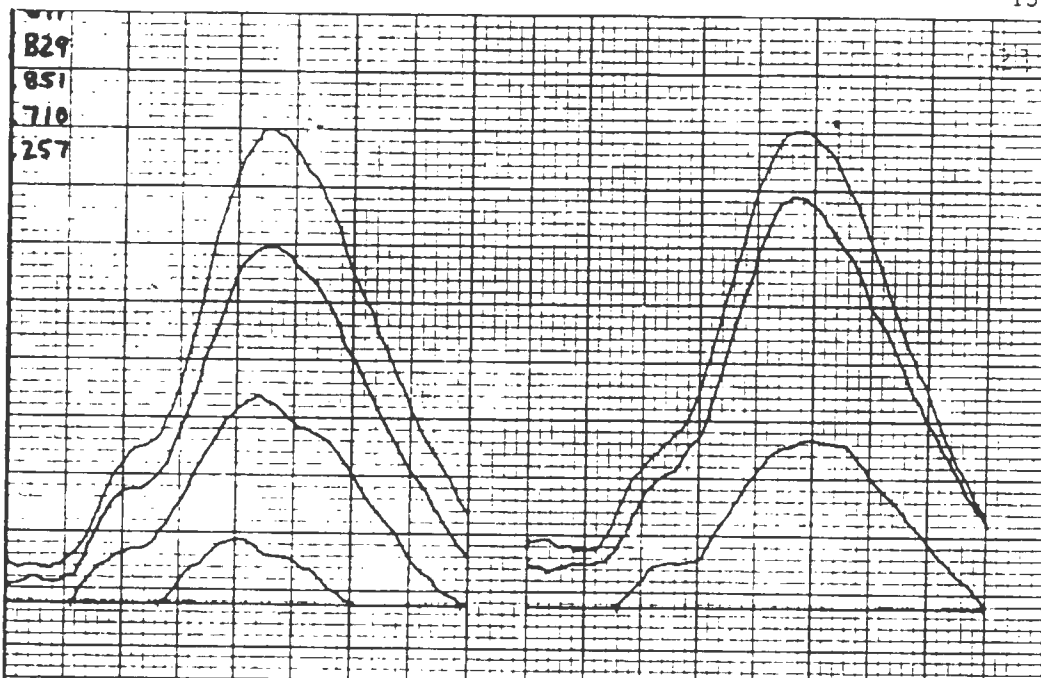
Test number 20



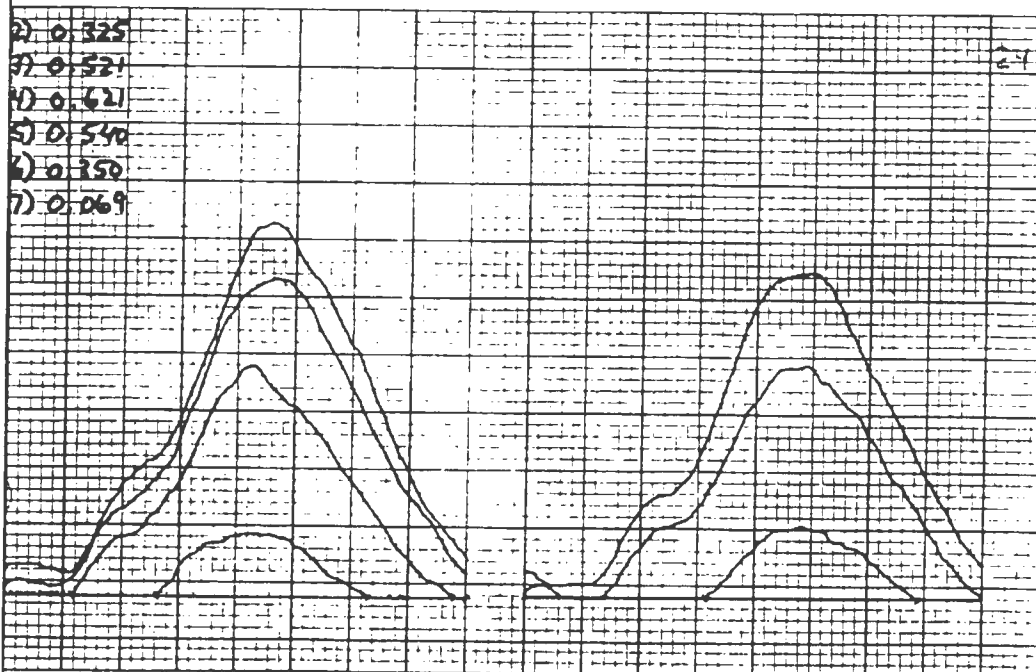
Test number 21



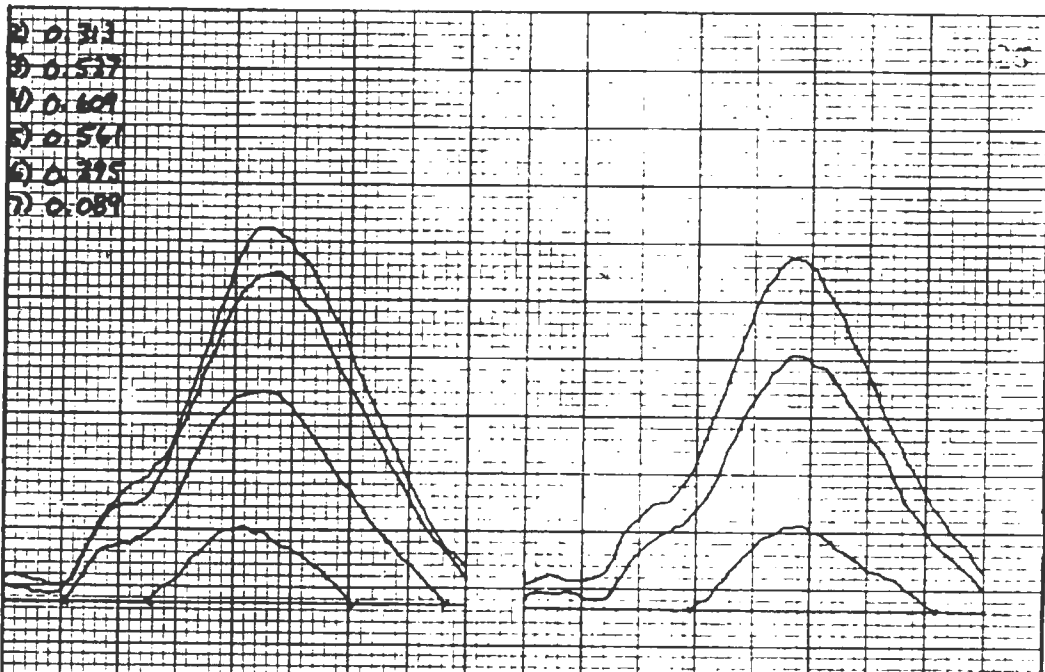
Test number 22



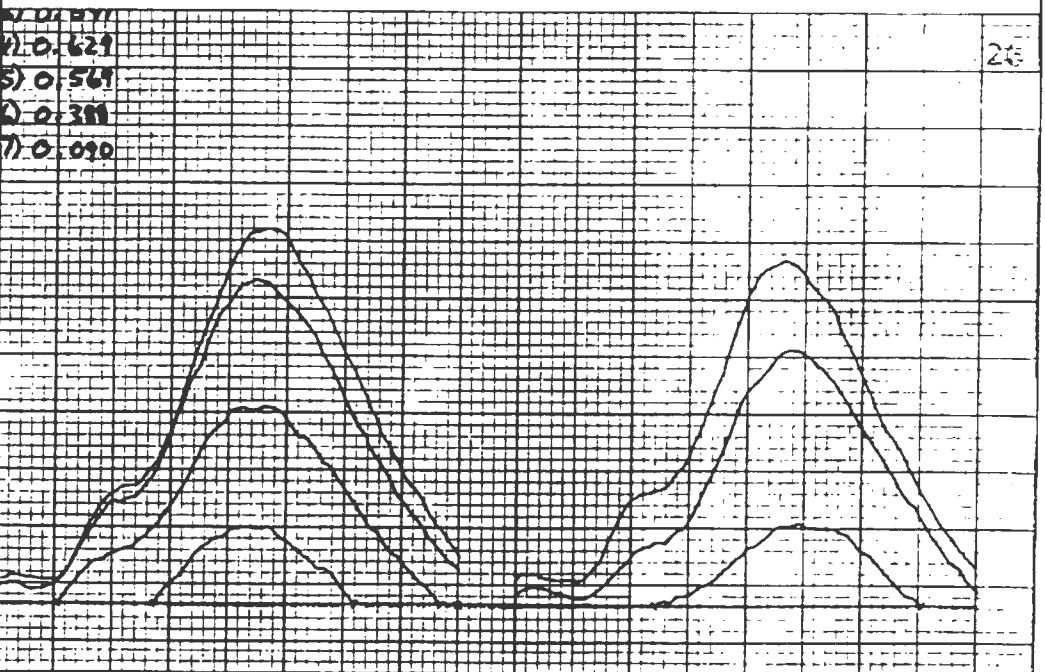
Test number 23



Test number 24



Test number 25



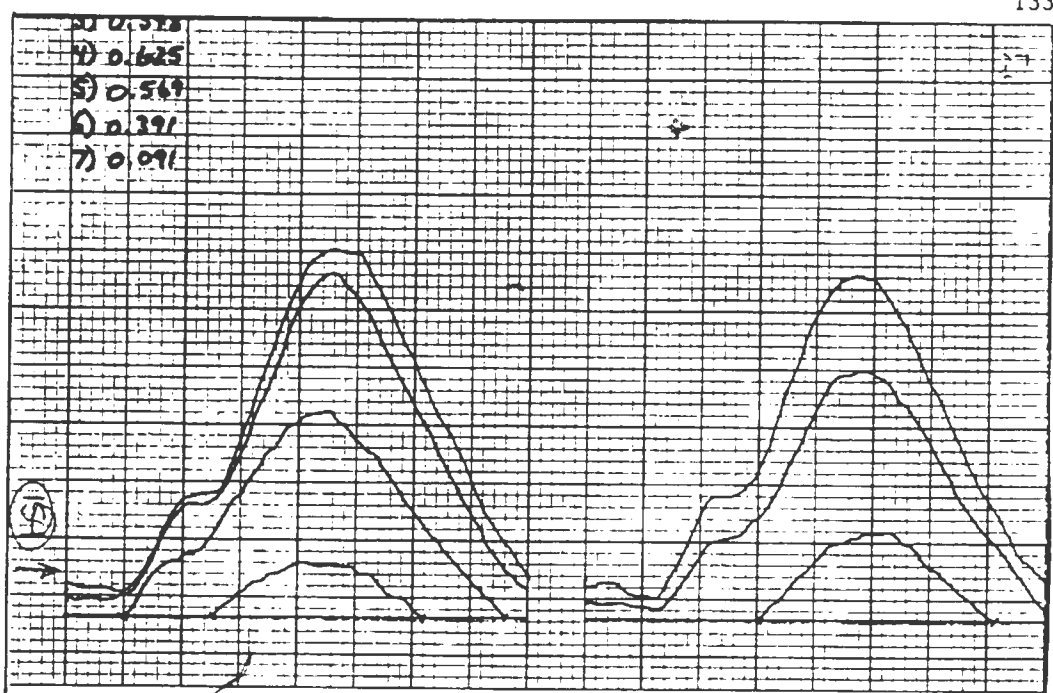
Test number 26

- 2) 0.313
- 3) 0.537
- 4) 0.609
- 5) 0.561
- 6) 0.325
- 7) 0.089

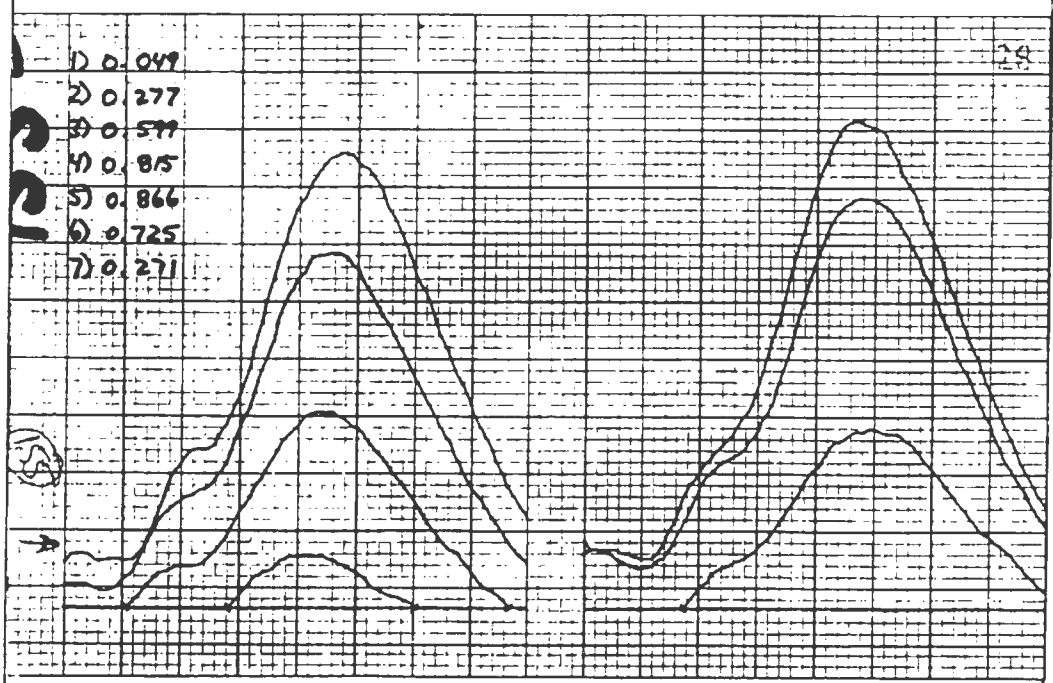
- 4) 0.629
- 5) 0.561
- 6) 0.311
- 7) 0.090

25

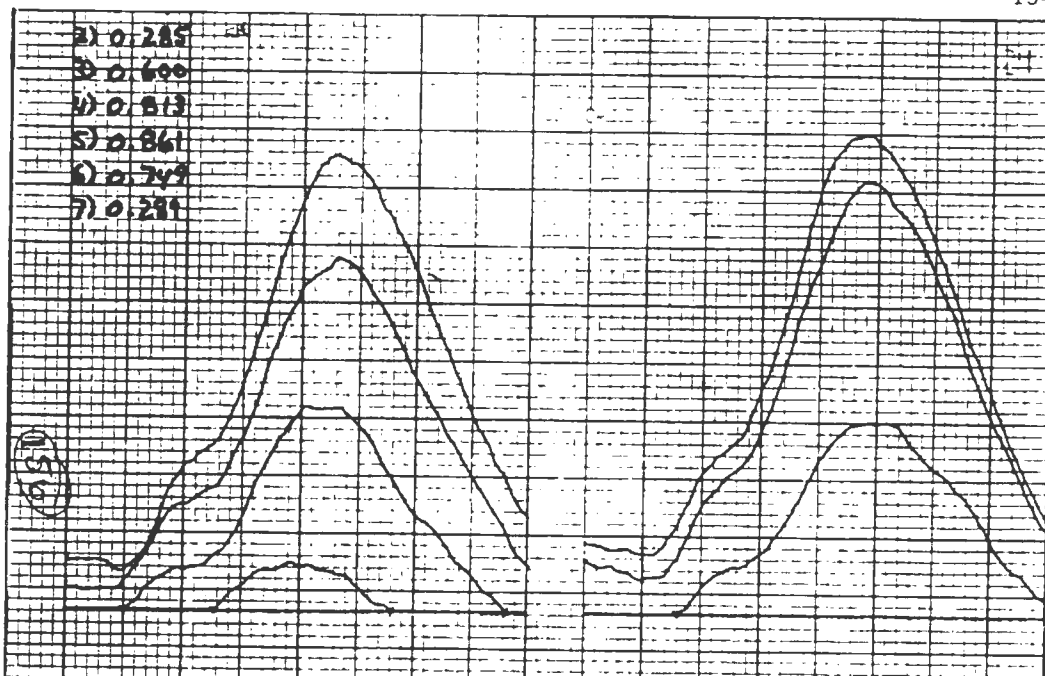
26



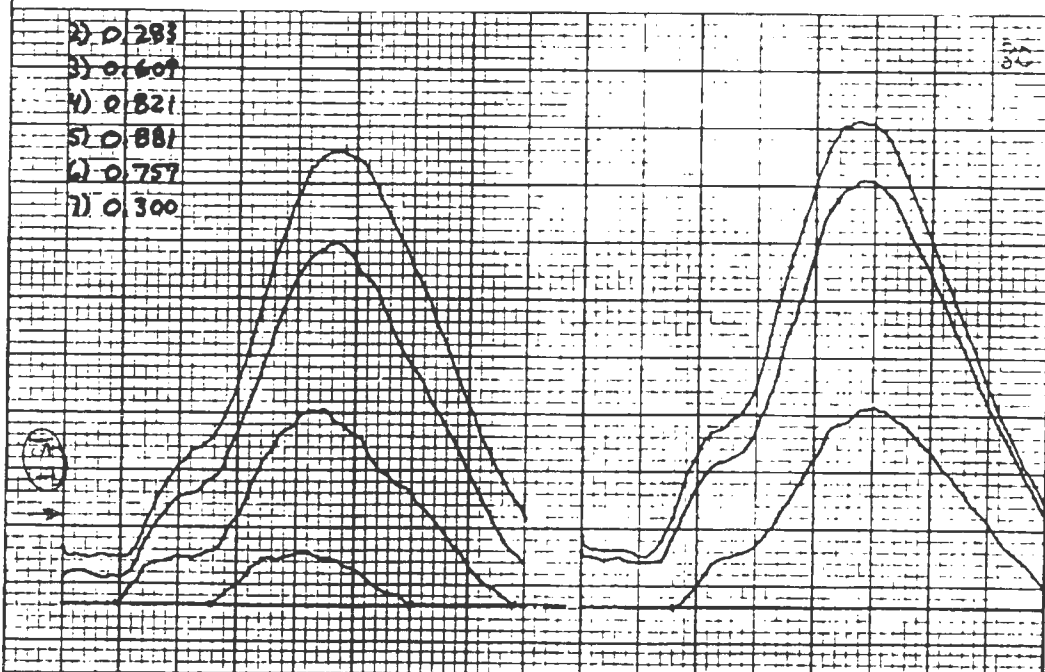
Test number 27



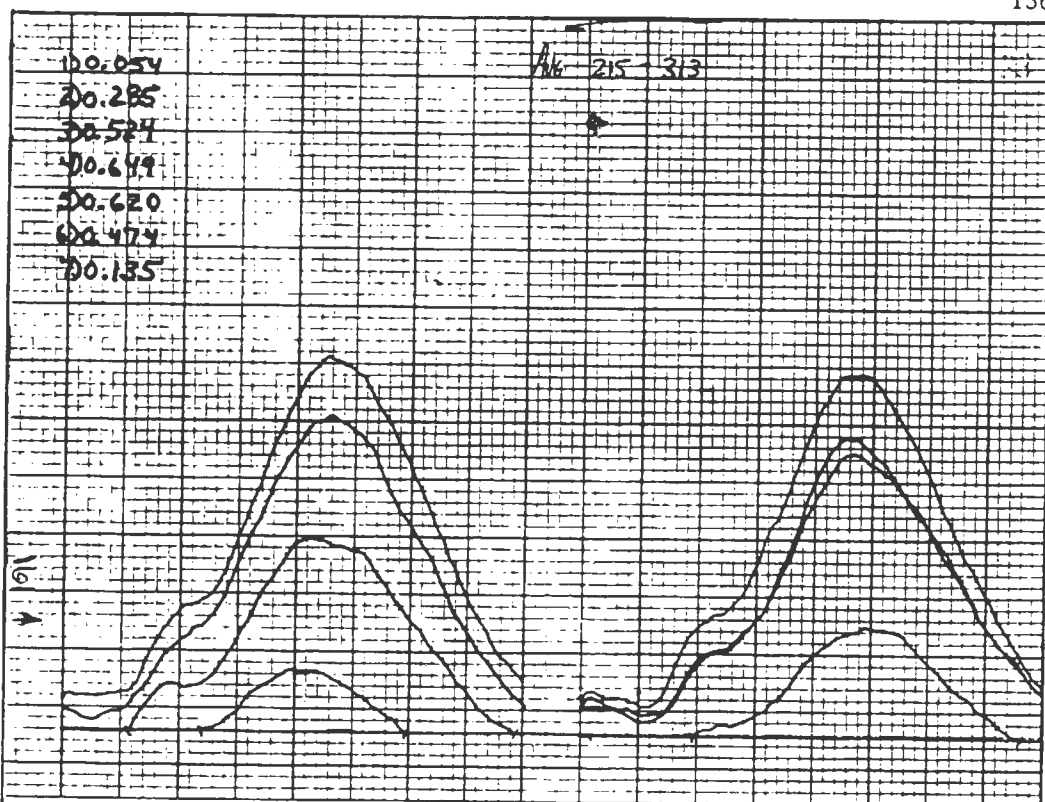
Test number 28



Test number 29



Test number 30



Test number 33

APPENDIX 6 Methane Combustion Inhibition by Bromine Compounds

ABSTRACT

The preferential reaction of H atoms and OH radicals with Br₂ and HBr, in a CH₄ - air flame, inhibits the chain reaction mechanisms of CH₄ combustion.

PREVIOUS RESEARCH and THEORY

Hydrogen bromide and bromine are efficient inhibitors of flame propagation. Inhibition results from reactions of HBr and Br₂ with chain propagating and chain branching radicals such as H and OH¹.

The HBr and Br₂ compounds can be introduced into a flame via the addition of any of several bromine compounds. The inhibiting characteristics of various brominated compounds have been investigated, and among these are:

1. Bromine^{2,3,4,5,6,7}
2. Hydrogen Bromide^{1,7,8,9,10,11}
3. Methyl Bromide^{7,12,13,14,15}
4. Bromotrifluoromethane^{7,16,17}
5. Dibromofluoromethane^{7,18}
6. 4,5,6,7 - Tetrabromophenolphthalein¹⁹

Steinberg has compiled a list of references on 18 other bromine compounds which have been investigated.¹⁸

The inhibition reactions are:



These three reactions rob the chain reaction of necessary radicals.

Precise knowledge of the combustion mechanism is a prerequisite for understanding inhibition phenomena. The high temperature combustion of methane is thought to involve these 18 steps²⁰:

- | | | |
|---|----------------------------|--------|
| 1. $\text{CH}_4 + \text{M} \rightleftharpoons \text{CH}_3 + \text{H} + \text{M}$ | Initiation | EQN 4 |
| 2. $\text{CH}_4 + \text{O}_2 \rightleftharpoons \text{CH}_3 + \text{HO}_2$ | Initiation | EQN 5 |
| 3. $\text{O}_2 + \text{M} \rightleftharpoons 2\text{O} + \text{M}$ | Initiation | EQN 6 |
| 4. $\text{CH}_4 + \text{O} \rightleftharpoons \text{CH}_3 + \text{OH}$ | Branching | EQN 7 |
| 5. $\text{CH}_4 + \text{H} \rightleftharpoons \text{CH}_3 + \text{H}_2$ | Propagating | EQN 8 |
| 6. $\text{CH}_4 + \text{OH} \rightleftharpoons \text{CH}_3 + \text{H}_2\text{O}$ | Propagating | EQN 9 |
| 7. $\text{CH}_3 + \text{O} \rightleftharpoons \text{H}_2\text{CO} + \text{H}$ | Terminating ^{1/2} | EQN 10 |
| 8. $\text{CH}_3 + \text{O}_2 \rightleftharpoons \text{H}_2\text{CO} + \text{OH}$ | Propagating | EQN 11 |
| 9. $\text{H}_2\text{CO} + \text{OH} \rightleftharpoons \text{HCO} + \text{H}_2\text{O}$ | Propagating | EQN 12 |
| 10. $\text{HCO} + \text{OH} \rightleftharpoons \text{CO} + \text{H}_2\text{O}$ | Terminating ^{2/2} | EQN 13 |
| 11. $\text{CO} + \text{OH} \rightleftharpoons \text{CO}_2 + \text{H}$ | Propagating | EQN 14 |

12. $\text{H} + \text{O}_2 \rightleftharpoons \text{OH} + \text{O}$	Branching	EQN 15
13. $\text{O} + \text{H}_2 \rightleftharpoons \text{OH} + \text{H}$	Branching	EQN 16
14. $\text{O} + \text{H}_2\text{O} \rightleftharpoons 2\text{OH}$	Branching	EQN 17
15. $\text{H} + \text{H}_2\text{O} \rightleftharpoons \text{H}_2 + \text{OH}$	Propagating	EQN 18
16. $\text{H} + \text{OH} + \text{M} \rightleftharpoons \text{H}_2\text{O} + \text{M}$	Terminating ²²	EQN 19
17. $\text{CH}_3 + \text{O}_2 \rightleftharpoons \text{HCO} + \text{H}_2\text{O}$	Propagating	EQN 20
18. $\text{HCO} + \text{M} \rightleftharpoons \text{H} + \text{CO} + \text{M}$	Propagating	EQN 21

At lower temperatures, a simpler scheme is thought to be followed²¹:

1. $\text{CH}_4 + \text{O}_2 \rightleftharpoons \text{CH}_3 + \text{HO}_2$	Initiation	EQN 5
2. $\text{CH}_3 + \text{O}_2 \rightleftharpoons \text{CH}_2\text{O} + \text{OH}$	Propagating	EQN 11
3. $\text{OH} + \text{CH}_4 \rightleftharpoons \text{H}_2\text{O} + \text{CH}_3$	Propagating	EQN 9
4. $\text{OH} + \text{H}_2\text{CO} \rightleftharpoons \text{H}_2\text{O} + \text{HCO}$	Propagating	EQN 12
5. $\text{H}_2\text{CO} + \text{O}_2 \rightleftharpoons \text{HCO} + \text{HO}_2$	Initiation	EQN 22
6. $\text{HCO} + \text{O}_2 \rightleftharpoons \text{CO} + \text{HO}_2$	Propagating	EQN 23
7. $\text{HO}_2 + \text{CH}_4 \rightleftharpoons \text{H}_2\text{O}_2 + \text{CH}_3$	Propagating	EQN 24
8. $\text{HO}_2 + \text{H}_2\text{CO} \rightleftharpoons \text{H}_2\text{O}_2 + \text{HCO}$	Propagating	EQN 25

The lower temperature reactions would dominate in the preflame zones, while the high temperature scheme would dominate within the flame itself.

Following is the reaction mechanism for H_2 and Br_2^{22} . It too is a complex chain reaction mechanism.

1. $M + Br_2 \rightleftharpoons 2Br + M$ Initiation EQN 26
2. $Br + H_2 \rightleftharpoons HBr + H$ Propagating EQN 27
3. $H + Br_2 \rightleftharpoons HBr + Br$ Propagating EQN 1
4. $H + HBr \rightleftharpoons H_2 + Br$ Propagating EQN 2
5. $M + 2Br \rightleftharpoons Br_2 + M$ Terminating²² EQN 28

Let us now assume that the reactions expressed in Equations 1, 2, and 3 are so rapid that no H or OH radicals are available to react with any compound containing a carbon atom. Also, we will assume that any HO_2 generated will decompose before it can react, as will H_2O_2 . HO_2 will decompose to either $OH + O$, or $H + O_2$. H_2O_2 will decompose to $2OH$.

With these restrictions and assumptions in mind, we can then postulate the following mechanism for "completely inhibited" methane combustion with bromine present.

1. $CH_4 + M \rightleftharpoons CH_3 + H + M$ Initiation EQN 4
2. $\dot{C}H_4 + O_2 \rightleftharpoons CH_3 + HO_2$ Initiation EQN 5
3. $O_2 + M \rightleftharpoons 2O + M$ Initiation EQN 6
4. $H_2 + M \rightleftharpoons 2H + M$ Initiation EQN 28
5. $CH_4 + O \rightleftharpoons CH_3 + OH$ Branching EQN 7
6. $CH_3 + O \rightleftharpoons H_2CO + H$ Terminating^{1/2} EQN 10

7.	$\text{CH}_3 + \text{O}_2 \rightleftharpoons \text{H}_2\text{CO} + \text{OH}$	Propagating	EQN 11
8.	$\text{H} + \text{O}_2 \rightleftharpoons \text{OH} + \text{O}$	Branching	EQN 15
9.	$\text{O} + \text{H}_2 \rightleftharpoons \text{OH} + \text{H}$	Branching	EQN 16
10.	$\text{O} + \text{H}_2\text{O} \rightleftharpoons 2\text{OH}$	Branching	EQN 17
11.	$\text{H} + \text{OH} + \text{M} \rightleftharpoons \text{H}_2\text{O} + \text{M}$	Terminating ²²	EQN 19
12.	$\text{CH}_3 + \text{O}_2 \rightleftharpoons \text{HCO} + \text{H}_2\text{O}$	Propagating	EQN 20
13.	$\text{HCO} + \text{M} \rightleftharpoons \text{H} + \text{CO} + \text{M}$	Propagating	EQN 21
14.	$\text{H}_2\text{CO} + \text{O}_2 \rightleftharpoons \text{HO}_2 + \text{HCO}$	Initiation	EQN 22
15.	$\text{HCO} + \text{O}_2 \rightleftharpoons \text{CO} + \text{HO}_2$	Propagating	EQN 23
16.	$\text{M} + \text{Br}_2 \rightleftharpoons 2\text{Br} + \text{M}$	Initiation	EQN 26
17.	$\text{Br} + \text{H}_2 \rightleftharpoons \text{HBr} + \text{H}$	Propagating	EQN 27
18.	$\text{H} + \text{Br}_2 \rightleftharpoons \text{HBr} + \text{Br}$	Propagating	EQN 1
19.	$\text{H} + \text{HBr} \rightleftharpoons \text{H}_2 + \text{Br}$	Propagating	EQN 2
20.	$\text{M} + 2\text{Br} \rightleftharpoons \text{Br}_2 + \text{M}$	Terminating ²²	EQN 28
21.	$\text{OH} + \text{HBr} \rightleftharpoons \text{H}_2\text{O} + \text{Br}$	Propagating	EQN 3
22.	$\begin{array}{c} \text{Bromine} \\ 2\text{CO} \rightleftharpoons \text{C}_{\text{soot}} + \text{CO}_2 \\ \text{Catalyst} \end{array}$		EQN 29

Some interesting developments are now coming to light. Combustion can still occur, but several important pathways have been eliminated. Compare the available paths for oxidation of

carbon compounds before the bromine additions, and after.

<u>Without Bromine</u>		<u>With Bromine</u>
$\text{CH}_4 + \text{M} \rightleftharpoons \text{CH}_3 + \text{H} + \text{M}$	(EQN 4)	$\text{CH}_4 + \text{M} \rightleftharpoons \text{CH}_3 + \text{H} + \text{M}$
$\text{CH}_4 + \text{O}_2 \rightleftharpoons \text{CH}_3 + \text{HO}_2$	(EQN 5)	$\text{CH}_4 + \text{O}_2 \rightleftharpoons \text{CH}_3 + \text{HO}_2$
$\text{CH}_4 + \text{O} \rightleftharpoons \text{CH}_3 + \text{OH}$	(EQN 7)	$\text{CH}_4 + \text{O} \rightleftharpoons \text{CH}_3 + \text{OH}$
$\text{CH}_4 + \text{H} \rightleftharpoons \text{CH}_3 + \text{H}_2$	(EQN 8)	
$\text{CH}_4 + \text{OH} \rightleftharpoons \text{CH}_3 + \text{H}_2\text{O}$	(EQN 9)	
$\text{CH}_3 + \text{O}_2 \rightleftharpoons \text{H}_2\text{CO} + \text{OH}$	(EQN 11)	$\text{CH}_3 + \text{O}_2 \rightleftharpoons \text{H}_2\text{CO} + \text{OH}$
$\text{CH}_3 + \text{O}_2 \rightleftharpoons \text{HCO} + \text{H}_2\text{C}$	(EQN 20)	$\text{CH}_3 + \text{O}_2 \rightleftharpoons \text{HCO} + \text{H}_2\text{O}$
$\text{CH}_3 + \text{O} \rightleftharpoons \text{H}_2\text{CO} + \text{H}$	(EQN 10)	$\text{CH}_3 + \text{O} \rightleftharpoons \text{H}_2\text{CO} + \text{H}$
$\text{H}_2\text{CO} + \text{O}_2 \rightleftharpoons \text{HCO} + \text{HO}_2$	(EQN 22)	$\text{H}_2\text{CO} + \text{O}_2 \rightleftharpoons \text{HCO} + \text{HO}_2$
$\text{H}_2\text{CO} + \text{OH} \rightleftharpoons \text{HCO} + \text{H}_2\text{O}$	(EQN 12)	
$\text{HCO} + \text{O}_2 \rightleftharpoons \text{CO} + \text{HO}_2$	(EQN 23)	$\text{HCO} + \text{O}_2 \rightleftharpoons \text{CO} + \text{HO}_2$
$\text{HCO} + \text{M} \rightleftharpoons \text{H} + \text{CO} + \text{M}$	(EQN 21)	$\text{HCO} + \text{M} \rightleftharpoons \text{H} + \text{OC} + \text{M}$
$\text{HCO} + \text{OH} \rightleftharpoons \text{CO} + \text{H}_2\text{O}$	(EQN 13)	
$\text{CO} + \text{OH} \rightleftharpoons \text{CO}_2 + \text{H}$	(EQN 11)	$2\text{CO} \rightleftharpoons \text{C}_{\text{soot}} + \text{CO}_2$

DISCUSSION

Tables of bond energy list the first broken C-H bond in methane to be kilocalories more than C-H bonds.²¹ The temperature of ignition for a methane/air mixture is higher than that for other hydrocarbons. This is because it does take so much energy to strip off that first hydrogen and begin the oxidation process. The energy of activation for the five CH₄ reactions (EQN's 4, 5, 7, 8, 9) are, respectively: 100,600 cal; 45,400 cal; 8,760 cal; 12,700 cal; and 5,000 cal. Only the three radical reactions have low energies of activation, and adding bromine eliminates two of these reactions (including that one having the lowest energy of the three). Thus we see that adding bromine has had two important effects on the initial combustion reactions.

1. We have decreased the number of species present with which methane could react.
2. We have increased the minimum energy needed for reaction.

In addition, one reaction of H₂CO to HCO has been removed. Likewise, one reaction of HCO to CO has been removed. Eliminating available reactions requires the hydrocarbon species in question to undergo additional collisions and will take longer to react.

In fact, by removing H and OH from the reaction mechanism for CH₄ combustion, we have completely altered the nature of that chain reaction mechanism. For instance, the step



which is propagating with respect to uninhibited reaction, now becomes effectively terminating. The same can be said of several other reactions (HCO + M \rightleftharpoons H + CO + M for instance). The H and OH radicals produced become separated from the hydrocarbon chain reaction system, and ultimately are converted to H₂O through the bromine system. The radical yield (more precisely, the effective yield) of the steps in the chain reaction for CH₄ \rightleftharpoons CO₂ is reduced by HBr or Br₂.

CONCLUSION

The removal of H and OH radicals from a methane/air flame by the action of HBr or Br₂ can account mechanistically for several of the observed inhibition phenomena.

1. Increased ignition temperature - The lowest energy of activation reaction is eliminated by tie up of OH and H.
2. Decreased flame speed - Reactions proceed more slowly due to increased number of collisions needed to react.
3. Sooting - CO conversion to CO₂ proceeds through a bromine catalyzed reaction



4. Minimum temperature of flame increased - Radical yield of chain reaction is lowered. Hence higher temperatures are required to generate sufficient reacting species.

APPENDIX 6 REFERENCES

- (1) Jourdain, J. L.; Le Bras, G.; Combourieu, J., Chem. Phys. Letts. 1981, 78(3), 483-7.
- (2) KoKurin, A. D.; Vinogradov, V. N.; Egorova, L. I.; ZH. Prikl. Khim. 1980, 53(9), 2083-5.
- (3) Phillips, L. F. and Sugden, T. M., Can. J. Chem. 1960, 38, 1804
- (4) Lask, G. W. and Wagner, H. G., Forschungsh Wes. Ing., 1961, 27, 52
- (5) Jost, W. and Wagner, H. G., special Publication No. 9, p. 197, The Chemical Society, London (1957)
- (6) Lask, G. W. and Wagner, H. G. 8th Symposium, p. 432
- (7) Rosser, W. A; Wise, H.; Miller, J. 7th Symposium, p. 175
- (8) W. E. Wilson; Donovan, J. T.; Fristrom, J. R.; 12th International Symposium on Combustion (Butterworths, London, 1969) p. 929
- (9) Drake, M. C.; Hastie, J. W.; Combust. Flame, 1981 40(2), 201-11
- (10) Westbrook, C.K.; Combust. Sci. Technol. 1980 23(5-6), pp. 1991-202
- (11) Aronowitz, S; Chang, S.; Scattergood, T.; Journal of Physical Chemistry, Vol. 85, No. 4, 1981
- (12) Simmons, R. F.; Wolfhard, H.G; Trans. Faraday Soc. 1955, 51, 53-59
- (13) Simmons, R. F.; Wolfhard, H. G; Trans. Faraday Soc. 1955, 51, 1211-1217
- (14) Bourdon, M.C.; Bourgoyne, J. H.; Weinberg, F. J. 5th Symposium, p. 647
- (15) Steacie, E. W. R., Atomic and Free Radical Reactions (Reinhold, New York, 1954) Vol. 1, p. 107, p. 258
- (16) Tucker, D. M.; Drysdale, D. D.; Rasbash, D. J.; Combust. Flame 1981, 41(3), 293-300
- (17) Parks, D. J.; Alvares, N. J.; Beason, D. G.; Fire Saf. J. 1980, 2(4), 237-42

- (18) Papp, J. F.; Lazzara, C. P.; Biordi, J. C.; Rep. Invest. - U.S., Bur. Mines 1981, RI-8551, 36pp
- (19) Lin, M.S; Pearce, E. M.; Journal of Polymer Science, Polymer Chemistry Edition, Vol. 19, 251-2160 (1981)
- (20) Serry, D.; Bowman, C. T.; Combust. Flame (1970), 14, 347
- (21) Glassman, I; Combustion (Academic Press, New York, 1977) p.49
- (22) Bodenstein, M. (1913). Z. Phys. Chem. 85, 329